QUANTIFYING PEATLAND CARBON DYNAMICS USING MECHANISTICALLY-BASED BIOGEOCHEMISTRY MODELS

by

Sirui Wang

A Dissertation

Submitted to the Faculty of Purdue University

In Partial Fulfillment of the Requirements for the degree of

Doctor of Philosophy

Department of Earth, Atmospheric, & Planetary Sciences

West Lafayette, Indiana

May 2019

THE PURDUE UNIVERSITY GRADUATE SCHOOL
STATEMENT OF COMMITTEE APPROVAL

Dr. Qianlai Zhuang

Department of Earth, Atmospheric, & Planetary Sciences

Dr. Lisa Welp

Department of Earth, Atmospheric, & Planetary Sciences

Dr. Harshvardhan

Department of Earth, Atmospheric, & Planetary Sciences

Dr. Tonglin Zhang

Department of Statistics

Approved by:

Dr. Daniel J. Cziczo

Head of the Graduate Program

To my Family

ACKNOWLEDGMENTS

I would like to express my sincerest gratitude and greatest appreciation to all who have been supporting me and helping me during my study and daily life. I would like to start by thanking Prof. Qianlai Zhuang for his guidance, support, and patience. During my PhD study time, Prof. Zhuang inspired me to accomplish my research with his innovative ideas and endless assistance. He always kept inspiring me when I had difficulties and was always optimistic, helping me overcome the obstacles. It is my great honor to work and learn under his guidance. I am also thankful to my committee members: Prof. Harshvardhan, Prof. Tonglin Zhang, and Prof. Lisa Welp. Atmospheric remote sensing was the first course I took after I came to Purdue and it was taught by Prof. Harshvardhan. He has in-depth knowledge on remote sensing and radiative transferring. His knowledge helped me greatly on my research regardless on or off the class. Prof. Zhang is from the Department of Statistics, I took multiple courses from him and learned how to parameterize and optimize the model for my dissertation research in a more efficient way. What he has taught speeded up my research progress. Prof. Welp is such a careful and rigorous scientist with great knowledge on ecosystem dynamics and hydrology. She kept following my research and gave me helpful advices.

I also would like to thank all my co-authors. They collaborated with us in multiple projects and provided us with valuable field and lab data for model calibration and verification. They also provided constructive comments and suggestions during my manuscript revision iterations. Their efforts and help made my publications possible. I am looking forward to working with them again in the near future.

Finally, I would like to thank our lab members at Purdue. It is their help that made both my PhD study and my life much easier and much more interesting. I really have enjoyed every single day with them. It has been a great time for me at Purdue.

TABLE OF CONTENTS

LIST OF TABLES

LIST OF FIGURES

ABSTRACT

Author: Wang, Sirui. PhD
Institution: Purdue University
Degree Received: May 2019
Title: Quantifying Peatland Carbon Dynamics Using Mechanistically-Based Biogeochemistry Models
Committee Chair: Qianlai Zhuang

Peatlands are the most efficient natural carbon sink on the planet. They are the most carbon-intensive storages than any other vegetation types. However, recent studies indicate that global peatlands can potentially release 6% of the global soil carbon into the atmosphere when they are drained or deforested. They cover only about 3% of the total global land area, but sequester over 30% of the Earth's soil organic carbon. Peatlands in northern mid-to-high latitudes (45°-90°N) occupy ~90% of the global peatland area and account for ~80% of the total global peat organic carbon stock. Those peatlands are mainly located in Canada, Russia, and the USA. Peatlands in tropical regions cover ~10% of the global peatlands area and store 15-19% of the global peat organic carbon. They are mainly distributed in Southeast Asia and South and Central America. The temperature at the global scale has been rising since the middle of the last century and has accelerated during the last 40 years and the warming will continue in this century. The large storage of soil organic carbon within the peatlands can significantly respond to the changing climate by varying the roles between their carbon sink (from atmosphere to soil) and source (from soil to atmosphere) activities. This dissertation focuses on quantifying the soil organic carbon dynamics in North America and South America using mechanistically-based biogeochemistry models.

Peatlands in Alaska occupy 40 million hectares and account for ~10% of the total peatland area in northern mid-to-high latitudes. The regional soil organic carbon dynamics and

its response to climate are still with large uncertainty. Most of the studies on peatlands to date are based on short-term site-level observation. This dissertation first used an integrated modeling framework that coupled the dynamics of hydrology, soil thermal regime, and ecosystem carbon and nitrogen to quantify the long-term peat carbon accumulation in Alaska during the Holocene. Modeled hydrology, soil thermal regime, carbon pools and fluxes and methane emissions were evaluated using long-term observation data at several peatland sites in Minnesota, Alaska, and Canada. The model was then applied for a 10,000-year (15 ka to 5 ka; 1 ka = 1000 cal yr before present) simulation at four peatland sites. The model simulations matched the observed carbon accumulation rates at fen sites during the Holocene ($R^2 = 0.88$, 0.87, 0.38 and -0.05 for four sites respectively using comparisons in 500-year bins from 15 ka to 5 ka). The simulated (2.04 m) and observed peat depths (on average 1.98 m) also compared well (R^2 = 0.91). The early Holocene carbon accumulation rates, especially during the Holocene thermal maximum (HTM) (35.9 g C m^{-2} yr^{-1}), were estimated up to 6-times higher than the rest of the Holocene (6.5 g C m^{-2} yr^{-1}). It suggested that high summer temperature and the lengthened growing season resulted from the elevated insolation seasonality, along with wetter-than-before conditions might be major factors causing the rapid carbon accumulation in Alaska during the HTM. The sensitivity tests indicated that, apart from climate, initial water-table depth and vegetation canopy were major drivers to the estimated peat carbon accumulation.

To further quantify the regional long-term soil organic carbon accumulation rates and the current carbon stocks in Alaska, the second part of my research focused on quantifying the soil organic carbon accumulation in multiple Alaskan terrestrial ecosystems over the last 15,000 years for both peatland and non-peatland ecosystems. Comparable with the previous estimates of 25-70 Pg carbon (C) in peatlands and 13-22 Pg C in non-peatland soils within 1-m depth in

Alaska using peat core data, our model estimated a total SOC of 36-63 Pg C at present, including 27-48 Pg C in peatland soils and 9-15 Pg C in non-peatland soils. Current living vegetation stored 2.5-3.7 Pg C in Alaska with 0.3-0.6 Pg C in peatlands and 2.2-3.1 Pg C in non-peatlands. The simulated average rate of peat soil C accumulation was 2.3 Tg C yr^{-1} with a peak value of 5.1 Tg C yr^{-1} during the Holocene Thermal Maximum (HTM) in the early Holocene, four folds higher than the average rate of 1.4 Tg C yr^{-1} over the rest of the Holocene. The accumulation slowed down, or even ceased, during the neo-glacial climate cooling after the mid-Holocene, but increased again in the 20th century. The model-estimated peat depths ranged from 1.1 to 2.7 m, similar to the field-based estimate of 2.29 m for the region. The changes in vegetation and their distributions were the main factors to determine the spatial variations of SOC accumulation during different time periods. Warmer summer temperature and stronger radiation seasonality, along with higher precipitation in the HTM and the 20th century might have resulted in the extensive peatland expansion and carbon accumulation.

Most studies on the role of tropical peatlands have focused on Indonesian peatlands. Few have focused on the Amazon basin, where peatlands remain intact and have been a long-term carbon sink. To address the problem, my third study quantified the carbon accumulation for peatland and non-peatland ecosystems in the Pastaza-Marañon foreland basin (PMFB), the most extensive peatland complex in the Amazon basin from 12,000 years before present to 2100 AD. Model simulations indicated that warming accelerated peat carbon loss while increasing precipitation accelerated peat carbon accumulation at millennial time scales. The uncertain parameters and spatial variation of climate were significant sources of uncertainty to modeled peat carbon accumulation. Under warmer and presumably wetter conditions over the 21st century, the warming effect on increasing peat carbon loss might overwhelm the wetter effect on

increasing peat carbon accumulation. Peat soil carbon accumulation rate in the PMFB slowed down to 7.9 (4.3~12.2) g C m^{-2} yr^{-1} from the current rate of 16.1 (9.1~23.7) g C m^{-2} yr^{-1} and the region might turn into a carbon source to the atmosphere at -53.3 (-66.8~-41.2) g C m^{-2} yr^{-1} (negative indicates source), depending on the level of warming. Peatland ecosystems showed a higher vulnerability than non-peatland ecosystems as indicated by the ratio of their soil carbon density changes (change of soil carbon/existing soil carbon stock) ranging from 3.9 to 5.8). This was primarily due to larger peatlands carbon stocks and more dramatic responses of their aerobic and anaerobic decompositions in comparison with non-peatland ecosystems under future climate conditions. Peatland and non-peatland soils in the PMFB might lose up to 0.4 (0.32~0.52) Pg C by 2100 AD with the largest loss from palm swamp. The carbon-dense Amazonian peatland might switch from a current carbon sink into a source in the 21st century.

Peatlands are important sources and sinks for greenhouse gases (carbon dioxide and methane). Their carbon (C) balance between soil and atmosphere remains unquantified due to the large data gaps and uncertainties in regional peat carbon estimation. My final study was to quantify the C accumulation rates and C stocks within North America peatlands over the last 12,000 years. I find that 85-174 Pg C have been accumulated in North American peatlands over these years including 0.37-0.76 Pg C in subtropical peatlands in this region. During the 10- 8 ka period, the warmer and wetter conditions might have played an important role in stimulating peat C accumulation by enhancing plant photosynthesis. The enhanced peat decomposition due to warming through the Holocene slows down carbon accumulation in the region.

CHAPTER 1. INTRODUCTION

1.1 Research Background

Global climate has experienced significant changes in the last few decades (Arctic Climate Impact Assessment, 2005; Intergovernmental Panel on Climate Change (IPCC), 2014). The mean global surface temperature started increasing since the middle of the 19th century and has risen 0.8℃ according to the reports (IPCC, 2013, 2014). In the northern mid-to-high latitudes, this warming is larger than other regions on the planet (Alexeev et al., 2005) and has accelerated at 0.3℃ per decade since 1970 (IPCC, 2014; McGuire et al., 2009). According to the predictions of global models, the warming trend will continue in the next 100 years (IPCC, 2013). Over 40% of the global soil organic carbon (SOC) is stored in northern mid-to-high latitudes (Melillo et al., 1995). The recent estimation of the SOC stocks in northern high latitudes was between 900 and 1300 Pg C (1 Pg C = 10^{15} g C), including 200-600 Pg C stored in northern peatlands and another 750 Pg C in non-peatland soils (Melillo et al., 1995; Gorham, 1990, 1991; Yu, 2012; Tarnocai et al., 2009; Hugelius et al., 2014). Peatlands in northern high latitudes store approximately 90% of global peat SOC, occupying 80% global peatland area. In Alaska, peatlands cover roughly 11% of the total land area and is one of the most peatland-extensive regions in northern high latitudes (Pastick et al., 2017). The responses of northern peatlands to warming and other climate trends is significant. Under warming conditions, northern peatlands may still act as a large C sink due to the stimulated plant C uptake (Loisel et al., 2012). Meanwhile, hydrological conditions of northern peatlands and the subsequent peat soil decomposition may be altered through the increased evapotranspiration and lowered water table (Hobbie et al., 2000; Yu et al., 2009).

So far, several studies have been conducted to understand the interaction between peat SOC accumulation and the climate factors. However, large uncertainty remains (Davidson and Janssens, 2006; Gerdol et al., 2008; Jones and Yu, 2010). There are limitations of the current studies. First, most of those studies were done based on short-term site-level field measurements (Turetsky et al., 2008, 2014; Bridgham et al., 2008). Those studies analyzed the C dynamics and hydrological conditions at several peatland sites within the last few decades. However, it may not be adequate for understanding the long-term trend of the peat SOC history and its response to climate change. Second, long-term peat accumulation data have been collected recently at northern peatland sites (Turunen et al., 2002; Roulet et al., 2007; Gorham et al., 2003; Yu et al., 2009). However, due to the intensive field work and the non-accessibility of most of peatlands, core analysis may not efficiently provide an estimation of peat SOC stocks at large regional scales. Third, some models have been developed in order to simulate the peat SOC dynamics (Frolking et al., 2010; Spahni et al., 2013). However, those models did not take advantage of the rich peat core data.

Apart from the peatlands in northern high latitudes, peatlands in tropical regions occupy ~11% of the global peatland area and account for 15%-19% of the total global peat SOC stock (Page et al., 2011). Mean surface air temperature in tropical regions, especially South America, has been projected to increase by 1.8-5.1℃ in the next 100 years, although large uncertainty exists (Marengo et al., 2012; Zulkafli et al., 2016). Understanding the responses of tropical peatlands to a changing climate will be as significant as the northern peatlands. The 120,000 km^2 Pastaza-Marañón foreland basin (PMFB) located in Peru is the most extensive peatland complex in the Amazon basin, with up to 7.5 m thick peat deposits (Lähteenoja et al., 2011, 2012). A very limited number of studies have been done for this area while most of studies have

been focusing on Indonesian peatlands. Recently, long-term field measurement data have been collected from the core analysis and satellite images have been analyzed to map the vegetation distribution in this area (Lähteenoja et al., 2009a, 2009b, 2011, 2012; Draper et al., 2014). However, due to the limitation of accessibility to the peatlands, the regional SOC estimation largely relies on the interpolation and extrapolation of the site-level measurements. The historical peat SOC accumulation trajectories and the current regional peat SOC stocks have been estimated by those studies. However, the regional carbon dynamics in future have not been yet evaluated.

1.2 Research Objectives

Given the limitations of site-level field measurements and the limitations of existing modeling studies, the first objective of my dissertation was to develop a new model that is able to simulate the peat SOC dynamics. My first study based on an extant biogeochemistry model, the Terrestrial Ecosystem Model (TEM, Zhuang et al., 2001, 2002, 2003, 2004, 2006), to develop a new model for peatland ecosystems (P-TEM, Peatland Terrestrial Ecosystem Model). By coupling and revising a series of modules (the carbon and nitrogen dynamics module, the soil thermal module, the methane dynamics module, and the hydrological module), P-TEM was developed explicitly for both peatland and non-peatland ecosystems. By taking advantage of the observational data of soil moisture, water-table depth, soil temperature, and methane fluxes at peatland sites, we calibrated and evaluated the P-TEM. The model was then applied to four peatland sites on the Kenai Peninsula, Alaska, and was compared to the peat core measurements for performance testing. Driven by the paleoclimate data from ECBilt-CLIO model output (Timm and Timmermann, 2007), simulations from 15 to 5 ka (15 ka to 5 ka; 1 ka = 1000 cal yr before present) were conducted to quantify the peat SOC accumulation rates and the variations of

the hydrological conditions during the Holocene period. To understand the interaction between climatic factors and the SOC dynamics, a series of sensitivity tests and statistical analysis were performed.

Using the peatland model (P-TEM), my second objective was to take a further step to quantify the regional SOC accumulation rates and current stocks for both peatland and non-peatland in Alaska. The model parameters were adjusted and optimized from the previous study for non-peatland ecosystems (Tang and Zhuang, 2008). Based on the parameterization in my previous study (Wang et al., 2016a) and the parameterization from the open fen and spruce bog sites, the P-TEM was re-adjusted for regional simulation. To obtain the vegetation distribution map during different paleo time periods, non-peatland ecosystems were classified into boreal deciduous broadleaf forest, boreal evergreen needleleaf and mixed forest, alpine tundra, wet tundra; and barren lands based on the pollen data (He et al., 2014). Non-peatland maps were then reclassified into peatland maps including *Sphagnum* spp. poor fens dominated by tundra and *Sphagnum* spp.-black spruce (*Picea mariana*) bog/ peatland dominated by forest ecosystems to represent the expansion and shrinkage of peatlands during each time period. Non-peatland and peatland ecosystem distribution for each grid cell was determined using the wetland inundation data extracted from the NASA/ GISS global natural wetland dataset (Matthews and Fung, 1987). The Alaskan C stock was simulated through the Holocene driven with vegetation data reconstructed and the paleoclimate data from 15 ka to present. A series of extra simulations were done to further examine how uncertain climates and vegetation distribution affect the results.

My third objective was to quantify the historical trajectories of the tropical peat SOC dynamics and predict their future fate. By using the available field measurements and satellite images, the region was classified into different ecosystems. P-TEM was parameterized for each

type of ecosystems. The model parameters were optimized using the published peat, vegetation and remote-sensing data for the PMFB. The model was then used to: 1) quantify past C accumulation from 12 ka to 2014 AD in peatlands, and 2) predict the future trends of C accumulation under different climate scenarios in the 21st century in peatland and non-peatland ecosystems within the PMFB.

My fourth objective in this dissertation was to combine the previous studies to overcome the large data gaps and uncertainties in the regional peat carbon estimation in North America. Peatlands in North America includes northern peatlands located in Canada, Alaska, the conterminous USA (mainly upper Michigan, Maine, and North Dakota), and subtropical peatlands distributed in Florida and Coastal areas of Mexican Gulf. The model was re-calibrated using the site-level long-term peat carbon accumulation data in northern part of North America and subtropical part of North America. The model was applied to the whole North America to simulate the peat soil carbon density distribution and total carbon stocks from 12 ka to 2014 AD based on the modern inundation map and peatland distribution map.

1.3 Dissertation Organization

My dissertation consists of four studies, each of which addresses one research objective. In Chapter 2, a new model for both peatland and non-peatland ecosystems (P-TEM) was developed based on the existing biogeochemistry model (TEM). Multiple site-level field measurements were utilized to parameterize the model with respect to carbon and water fluxes, and soil temperature profiles. The long-term peat SOC accumulation rates were simulated using the adjusted model and were tested against the peat core analysis data at four sites in Alaska. In Chapter 3, to conduct regional simulations of SOC accumulation for both non-peatlands and peatlands, P-TEM was parameterized for representative ecosystems in Alaska. Second, the

regional vegetation and peatland distribution data were organized. Spatial basal age data for all peatland grid cells based on site-level soil core data, and climate data for each period during the Holocene were also organized. Finally, the regional simulations and sensitivity analysis were conducted. In Chapter 4, the model was used to quantify the SOC accumulation for peatland and non-peatland ecosystems in the Pastaza-Marañon foreland basin (PMFB) in the Peruvian Amazon from 12,000 years before present to 2100 AD. In Chapter 5, the model was re-parameterized and applied to simulate the regional peat carbon density and total carbon stocks within North America from 12 ka to present day. In Chapter 6, the conclusions and the limitations of my dissertation research were discussed. A new study in progress and the future related works are described.

CHAPTER 2. QUANTIFYING PEAT CARBON ACCUMULATION IN ALASKA USING A PROCESS-BASED BIOGEOCHEMISTRY MODEL[1]

2.1 Introduction

The Arctic has experienced significant warming in the 20th century, and this warming is predicted to continue in this century (Arctic Climate Impact Assessment, 2005; Intergovernmental Panel on Climate Change (IPCC), 2014). Terrestrial ecosystems in this region occupy a large portion (22%) of the global land surface with approximately 40% of global soil carbon (McGuire et al., 1995, 1997). The ongoing and future warming is expected to change the cycling of the Arctic soil carbon, leading to either a negative (Davidson and Janssens, 2006) or a positive feedback to the global climate system (Christensen et al., 2007; Jones and Yu, 2010).

Northern peatlands store 200 - 600 Pg (1 Pg = 10^{15} g) carbon depending on depth considered (Gorham, 1991; Turunen et al., 2002; McGuire et al., 2009; Yu et al., 2010), which accounts for up to one-third of the world's soil carbon (Post et al., 1982; Gorham, 1991). They are mainly located in Russia, Canada, the USA, and Fennoscandian countries (Lappalainen, 1996; Turunen et al., 2002). A number of studies have quantified the climate impact on carbon dynamics in peatlands (e.g., Kirschbaum, 1993, 1995; Wang and Polglase, 1995; Deng et al., 2015; Zhuang et al., 2015; Knorr et al., 2005), but no consensus on the net effect of climate change on peat carbon accumulation has been reached. A number of soil core analyses and modeling indicate that warming reduces soil organic carbon storage (e.g., Kirschbaum, 2000, 2006; Davidson and Janssens, 2006; Gerdol et al., 2008), but others suggest there is an acceleration of soil carbon sequestration (Yu et al., 2009; Jones and Yu, 2010).

---

[1]**Wang, S**., Zhuang, Q., Yu, Z., Bridgham, S., and Keller, J., Quantifying peat carbon accumulation in Alaska using a process-based biogeochemistry model, J. Geophys. Res. Biogeosci., 121, doi:10.1002/2016JG003452, 2016.

Many existing studies on peatland carbon dynamics are based on short-term observation and model simulations (e.g., Turetsky et al., 2008, 2014; Bridgham et al., 2008; Deng et al., 2015). These short-term analyses may not be adequate for understanding the response of peat carbon to long-term climate change. To overcome this, peat core data have been used to infer the peat carbon accumulation rates during the Holocene in various regions (e.g., Turunen et al., 2002; Roulet et al., 2007; Gorham et al., 2003; Yu et al., 2009). Most long-term observational studies have focused on individual sites, but recently some large-scale syntheses have been carried out (Yu et al., 2010; Loisel et al., 2014). Models are another means of examining long-term response to climate change. Spahni et al. (2013) imbedded a peatland module into a dynamic global vegetation and land surface process model (LPX-Bern 1.0), and conducted a transient simulation of carbon dynamics in northern peatlands from the Last Glacial Maximum to the 21st century. Frolking et al. (2010) also modeled the peat carbon accumulation rate and peat depth profile for an 8000-years old ombrotrophic bog (Mer Bleue) in Canada. However these models have not explicitly considered the effects of permafrost dynamics or were based on a simple algorithm to model soil temperature effects on peat carbon dynamics. Further, some of these models have not considered the nitrogen feedbacks to the carbon cycling in nitrogen-limited northern peatlands.

In the past few decades, peat core data have been collected in the circum-Arctic region (Yu et al., 2009). Fluxes of carbon, water and energy in peatland ecosystems in the region have also been measured (Turetsky et al., 2008; Churchill, 2011). However, existing peatland modeling studies have not taken advantage of these rich data. Here, we develop and evaluate a peatland biogeochemistry model (P-TEM) based on an extant biogeochemistry model, the Terrestrial Ecosystem Model (TEM; Zhuang et al., 2003; 2004). The model explicitly considers

the effects of permafrost and hydrological dynamics as well as nitrogen feedbacks to the carbon cycling of peatland ecosystems. The model is then used to examine peat carbon accumulation rates for Alaskan peatlands during the Holocene.

2.2 Methods

2.2.1 Overview

We first develop the P-TEM by coupling and revising a core carbon and nitrogen dynamics module (CNDM) of TEM (Zhuang et al., 2003), the soil thermal module (STM) (Zhuang et al., 2001), the methane dynamics module (MDM) (Zhuang et al., 2004; 2006), a hydrological module (HM) (Zhuang et al., 2002) (Figure 2.1). Second, we evaluate hydrological dynamics using observed data of soil moisture at upland sites in Canada and water-table depth at peatland sites in Alaska. We evaluate soil temperature estimates using data collected at the same upland and peatland sites. We also evaluate methane emission estimates using methane flux data of a peatland in Minnesota. Third, we apply the model to four peatlands sites on the Kenai Peninsula, Alaska, driven with paleoclimate data from ECBilt-CLIO model output (Timm and Timmermann, 2007) to evaluate peat carbon accumulation rate and depth profile by comparing to peat core data. Finally, we test the model sensitivity to various controls and factors as a way to identify the main factors that influence peat carbon dynamics.

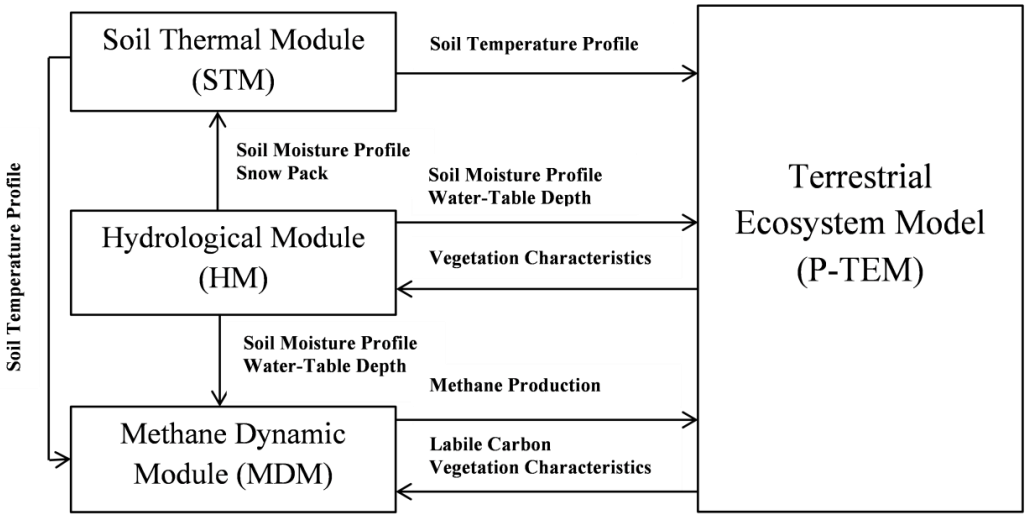

Figure 2.1. P-TEM modeling framework includes a soil thermal module (STM), a hydrologic module (HM), a carbon/ nitrogen dynamic model (TEM), and a methane dynamics module (MDM) (Zhuang et al., 2002, 2004, 2006).

2.2.2 Model Modification

Peat soil organic carbon (SOC) accumulation is determined by the net primary production (NPP) and aerobic and anaerobic respiration. Peatlands accumulate carbon where NPP is greater than decomposition, resulting in positive net ecosystem production (NEP). The core carbon and nitrogen dynamics module of TEM was developed for upland ecosytsems (Zhuang et al., 2003), where NEP is calculated at a monthly time step:

$$NEP = NPP - R_H \qquad (1)$$

SOC heterotrophic respiration (R_H) is calculated as (Table 2.1):

$$R_H = K_d C_S f(M_V) e^{0.069 H_T} \qquad (2)$$

where $f(M_V)$ is a nonlinear relationship that describes the effect of soil moisture in the unsatureted zone on microbial activity for decomposition. Soil moisture affects oxygen level in

soils. K_d is the logarithm of heterotrophic respiration rate at 0℃. C_S is the total amount of upland mineral SOC above the plant rooting depth. H_T is mean monthly temperature of the organic layer.

Here we revise the decomposition to include both aerobic heterotrophic respiration above the water table which produces CO_2 and anaerobic respiration below water table, which produces both CO_2 and methane (CH_4) at the same time with certain amount of CH_4 transferred to CO_2 through oxidation. The soil organic carbon accumulation rate (ΔSOC) is equal to NEP, where NEP is calculated:

$$NEP = NPP - R_H^{'} - R_{CH_4} - R_{CWM} - R_{CM} - R_{COM} (3)$$

R_{CH_4} represents the monthly methane emission after methane oxidation and R_{CWM} represents the CO_2 emission due to methane oxidation (Zhuang et al., 2015). A ratio of 1:1 is assumed to calculate the CO_2 release (R_{CM}) accompanied with the methanogenesis (Tang et al., 2010; Conrad, 1999). R_{COM} represents the CO_2 release from other anaerobic processes (e.g., fermentation, terminal electron acceptor (TEA) reduction) (Keller and Bridgham, 2007; Keller and Takagi, 2013). The ratio of $R_{COM}: R_{CH_4}$ varies largely according to previous studies. The molar ratios ($CO_2: CH_4$) of the emission rates under inundated conditions were 4-173 for the fen and bog, respectively (Moore and Knowles, 1989), while Freeman et al. (1993) and Yavitt et al. (1987) estimated this ratio as 1. Here we assume $R_{COM}: R_{CH_4}$ (CO_2 release from other anaerobic processes : CH_4 release after oxidation) to be 5 so that the simulated $CO_2: CH_4$ of the emission rates from the anearobic processes is ~10 for a fen (see Discussion). $R_H^{'}$ now represents the monthly aerobic respiration related to the variability of water-table depth (WTD) (Table 2.1):

$$R_H^{'} = K_d C_{S1} f(M_V^{'}) e^{0.069 H_T} \times \frac{WTD}{LWB} \quad (4)$$

where $M_V^{'}$ represents the soil water content in the unsaturated zone above the WTD. The SOC between the lowest water-table boundary (LWB, a fixed model parameter, the soil below which is set saturated; see Table 2.1) and soil surface (C_{S1}) in the transient condition is obtainted after a 2000-year equilibrium run.

We model peatland soils as a two-layer system based on the three-layer system for upland (Tables 2.2, 2.3) in the hydrological module (HM). The soil layers above the LWB are divided into 1-cm sub-layers where peat soil characteristics in the upper peat are constant above 7 cm peat depth and changed linearly in the section interval of 1 cm below (Table 2.3) (Granberg et al., 1999; Zhuang et al., 2004). P_{tot} is the total porosity (Table 2.3) and is set to 0.98 below the WTD. The actual WTD is estimated based on the total amount of water content above the LWB within upper two boxes. Using the calculated WTD, the water content at each 1cm above the water table can be then determined after solving the water balance equations.

In the STM module, the soil vertical profile is divided into four layers: (1) snowpack in winter; (2) moss (or litter) layer; (3) organic soil (upper organic layer and lower organic layer for peatland soils) and (4) mineral soil. The mineral layer is set to be water saturated for peatland soils (Table 2.3). Each of these soil layers is characterized with a distinct soil thermal conductivity and heat capacity. The observed soil water content data are used to drive STM.

The methane dynamics module (MDM) (Zhuang et al., 2004) explicitly considers the process of methane production (methanogenesis), methane oxidation (methanotrophy) and the transportation pathways including: (1) diffusion through the soil profile; (2) plant-aided transportation; and (3) ebullition. Methane oxidation is simulated as an aerobic process that

occurs only in the unsaturated zone. Hourly methanotrophy is estimated within each 1-cm layer. The MDM gets the soil temperature inputs calculated from STM. HM estimated the WTD and soil water content in the unsaturated zone affects methane production and emission. Net primary production (NPP) is calculated from the CNDM. Soil-water pH is prescribed from the site observed data, and the root distribution determines the redox potential.

Table 2.1. Variables and model parameters used for calculating heterotrophic respiration in this study.

Variables	Description	Unit
R_H	Monthly heterotrophic respiration of soil organic carbon (upland soils)	g C m^{-2} mon^{-1}
R'_H	Monthly aerobic heterotrophic respiration of soil organic carbon (peatland soils)	g C m^{-2} mon^{-1}
R_{CH_4}	Monthly methane emission	g C m^{-2} mon^{-1}
R_{CWM}	Monthly CO_2 emission due to methane oxidation	g C m^{-2} mon^{-1}
R_{CM}	Monthly CO_2 emission due to methane production	g C m^{-2} mon^{-1}
R_{COM}	Monthly CO_2 emission due to other anaerobic processes	g C m^{-2} mon^{-1}
K_d	Logarithm of heterotrophic respiration rate at 0℃	g C g^{-1} mol^{-1}
C_S	Quantity of the state variable describing total amount of soil organic carbon (SOC)	g C m^{-2}
C_{S0}	SOC between the lowest water-table boundary and soil surface (Equilibrium)	g C m^{-2}
C_{S1}	SOC between the lowest water-table boundary and soil surface (Transient)	g C m^{-2}
M_V	Soil water content (upland soils)	%
M'_V	Soil water content in the unsaturated zone (peatland soils)	%
H_T	Mean monthly temperature of the organic soil layer	℃
LWB	Lowest water-table boundary (fixed model parameter)	mm
WTD	Water-table depth	mm

Table 2.2. Optimized parameters used for simulation of soil moisture content in the unsaturated zone for hydrological module (HM) based on observation (Zhuang et al., 2002, 2004).

Parameters	Definition	SK 1977	Delta Junction 1920	Delta Junction 1999	Units
I_{RMAX}	The maximum daily canopy interception of rain	0.26	0.26	0.0	mm mm^{-1}
I_{SMAX}	Snow interception rate	0.5	0.5	0.5	LAI^{-1} d^{-1}
PFC_{mo}	Field capacity of moss plus fibric layer	50	45	45	%
PFC_{humic}	Field capacity of humic organic layer	40	35	36	%
PFC_{min}	Field capacity of mineral layer	35	30	30	%
PC_{mo}	Percolation coefficients for moss plus fibric layer	6	6	6	unitless
PC_{humic}	Percolation coefficients for humic layer	4.5	4.5	4.5	unitless
PC_{min}	Percolation coefficients for mineral layer	4	4	4	unitless
$DEPT_{mo}$	Depth for moss plus fibric layer	0.1	0.1	0.1	m
$DEPT_{humic}$	Depth for humic layer	0.4	0.4	0.4	m
$DEPT_{min}$	Depth for mineral layer	0.5	0.5	0.5	m
$PHASE_{mo}$	Percentage of water which will become ice form during winter	80	80	80	%
$PHASE_{humic}$		70	70	70	%
$PHASE_{min}$		0	0	0	%

Table 2.3. Optimized parameters used for simulation of water-table depth based on observation (Granberg et al., 1999; Zhuang et al., 2004).

Parameter	Thickness of moss layer (cm)	Thickness of organic layer above *LWB* (cm)	Lowest water-table boundary(*LWB*) (cm)	P_{tot} (%) of two layers	Minimum vegetation surface soil moisture (%)	Maximum depth below the peat surface which the soil moisture above starts to decrease linearly (cm)
APEXCON	10	20	30	94, 88	25	7
SPRUCE	10	20	30	95, 88	33	7

2.2.3 Model Evaluation

We evaluate the modeling framework with respect to hydrological dynamics, peat soil thermal dynamics, and carbon and methane dynamics using observed data at various peatland sites. We first evaluate the modeled volumetric soil moisture (%) at three upland sites in Alaska (Delta Junction 1920 and 1999) and Canada (SK 1977) (Table 2.4). The forcing climate data from the local sites including air temperature, precipitation, global incoming solar radiation or photosynthetically active radiation (PAR), and water vapor pressure were aggregated into monthly time step. The water vapor pressure is obtained from the calculation of observed air temperature at canopy height and relative humidity. The snow rate is obtained by equally splitting the total annual accumulated snowfall into months during the winter. Second, we evaluate the simulated water-table depth and methane emissions at APEXCON and SPRUCE sites (Table 2.4). The APEXCON site, characterized as a lowland open fen, is located outside the boundaries of the Bonanza Creek Experimental Forest. The APEXCON site is a moderate rich fen with mean pH of 5.3, which lacks trees and is dominated by a diverse community of emergent aquatic plants (Carex, Equisetum), brown moss, and Sphagnum with the thickness of peat approximately 1 m. The weekly observed methane fluxes using static chambers during the growing seasons are for the period of 2005-2011. Hourly water-table depth was continuously recorded from June to October each year. The SPRUCE site is characterized as a Picea mariana

(black spruce) – Sphagnum spp. bog forest. The 0.5-hour observed meteorological data (Hanson et al., 2015), water-table depth and methane flux data during the growing seasons from 2011 to 2014 (Iverson et al., 2014; Hanson et al., 2014) were aggregated to a monthly time step for model input.

Third, we evaluate the simulated soil temperature profile using observed data at Saskatchew 1977 Fire and Delta Junction 1920 sites for upland soils and APEXCON for peatland soils. We also evaluate the simulated carbon dynamics of a fen at the APEXCON site.

2.2.4 Model Application

We apply P-TEM to four peatlands on the Kenai Peninsula, Alaska (Jones and Yu, 2010; Yu et al., 2009) (Table 2.5). The observed data includes the peat depth, percentage of organic matter, and bulk density of both organic and inorganic matter at 1-cm intervals. The percentage of organic matter in the peat sample and the bulk density are used to convert the simulated peat carbon to the total peat depth profile. The ratio of the peat SOC over peat organic matter is set to be 0.468 from the soil carbon amount distribution database (Loisel et al., 2014).

In the simulation, we assume that the initial waterlogging event occurred 2000 years before peat starts to form, which provides the necessary hydrological conditions for peatland formation. We run the model for 2000 years using the climate data from 17 ka to 15 ka (see below for climate data description) to rearch equilibrium to get the initial soil carbon C_{S0}. The transient simulation starts after reaching the equilibrium as C_{S0} no longer changes, providing a stable soil carbon amount from the LWB to soil surface at 15 ka.

The accumulation of peat carbon is examined at four subsequent time slices (15 ka to 5 ka) after the 2000-year equilibrium run (17 ka to 15 ka) including a time slice encompassing a millennial-scale warming event during the last deglaciation known as the BØlling-AllerØd at 15-

13 ka, the Holocene Thermal Maximum (HTM) during the early Holocene at 11-10 and 10-9 ka, and the mid-Holocene at 7-5 ka BP. The climate data in two time periods, from 13 to 11 ka and from 9 to 7 ka were not explicitly simulated, but we used the linear interpolation from adjacent slices and filled these two missing slices. Climate data were downscaled from ECBilt-CLIO model output (Timm and Timmermann, 2007; He et al., 2014). Climate fields include monthly precipitation, monthly air temperature, monthly net incoming solar radiation (NIRR) and monthly vapor pressure ($2.5° \times 2.5°$). The ECBilt-CLIO model has been used in other HTM studies where the model produced the interaction between orbital-induced summer insolation and ice sheet configuration that were reflected in proxy records (Renssen et al., 2009). We apply delta-ratio bias-correction with observed half-degree data from the Climate Research Unit (CRU2.0) and the inverse-square distance interpolation method, similar to the approach taken to downscale and bias-correct future climate scenarios (Hay et al., 2000), to correct the climate anomalies for the detailed topography and coastlines of northern high latitudes at a resolution of $0.5° \times 0.5°$. To drive the P-TEM, we use the same time-dependent forcing atmospheric carbon dioxide concentration data as were used in ECBilt-CLIO transient simulations from the Taylor Dome (Timm and Timmermann, 2007).

We also conduct a sensitivity analysis for peat carbon accumulation in response to variations of the lowest water-table boundary (LWB) and the leaf area index (LAI). In the "standard" simulation, the LWB is set to 30 cm below the soil surface, while in the "more saturated" and "less saturated" scenarios, it is set to 22 cm and 38 cm, respectively. We conduct the test with other variables remaining unchanged. As the water-table position is raised, less space will be available for the microbial aerobic respiration, leading to an increasing amount of

methane production, and vice versa. We are interested in estimating the long-term influence of different LWB on the simulation of peatland carbon accumulation in P-TEM.

Leaf Area Index (LAI) defines the leaf area for snow and rain interception by the vegetation canopy. Different values of LAI lead to different hydrological conditions. We conduct three simulations: the forested peatland with the LAI set to 5.0 (Coughlan and Running, 1997) and the maximum daily canopy interception of rain (I_{RMAX}) (Table 2.2) set to 0.26 (Helvey, 1971; Zhuang et al., 2002) through the year; a partly forested peatland with LAI 2.8 and I_{RMAX} set to 0.1; and an open peatland (Sphagnum) with LAI set to 0.4 and I_{RMAX} set to 0.0. The "standard" simulation is the open fen and we also conduct simulations for two other vegetation types to investigate how the different LAI can influence the interception of monthly precipitation, and thus cause the change of peat carbon accumulation.

Table 2.4. Sites used for parameterization for hydrological module (HM), methane dynamics module (MDM) and soil thermal module (STM).

Site	Description	Vegetation	Simulation Period	Observed variables for HM (or MDM) parameterization	Observed variables for STM parameterization
Saskatchew (SK) 1977 Fire	Evergreen broadleaf forest site in Saskatchewan, Canada. Mean annual temperature is 0.4℃, with mean total precipitation 467.2 mm (1971-2000 Waskesiu normals)	Jack pine black spruce	Jan 2004 -Dec 2005	VSM at 30 cm	Soil temperature at depths 10cm, 20cm, and 50cm
Delta Junction 1920 Control	Evergreen needleleaf forest located near Delta Junction, to the north of the Alaska Range in Interior Alaska (Senkowsky, 2001)	Evergreen needleleaf forest	Jan 2002 -Dec 2003	VSM at 4cm, 11cm, and 37cm	Soil temperature at depths 10cm and 20cm
Delta Junction 1999 Burn	Located near Delta Junction, to the north of the Alaska Range in Interior Alaska, within 15-km of Delta Junction 1920 Control. 70% of the area is not covered by vascular plants, with mean annual temperature -2.3℃, annual accumulated rainfall 304 mm and snowfall 940 mm (Liu et al., 2005)	Open shrublands	Jan 2002 - Dec 2003	VSM at depth 4cm and 11cm	Not used
APEXCON	Low land open fen along Bonanza Creek Road at the base of the bluff, Bonanza Creek, Interior Alaska. The area is classified as continental boreal with a mean annual temperature of -2.9℃ and annual accumulated precipitation of 269 mm, of which 30% is snow (Hinzman et al., 2006)	Moderate rich open fen with sedges (*Carex* sp.), spiked rushes (*Eleocharis* sp.), *Sphagnum* spp., and brown mosses (*Drepanocladus aduncus*)	Growing Season in 2007, and from 2009 to 2011	Water-table depth and methane emission	Soil temperature at depths 10cm, 25cm, and 50cm
SPRUCE	Bog forest in northern Minnesota, 40 km of Grand Rapids in the USDA Forest Service Marcell Experimental Forest (MEF). Mean annual temperature from 1961 to 2005 is 3.3℃, annual accumulated precipitation is 768 mm, with 75% of it occurs in the snow-free period from mid-April to early November (Crill et al., 1988)	*Picea mariana-Sphagnum* spp. bog	Growing Season from 2011 to 2014	Water-table depth and methane emissions	-

Table 2.5. Sites used for comparison of carbon accumulation rates between simulation and observation (Jones and Yu, 2010)

Site name	Location	Peatland type	Latitude	Longitude	Dating method	No. of dates	Basal age (cal yr BP)	Time-weighted Holocene accumulation rates (g C m^{-2} yr^{-1})
Kenai Gasfield	Alaska, USA	fen	60º27'N	151º14'W	AMS	12	11,408	13.1
No Name Creek	Alaska, USA	fen	60º38'N	151º04'W	AMS	11	11,526	12.3
Horsetrail fen	Alaska, USA	rich fen	60º25'N	150º54'W	AMS	10	13,614	10. 7
Swanson fen	Alaska, USA	poor fen	60º47'N	150º49'W	AMS	9	14,225	5.7

2.3 Results and Discussion

2.3.1 Model Evaluation

Based on the adjusted parameters for upland (Table 2.2) and peatland (Table 2.3) in the HM, the result of the shallowest layer of soils in Delta Junction 1999 and 1920 suggest that the HM can accurately simulate the soil moisture content in both open tundra and boreal forest ($R^2 = 0.94$ and 0.76 for Delta Junction 1920 and 1999, respectively) (Figures 2.2(a) and (b)). Especially during the growing season, the water content is much higher at the tundra site, suggesting a higher rainfall through the plant canopy due to the smaller leaf interception area (Figure 2.2(e)). Similarly, HM has the capacity to simulate the soil moisture content for the deeper layer ($R^2 = 0.92$ and 0.83 for SK 1977 Fire and Delta Junction 1920, respectively) (Figures 2.2(c) and (d)). The HM well simulates the monthly water-table depth at both APEXCON and SPRUCE sites ($R^2 = 0.92$ and 0.52, respectively) (Figure 2.3).

Based on the adjusted parameters in the STM (Table 2.6), the model reproduces the soil temperature profile with R^2 values of 0.94, 0.96, and 0.67 at 10 cm, 20 cm and 50 cm,

respectively, at the SK 1977 Fire site (Figure 2.4). Similarly, compared with observations, the model captures the soil temperature for the Delta Junction 1920 site with R^2 values 0.83 and 0.85 at 10 cm and 20 cm, and for the APEXCON site with R^2 values of 0.96, 0.92, and 0.81 at 10 cm, 25 cm and 50 cm, respectively (Figure 2.4). Furthermore, the MDM estimated methane fluxes match observations with R^2 values of 0.90 and 0.40 for the two sites after incorporating the calculated soil moisture in the unsaturated zone, water-table depth, and soil temperature profile from other modules (Figure 2.5).

Based on the adjusted parameters in the CNDM, the simulated annual fluxes and pools of carbon and nitrogen are within the range of the observations at APEXCON in 2009 and other references (Table 2.7).

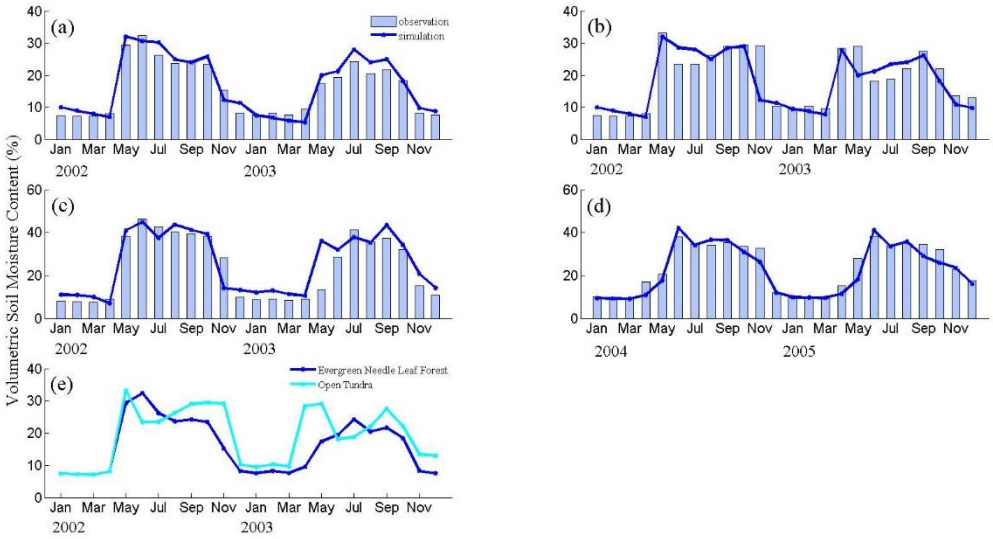

Figure 2.2. Comparison between observed and simulated soil moisture for the shallowest layer (moss layer) (a) at Delta Junction 1920 (evergreen needleleaf forest) and (b) Delta Junction 1999 (open tundra) in 2002 and 2003 (the value for comparison is calculated using the average of the moisture at 2 cm, 4 cm and 11 cm). Comparison between observed and simulated soil moisture for the organic layer at (c) (Delta Junction 1920 (37 cm) in 2002 and 2003, and (d) SK 1977 Fire (30 cm) in 2004 and 2005. (e) Comparison between the observed soil moisture for the 0-10 cm layer at Delta 1920 (forest site) and Delta 1999 (open tundra site).

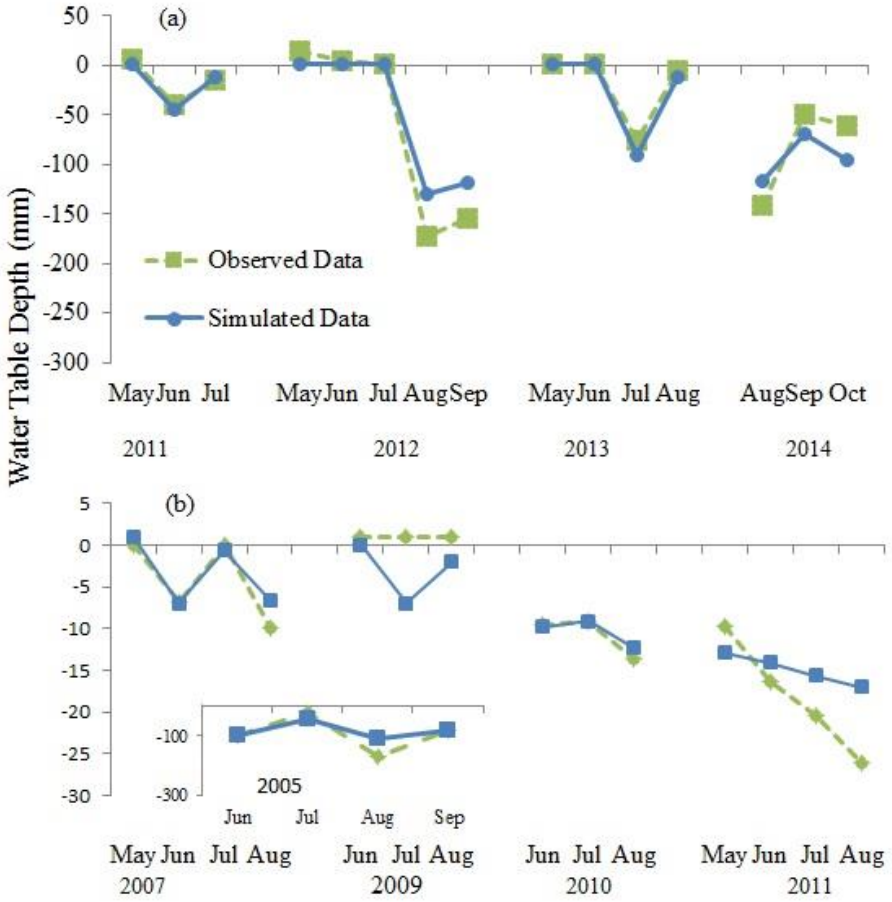

Figure 2.3. Comparison of the water-table depth between the observed data and simulated data for the growing seasons of SPRUCE (top) from 2011 to 2014 (Iverson et al., 2014; Shi et al., 2015) and APEXCON (bottom) in 2005, 2007, and 2009 to 2011. The inset of the bottom figure is the comparison of 2005 for APEXCON (Turetsky et al., 2008).

Table 2.6. Parameters used for simulation of soil temperature profile for three sites in soil thermal module (STM) (Zhuang et al., 2001).

Parameter	SK 1977	Delta Junction 1920	APEXCON	Units
Moss thickness	10	10	10	cm
Organic thickness	40	40	20	cm
Mineral layer thickness	50	50	70	cm
Moss water content	20	25	85	%
Moss thawed thermal conductivity	0.4	0.35	0.5	$W^{-1}\ m^{-1}\ K^{-1}$
Moss frozen thermal conductivity	0.53	0.55	0.6	$W^{-1}\ m^{-1}\ K^{-1}$
Moss thawed volumetric heat content	1.7	1.6	1.8	$MJ^{-1}\ m^{-1}\ K^{-1}$
Moss frozen volumetric heat content	1.5	1.5	1.5	$MJ^{-1}\ m^{-1}\ K^{-1}$
Organic water content	30	35	88	%
Organic thawed thermal conductivity	0.45	0.45	0.6	$W^{-1}\ m^{-1}\ K^{-1}$
Organic frozen thermal conductivity	1.0	1.1	1.2	$W^{-1}\ m^{-1}\ K^{-1}$
Organic thawed heat content	2.6	2.6	2.6	$MJ^{-1}\ m^{-1}\ K^{-1}$
Organic frozen heat content	2.4	2.4	2.4	$MJ^{-1}\ m^{-1}\ K^{-1}$
Mineral water content	43	40	90	%
Mineral thawed thermal conductivity	0.5	0.55	0.6	$W^{-1}\ m^{-1}\ K^{-1}$
Mineral frozen thermal conductivity	1.2	1.2	1.3	$W^{-1}\ m^{-1}\ K^{-1}$
Mineral thawed heat content	3.1	3.1	3.4	$MJ^{-1}\ m^{-1}\ K^{-1}$
Mineral frozen heat content	1.7	1.7	1.7	$MJ^{-1}\ m^{-1}\ K^{-1}$
Snow thermal conductivity	0.2	0.2	0.2	$MJ^{-1}\ m^{-1}\ K^{-1}$

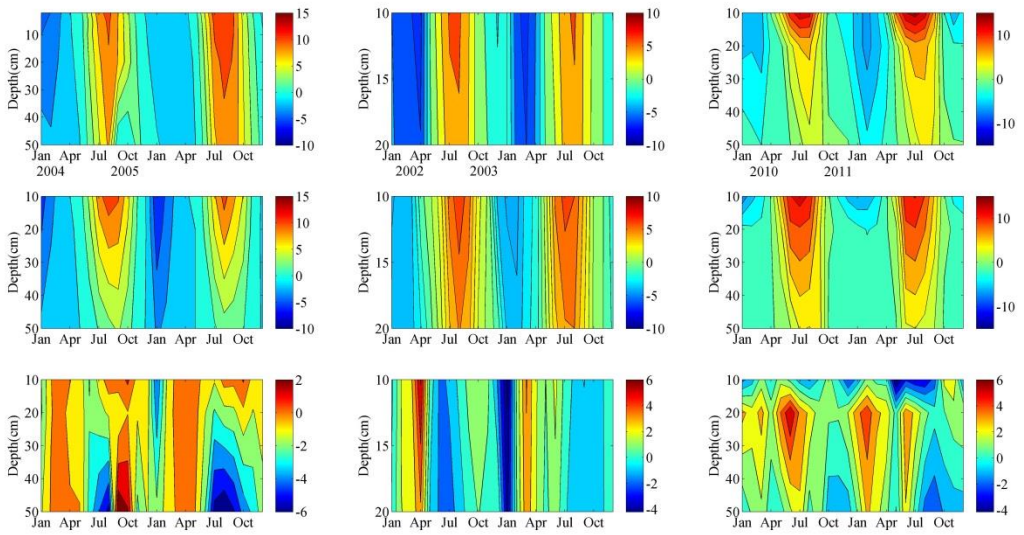

Figure 2.4. Top row: Observed soil temperature (°C) at depths 10 cm, 20 cm and 50 cm for SK 1977 site (left), observed soil temperature at 10cm, 20cm for Delta Junction 1920 (middle), observed soil temperature at 10cm, 25cm and 50cm for APEXCON (right). Middle row: Simulated soil temperature at 10cm, 20cm and 50cm for SK 1977 site (left), Simulated soil temperature at 10cm, 20cm for Delta Junction 1920 (middle), Simulated soil temperature at 10cm, 25cm and 50cm for APEXCON (right). Bottom row: Residual of simulated and observed soil temperature at 10cm, 20cm and 50cm for SK 1977 site (left), Residual of simulated and observed soil temperature at 10cm, 20cm for Delta Junction 1920 (middle), Residual of simulated and observed soil temperature at 10cm, 25cm and 50cm, respectively for APEXCON (right).

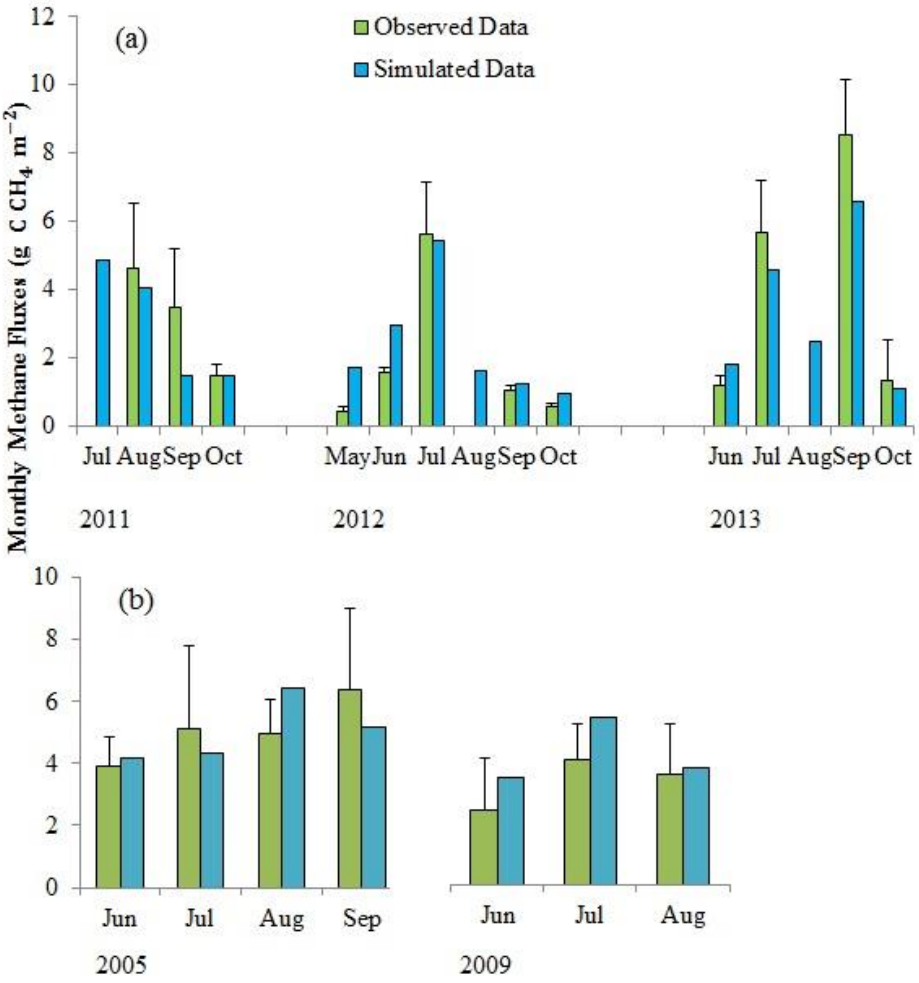

Figure 2.5. Comparison of the methane emission between observation and simulation for SPRUCE (a) from 2011 to 2013 (Hanson et al., 2014), and APEXCON (b) in 2005 and 2009. In (a), the blanks reflect missing observation data.

Table 2.7. Parameters of calculating carbon and nitrogen fluxes and pools for a fen site in carbon and nitrogen dynamics module (CNDM).

Annual Carbon and Nitrogen Fluxes or Pools[a]	Simulated Using Adjusted Model Parameters	Amount from references or site-level observations	References
NPP	350	445 ± 260	Turetsky et al. (2008),
Vegetation Carbon	750	682-904	Churchill (2011)
Litter Fall Carbon	333	300	Moore et al. (2002)
Nitrogen uptake by vegetation	2.0	1.8	Zhuang et al. (2002)
Soil carbon in 1 m	20000	5000-90000	Tarnocai et al. (2009)
Soil carbon : Soil nitrogen	70	48-90	Kuhry and Vitt (1996)

[a]Units for annual net primary production (NPP), litter fall carbon are g C m^{-2} yr^{-1}. Units for vegetation carbon and soil carbon in 1 m depth are g C m^{-2}. Unit for annual nitrogen uptake by plants is g N m^{-2} yr^{-1}. Soil carbon in 1 m depth represents the amount of carbon in the wet tundra (the depth is 1 m in the model), e.g. the initial carbon amount for peatland.

2.3.2 Peatland Carbon Accumulation

P-TEM simulations for the six grid cells in Kenai Peninsula show a large variation from 15 ka to 5 ka, ranging from a peat carbon loss to peat carbon gain of 100 g C m^{-2} yr^{-1} on average (Figure 2.6). The most obvious long-term pattern is a large peak of peat carbon accumulation rates at 11 ka – 9 ka (HTM), and a secondary peak at 6 ka – 5 ka (mid-Holocene). The model captures the largest peak during the HTM at almost all sites, among which the magnitude is accurately estimated at No Name Creek and Horse Trail Fen sites, while there are time shifts and over-estimates in magnitude at Kenai Gasfield and Swanson Fen sites. The secondary accumulation peak is captured at No Name Creek, Kenai Gasfield and Swanson Fen sites, while the model slightly over-estimated the rate at mid-Holocene at Horse Trail Fen site. In addition, there is a high-frequency (20-year resolution) variability in magnitude due to changing climate. When the temporal resolution of the results is reduced to 500-year bins (Figure 2.7), the simulations match the observations well, especially at No Name Creek and Horse Trail Fen sites. The simulated trend of carbon accumulation rates is consistent with the synthesis curves from all four sites (Jones and Yu, 2010). The R^2 coefficient between the simulation and observation are

0.88 for Horse Trail Fen, 0.87 for No Name Creek, 0.38 for Gasfiled and -0.05 for Swanson Fen (Figure 2.8). The negative correlation at Swanson Fen may be due to the time shift between the simulated accumulation peak in the late HTM and the observed peak in the early HTM. This could be resulted from the dating resolution on the actual cores as more dates (e.g., 20-year bins) would probably shift the peaks in the HTM slightly compared with less dates (e.g., 500-year bins) (Figures 2.6(d) and 2.6(d))

The frequency distribution of peat carbon accumulation rates over the simulated time period shows a large temporal variability (Figure 2.9), with a mean rate 10.82 g C m^{-2} yr^{-1} and standard deviation 29.22 g C m^{-2} yr^{-1}. There is a relatively large proportion of negative accumulation rates, suggesting a loss of carbon from the soil occurred in some years, especially before the Holocene and in the mid-Holocene (Figure 2.6). Most rates are within the range of -40 to 40 g C m^{-2} yr^{-1}. The rates exceeding 60 g C m^{-2} yr^{-1} occurred mainly during the HTM when there was expansive peatland development. These simulations are consistent with field observations (Yu et al., 2009). The rates exceeding 15 g C m^{-2} yr^{-1} can be approximated with a normal distribution (μ = 10.82 g C m^{-2} yr^{-1}, σ = 29.22 g C m^{-2} yr^{-1}). However, the rates smaller than 15 g C m^{-2} yr^{-1} exhibits a non-normal distribution pattern with a very high frequency from 0 to 15 g C m^{-2} yr^{-1}.

Using the observed peat depth bulk density, we estimate the peat depth profile from 15 ka to 5 ka (Figure 2.10). At No Name Creek, a total depth of 2.5 m is comparable with observed 2.47 m. Although there is a high correlation between simulated and observed peat depth at Horse Trail Fen, the rapid observed carbon accumulation started almost 2000 years before the model estimation. We model a 2.49 m depth versus an observed depth of 2.93 m. The modeled depth profile has a very high correlation with the observation at Kenai Gasfield. The simulated and

observed trends stay almost the same with a total depth of 1.2 m and 1.1 m. The observed depth at Swanson Fen started to increase approximately 3500 years before the model estimation. The total peat depth reaches 1.92 m from simulation compared with 1.76 m from observation. In general, Noname Creek and Kenai Gasfield have the best comparison while the modeled starting points of peat depth are later than the field estimation at Horse Trail Fen and Swanson Fen sites.

On average, the simulated carbon accumulation rate is 10.82 g C m^{-2} yr^{-1} from 15 ka to 5 ka, while the rate of the HTM is 35.9 g C m^{-2} yr^{-1}, which is up to six-times higher than the rest of the Holocene (6.5 g C m^{-2} yr^{-1}) excluding the rate during the HTM. These are consistent with findings of Jones and Yu (2010), which estimated the carbon accumulation rate was ~20 g C m^{-2} yr^{-1} from 11.5 ka to 8.6 ka, four-times higher than the average rate of ~5 g C m^{-2} yr^{-1} over the rest of the Holocene. They found that by 8.6 ka, around 75% of modern Alaskan peatland had formed, followed by a six-fold decrease afterwards.

The simulated climate by ECBilt-CLIO shows that, among all time periods, the coolest temperature appeared at 15 ka – 13 ka, followed by the mid-Holocene (7 ka – 5 ka) (Figures 2.11(c), and (d)). Those two periods were also generally dry (Figures 2.11(e) and (f)). The former represents colder and drier climate before the onset of the HTM (Barber and Finney, 2000; Edwards et al., 2001). The latter represents post-HTM cooling before the neo-glacier period, which caused permafrost aggradation across northern high latitudes (Oksanen et al., 2001; Zoltai, 1995). Before the HTM, the mean annual net incoming solar radiation (NIRR) of the chosen six pixels is the lowest among all time periods, approximately 75 W m^{-2} (Figure 2.11(b)). Similarly, the mean annual temperature before the HTM for the selected grids is also the lowest among all periods, which is -0.5℃ with the lowest mean monthly temperature -10℃ and highest 8℃ (Figures 2.11(c) and (d)). In the early HTM period (11 ka - 10 ka), the radiation

started to increase and reached 83 W m^{-2}. Meanwhile, the annual temperature increased considerably, reaching 2.36℃. The temperature had its largest increase in summer. The monthly temperature variation suggests that the growing season (monthly temperature above 0℃) had lengthened 10 – 15 days (Figure 2.11(c)). There was also an increase of radiation during the growing season in the early HTM (Figure 2.11(a)). We find that the total annual precipitation increased by 75 mm from 510 mm during the early HTM (Figure 2.11(f)), with a greater increase in summer than in winter (Figure 2.11(e)). It followed by a wetter-than-before condition in the late HTM (10 ka – 9 ka). The solar radiation in growing season continued to increase, reaching the maximum value 87 W m^{-2} at the time, characterized by the highest summer insolation and highest summer temperature as described in Jones and Yu (2010) and Huybers et al. (2006). Cooler and drier conditions occurred during the mid-Holocene, accompanied by a greater decrease of precipitation in winter than in summer.

The large expansion of Alaskan peatland during the HTM coincides with the maximum summer temperature and NIRR, as well as a wetter-than-before condition. Furthermore, ECBilt-CLIO simulated the increase of temperature and radiation in the growing season, but they remain unchanged in winter among all time periods (Figure 2.11(a)). This obviously leads to a stronger seasonality of radiation in the HTM, which has been described in Kaufman et al. (2004, 2016) and Yu et al. (2009). The rapid peat carbon accumulation in the HTM corresponds to the highest summer temperature along with the highest seasonal radiative forcing. Warmer conditions in summer and the lengthened vegetation growing season, and probably earlier snow melt during the HTM positively affects NPP by increasing plant productivity, leading to more carbon input to soils (Running et al., 2004). Warmer conditions could also lead to a higher decomposition rate of

peat SOC (Nobrega et al., 2007; Dorrepaal et al., 2009). However, these increases in NPP appear to more than offset warming-induced increases in decomposition.

Hydrological effect can be significant as water-table depth could be raised with an increase in precipitation. Higher water tables allow less space for aerobic respiration and give larger space for anaerobic respiration, which reduce the soil carbon loss as aerobic respiration is faster than anaerobic respiration (Hobbie et al., 2000).

A forward stepwise linear regression model between carbon accumulation rates and climate variables were applied. Monthly temperature, monthly NIRR, monthly precipitation and their seasonalities were put into the regression model. The result suggests that a number of factors are significant ($P<0.001$; Table 2.8), temperature has the most significant effect on carbon accumulation rate according to the biggest F-value in the analysis of variance table (ANOVA). The seasonality of NIRR also plays an important role, but monthly NIRR, as we thought important above is not a significant factor. The seasonality of temperature, the interaction of temperature and precipitation, and precipitation alone have relatively minor effects (lower F-values) among all significant variables. The seasonality of precipitation is not important. Enhanced temperature, larger climate (radiation) seasonality and enhanced precipitation may help explain the onset of explosive peatland initiation in Alaska during the HTM. The low, even negative carbon accumulation rate during the mid-Holocene is consistent with the unfavorable cool and dry climate conditions. This period experienced lower snowfall than the HTM (Figure 2.11(e)). The combination of decreased snowfall and lower temperature (Table 2.8) resulted in deeper frost depth due to the decreased insulative effects of the snowpack, and therefore shortening the period for active photosynthetic C uptake, leading to an overall low plant productivity (McGuire et al., 2000; Stieglitz et al., 2003).

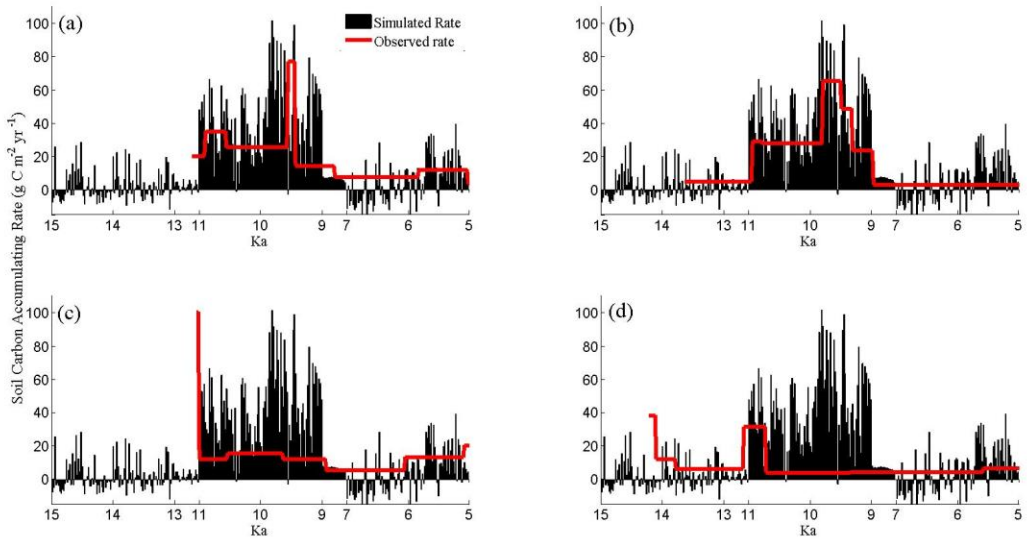

Figure 2.6. Simulated and observed carbon accumulation rates from 15 ka to 5 ka. Red solid lines represent the observed time-weighted rates for (a) No Name Creek; (b) Horse Trail Fen; (c) Kenai Gasfield; and (d) Swanson Fen. Black solid lines represent the simulated averaged carbon accumulation rate of every 20 years

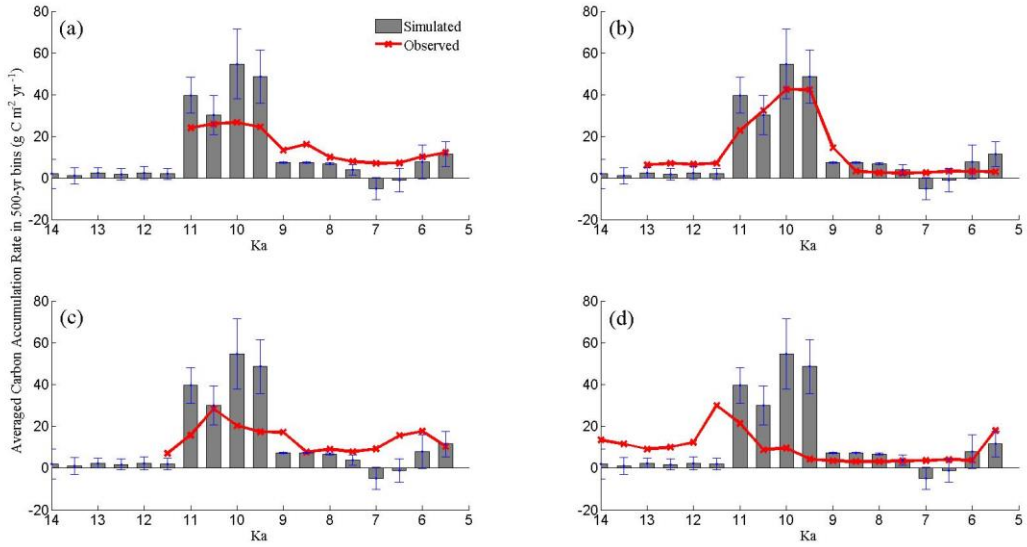

Figure 2.7. Simulated and observed carbon accumulation rates from 14.5 ka to 5 ka in 500-year bins with standard deviations for (a) No Name Creek; (b) Horse Trail Fen; (c) Kenai Gasfield; and (d) Swanson Fen.

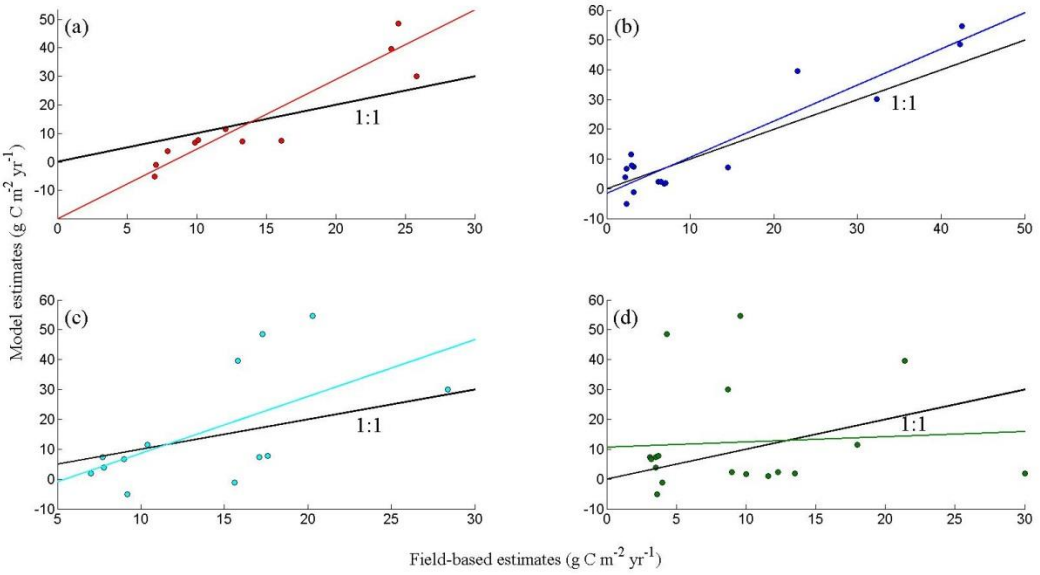

Figure 2.8. Field-based and model estimates of annual peat carbon accumulation rates in 500-year bins. Linear regressions between simulated and observed estimates are compared with the 1:1 line. For (a) No Name Creek, the linear regression is significant (P<0.001, N = 12), with R^2 = 0.87, slope = 2.43, and intercept = -19.85 $g\ C\ m^{-2}\ yr^{-1}$. For (b) Horse Trail Fen, the linear regression is significant (P<0.001, N = 16), with R^2 = 0.88, slope = 1.21, and intercept = -1.46 $g\ C\ m^{-2}\ yr^{-1}$; For (c) Kenai Gasfield, the linear regression is significant (P<0.001, N = 13), with R^2 = 0.38, slope = 1.90, and intercept = -10.40 $g\ C\ m^{-2}\ yr^{-1}$ and for (d) Swanson Fen, the linear regression is significant (P<0.001, N = 18), with R^2 = -0.05, slope = 0.17, and intercept = 10.69 $g\ C\ m^{-2}\ yr^{-1}$.

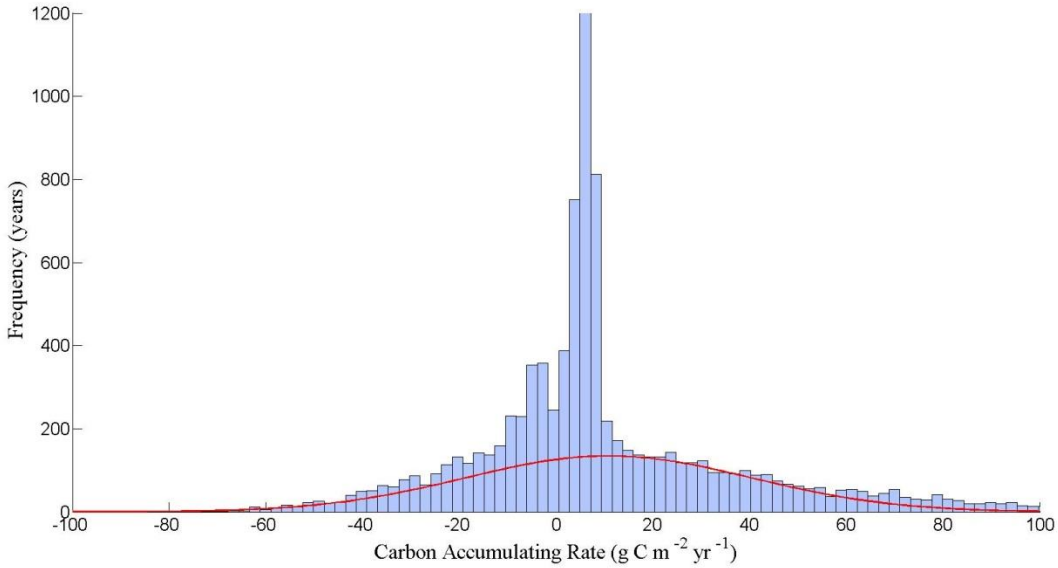

Figure 2.9. Frequency histogram of simulated peat carbon accumulation rates from 15 ka to 5 ka, characterized with a normal distribution (μ = 10.82 $g\ C\ m^{-2}\ yr^{-1}$, σ = 29.22 $g\ C\ m^{-2}\ yr^{-1}$).

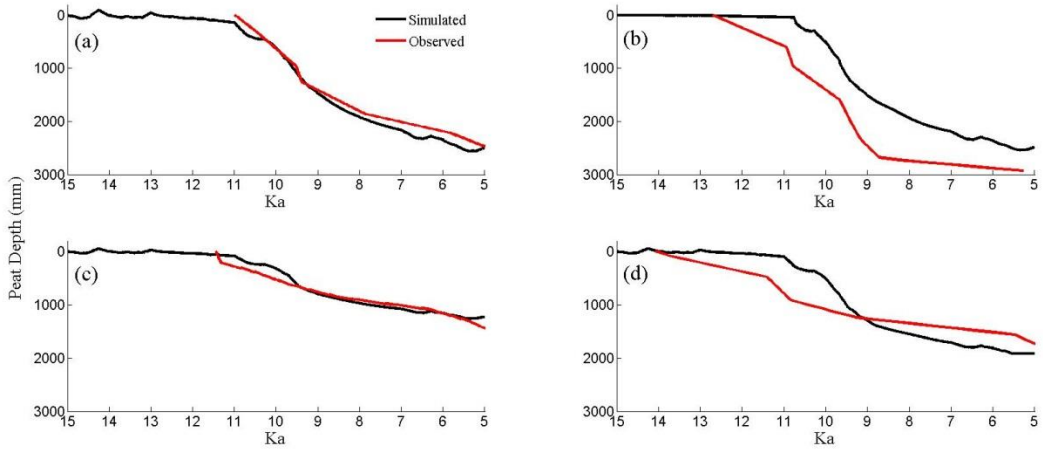

Figure 2.10. Comparisons between simulated and observed peatland depth profile: (a) No Name Creek; (b) Horse Trail Fen; (c) Kenai Gasfield; and (d) Swanson Fen.

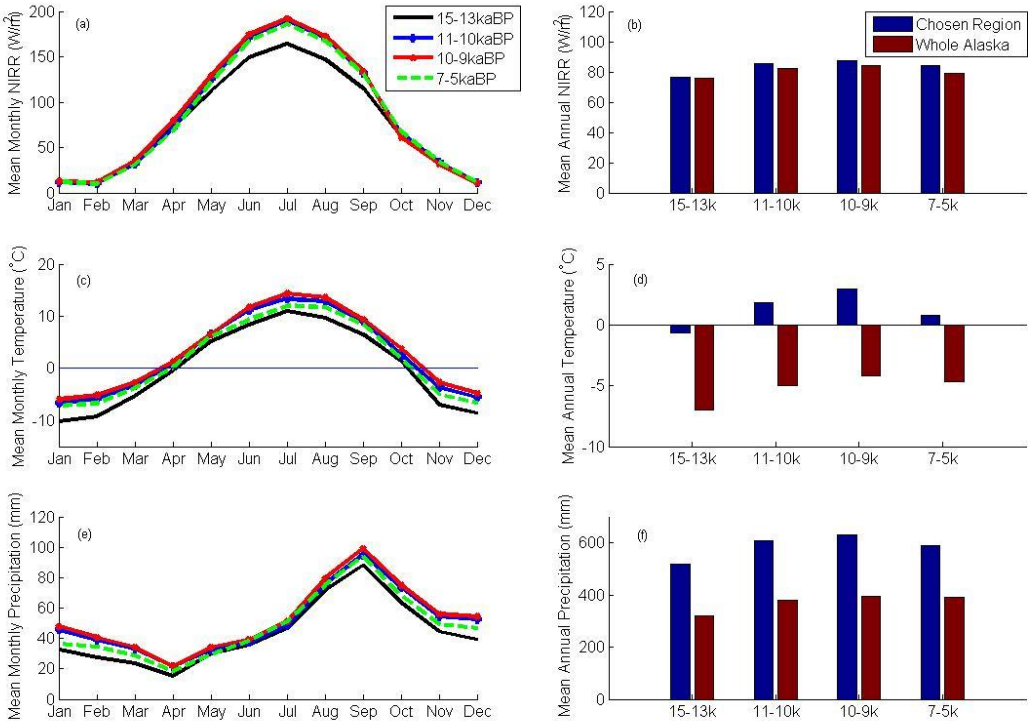

Figure 2.11. Climate data output from the paleoclimate simulations during the post-glacial period (15-13, 11-10, 10-9, and 7-5 ka): (a) Mean monthly and (b) mean annual net incoming solar radiation (NIRR) of the whole of Alaska and the chosen pixels; (c) mean monthly and (d) mean annual temperature of the whole of Alaska and the chosen pixels; (e) mean monthly and (f) mean annual precipitation of the whole of Alaska and the chosen pixels.

Table 2.8. Analysis of variance table of the forward stepwise linear regression between carbon accumulation rates (response) and climate variables (predictors).

Variables [a]	F value	R^2
temp	456.14	0.37
NIRR_season	223.86	0.18
temp_season	27.26	0.02
temp×prec	24.93	0.019
prec	8.45	0.007

[a] Temperature (temp) and net incoming solar radiation (NIRR) are annual means, precipitation (prec) is annual total. Seasonality of nirr (NIRR_season) and temperature (temp_season) are the annual differences between averages of JJA and DJF.

2.3.3 Model Sensitivity Analysis

Peat carbon accumulation, water-table depth, aerobic respiration in the unsaturated zone, and methane production in the saturated zone, are all affected by varying the lowest water-table boundary (LWB). In the "standard" simulation, the mean water-table depth is 14 cm below soil surface (Figure 2.12(b)), with fluctuation above and below this value. Considering there is a small change of precipitation among all the time slices (less than 20%), there is no apparent change for the mean water-table depth over the simulation period. The simulation under "more saturated" condition after setting the LWB to 22 cm indicates that mean water-table depth increases approximately 5 cm closer to the soil surface, resulting in a slight increase of aerobic respiration in the unsaturated zone (Figure 2.12(d)) and increase of methane production and emission (Figure 2.12(c)). Despite the positively affected decomposition, rising water table still resulted in an increase of carbon accumulation rate by up to 40 g C m^{-2} yr^{-1} during the HTM, which may suggest an overwhelming effect of hydrological condition on NPP rather than decomposition. The lower amount of peat SOC in the early Holocene determines the low aerobic respiration (Figure 2.12(a)). Respiration subsequently increases coincident with increasing SOC. In contrast, water table drops by 3 cm after setting the LWB to 35 cm, which decreases the carbon accumulation rate by up to 20 g C m^{-2} yr^{-1} in the HTM. An overall methane production rate is simulated at approximate 13 g C m^{-2} yr^{-1} during the HTM. The simulated methane emission is 7 g C m^{-2} yr^{-1}, about 60% of the methane production. Assuming that R_{COM}: R_{CH_4} is 5 as indicated previously, we get the ratio (CO_2: CH_4) of the emission rates around 10 under anaerobic conditions after accounting for the oxidized CH_4 (~40% of total CH_4 production) for CO_2 release. We estimate that ~78 g C m^{-2} yr^{-1} CO_2 is released via anaerobic respiration, which

is ~26% of the aerobic CO_2 production (including CO_2 production from CH_4 oxidation) during the HTM (Figure 2.12(d)). This is consistent with observed 24% in Glatzel et al. (2004).

At open fen site, when LAI is 0.4, the mean water-table depth is at approximately 14 cm (Figure 2.13(b)). Under partly forested fen condition with LAI of 2.8, the mean water-table depth slightly decreases as the interception of precipitation increases and more water is evaporated. The decreasing water-table position enhances aerobic respiration, leading to a slight decrease in peat SOC accumulation over the Holocene (Figures 2.13(a) and (d)). In forested peatland with LAI of 5.0, the interception of precipitation continues to increase, making the mean water-table depth decrease from 14 cm to 16 cm, resulting in a decrease in peat SOC accumulation. However, the effect of LAI may not be as significant as LWB on the long-term peat SOC accumulation.

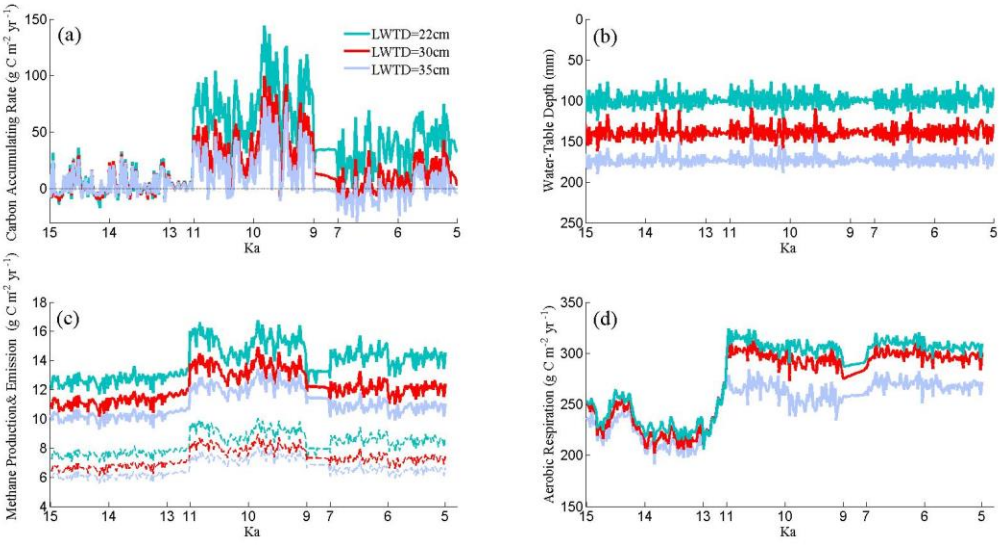

Figure 2.12. Sensitivity test of the lowest water-table depth/ boundary (LWTD/ LWB) effect on peatland dynamics: The lowest water-table depth was set to 22cm, 30cm and 35cm below the peat surface, while other variables remained constant. 20 years average of: (a) SOC accumulation rate, (b) water-table depth, (c) methane production (solid) and emission (dash), (d) aerobic respiration.

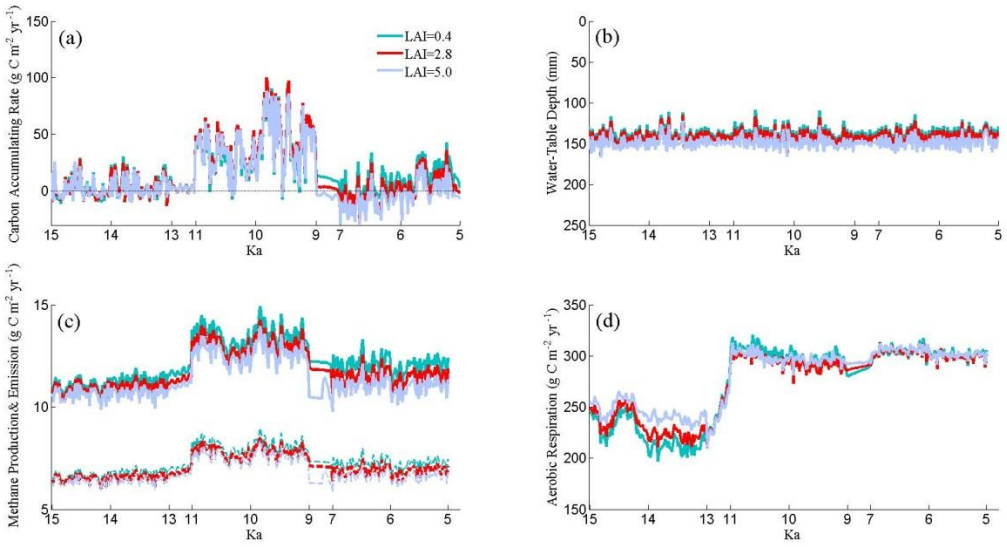

Figure 2.13. Sensitivity test of LAI effects on peatland dynamics. The parameters for LAI were changed to make LAI equal to 0.4 (open fen), 2.8 (partially forested peatland), 5.0 (forested peatland), while other variables remained constant. Clockwise: 20 years average of: (a) SOC accumulation rate, (b) water-table depth, (c) methane production (solid) and emission (dash), (d) aerobic respiration.

2.4 Conclusions

We develop a peatland ecosystem model to quantify long-term peat carbon accumulation rates in Alaska during the Holocene. The model is evaluated with observational data of soil moisture, water-table depth, soil temperature profile, methane and carbon fluxes and pools. The model is then applied to four Alaskan peatlands on the Kenai Peninsula. The model estimates well the peat carbon accumulation rate and peat depths throughout the Holocene. The average carbon accumulation rate is 10.82 g C m^{-2} yr^{-1}, while the rate of the HTM is 35.9 g C m^{-2} yr^{-1}, which is up to six times higher than the rest of the Holocene (6.5 g C m^{-2} yr^{-1}). Simulations are consistent with observational data. The warming event in the HTM characterized by increased summer temperatures and increased seasonality of solar radiation, along with the wetter-than-before conditions, might have played an important role in determining the carbon accumulation rate. From the sensitivity analysis, we identify that initial

water-table depth and vegetation canopy are major drivers of carbon accumulation. We plan to use the developed peatland model to quantify regional peat carbon accumulations under changing climate conditions when it is parameterized for various peatland ecosystems.

Acknowledgment. We appreciate the insightful and constructive comments from two anonymous reviewers. We acknowledge the funding support from a NSF project IIS-1027955 and a DOE project DE-SC0008092. We also acknowledge the SPRUCE project to allow us use its data. We also appreciate the comments and suggestions from Paul J. Hanson to this study. The model driving data (forcing data) presented in this paper are publicly accessible: ECBilt-CLIO Paleo-simulation (http://apdrc.soest.hawaii.edu/datadoc/sim2bl.php), CRU2.0 (http://www.cru.uea.ac.uk/data).

CHAPTER 3. QUANTIFYING SOIL CARBON ACCUMULATION IN ALASKAN TERRESTRIAL ECOSYSTEMS DURING THE LAST 15,000 YEARS[2]

3.1 Introduction

Global surface air temperature has been increasing since the middle of the 19th century (Jones and Mogberg, 2003; Manabe and Wetherald, 1980, 1986). Since 1970, the warming trend has accelerated at a rate of 0.35 ℃ per decade in northern high latitudes (Euskirchen et al., 2007; McGuire et al., 2009). It is projected that the warming will continue in the next 100 years (Arctic Climate Impact Assessment 2005; Intergovernmental Panel on Climate Change (IPCC), 2013, 2014). The land surface in northern high latitudes (>45° N) occupies 22% of the global surface and stores over 40% of the global soil organic carbon (SOC) (McGuire et al., 1995; Melillo et al., 1995; McGuire and Hobbie, 1997). Specifically, the northern high latitudes were estimated to store 200-600 Pg C (1 Pg C = 10^{15} g C) in peatland soils depending on the depth considered (Gorham, 1990, 1991; Yu, 2012), 750 Pg C in non-peatland soils (within 3 m) (Schuur et al., 2008; Tarnocai et al., 2009; Hugelius et al., 2014), and additional 400 Pg C in frozen loess deposits of Siberia (Zimov et al., 2006a). Peatland area is around 40 million hectares in Alaska compared with total 350 million hectares in northern high latitudes (Kivinen and Pakarinen, 1981). Alaskan peatlands account for the most peatland area in the USA and cover at least 8% of the total land area (Bridgham et al., 2006). To date, the regional soil C and its responses to the climate change are still with large uncertainties (McGuire et al., 2009; Loisel et al., 2014).

[2]**Wang, S**., Zhuang, Q., and Yu, Z.: Quantifying soil carbon accumulation in Alaskan terrestrial ecosystems during the last 15 000 years, Biogeosciences, 13, 6305-6319, doi:10.5194/bg-13-6305-2016, 2016.

The warming climate could increase C input to soils as litters through stimulating plant net primary productivity (NPP) (Loisel et al., 2012). However, it can also decrease the SOC by increasing soil respiration (Yu et al., 2009). Warming can also draw down the water table in peatlands by increasing evapotranspiration, resulting in higher decomposition as the aerobic respiration has a higher rate than anaerobic respiration in general (Hobbie et al., 2000). SOC accumulates where the rate of soil C input is higher than decomposition. The variation of climate may switch the role of soils between a C sink and a C source (Davidson and Janssens, 2006; Davidson et al., 2000; Jobbagy and Jackson, 2000). Unfortunately, due to the data gaps of field-measurement and uncertainties in estimating regional C stock (Yu, 2012), with limited understanding of both peatlands and non-peatlands and their responses to climate change, there is no consensus on the sink and source activities of these ecosystems at northern high latitudes (Frolking et al., 2011; Belyea, 2009; McGuire et al., 2009).

Both observation and model simulation studies have been applied to understand the long-term peat C accumulation in northern high latitudes. Most field estimations are based on series of peat-core samples (Turunen et al., 2002; Roulet et al., 2007; Yu et al., 2009; Tarnocai et al., 2009). However, those core analyses may not be adequate for estimating the regional C accumulation due to their limited spatial coverage. To date, a number of model simulations have also been carried out. For instance, Frolking et al. (2010) developed a peatland model considering the effects of plant community, hydrological dynamics and peat properties on SOC accumulation. The simulated results were compared with peat-core data. They further analyzed the contributions of different plant functional types (PFTs) to the peat C accumulation. However, this 1-D model has not been evaluated with respect to soil moisture, water-table depth, methane fluxes, and carbon and nitrogen fluxes and has not been used in large spatial-scale simulations by

considering other environmental factors (e.g., temperature, vapor pressure, and radiation). In contrast, Spahni et al. (2013) used a dynamic global vegetation and land surface process model (LPX), based on LPJ (Sitch et al., 2003), imbedded with a peatland module, which considered the nitrogen feedback on plant productivity (Xu-Ri and Prentice, 2008) and plant biogeography, to simulate the SOC accumulation rates of northern peatlands. However, climatic effects on SOC were not fully explained, presumably due to its inadequate representation of ecosystem processes (Stocker et al., 2011, 2014; Kleinen et al., 2012). The Terrestrial Ecosystem Model (TEM) has been applied to study C and nitrogen dynamics in the Arctic (Zhuang et al., 2001, 2002, 2003, 2015; He et al., 2014). However, the model has not been calibrated and evaluated with peat-core C data, and has not been applied to investigate the regional peatland C dynamics. Building upon these efforts, recently we fully evaluated the peatland version of TEM (P-TEM) including modules of hydrology (HM), soil thermal (STM), C and nitrogen dynamics (CNDM) for both upland and peatland ecosystems (Wang et al., 2016).

Here we used the peatland-core data for various peatland ecosystems to parameterize and test P-TEM (Figure 2.1). The model was then used to quantify soil C accumulation of both peatland and non-peatland ecosystems across the Alaskan landscape since the last deglaciation. This study is among the first to examine the peatlands and non-peatlands C dynamics and their distributions and peat depths using core data at regional scales.

3.2. Methods

3.2.1 Overview

To conduct regional simulations of carbon accumulation for both uplands and peatlands, we first parameterized the P-TEM for representative ecosystems in Alaska. Second, we organized the regional vegetation and peatland distribution data, spatial basal age data for all

peatland grid cells based on site-level soil core data, and climate data for each period during the Holocene. Finally, we conducted the regional simulations and sensitivity analysis.

3.2.2 Model Description

See Section 2.2.2 and Wang et al. (2016a, 2016b) for model details.

3.2.3 Model Parameterization

We have parameterized the key parameters of the individual modules including HM, STM, and MDM in Wang et al. (2016). The parameters in CNDM for upland soils and vegetation have been optimized in the previous studies (Zhuang et al 2002, 2003; Tang and Zhuang 2008). Here we parameterized P-TEM for peatland ecosystems using data from a moderate rich *Sphagnum* spp. open fen (APEXCON) and a *Sphagnum*-black spruce (*Picea mariana*) bog (APEXPER) (Table 3.1). Both are located in the Alaskan Peatland Experiment (APEX) study area, where *Picea mariana* is the only tree species above breast height in APEXPER. Three water table position manipulations were established in APEX including a control, a lowered, and a raised water table plots (Chivers et al., 2009; Turetsky et al., 2008; Kane et al., 2010; Churchill et al., 2011). The annual NPP and aboveground biomass at both sites have been measured in 2009. There were no belowground observations at APEX, however at a Canadian peatland, Mer Bleue (Moore et al., 2002), with *Sphagnum* spp. bog (shrubs and *Sphagnum*) and pool fen (sedges and herbs and *Sphagnum*). The belowground biomass was also observed at Suurisuo mire complex, southern Finland, a sedge fen site dominated by *Carex rostrate* (Saarinen et al., 1992). We used the ratio (70%) of belowground biomass to total biomass from these two study sites to calculate the missing belowground biomass values at APEXCON and APEXPER (Table 3.2). We conducted 100,000 Monte Carlo ensemble simulations to calibrate the model for each site using a Bayesian approach

and parameter values with the modes in their posterior distributions were selected (Tang and Zhuang, 2008, 2009).

3.2.4 Regional Model Input Data

The Alaskan C stock was simulated through the Holocene driven with vegetation data reconstructed for four time periods including a time period encompassing a millennial-scale warming event during the last deglaciation known as the BØlling-AllerØd at 15-11 ka (1 ka = 1000 cal yr Before Present), HTM during the early Holocene at 11-10 and 10-9 ka, and the mid- (9-5 ka) and late- Holocene (5 ka-1900 AD) (He et al., 2014). We used the modern vegetation distribution for the simulation during the period 1900-2000 AD (Figure 3.1). We assumed that the vegetation distribution remained static within each corresponding time period. Upland ecosystems were classified into boreal deciduous broadleaf forest, boreal evergreen needleleaf and mixed forest, alpine tundra, wet tundra; and barren lands (Table 3.3). By using the same vegetation distribution map, we reclassified the upland ecosystems into two peatland types including *Sphagnum* spp. poor fens (SP) dominated by tundra and *Sphagnum* spp.-black spruce (*Picea mariana*) bog/ peatland (SBP) dominated by forest ecosystems (Table 3.3).

Upland and peatland ecosystem distribution for each grid cell was determined using the wetland inundation data extracted from the NASA/ GISS global natural wetland dataset (Matthews and Fung, 1987). The resolution was resampled to $0.5° \times 0.5°$ from $1° \times 1°$. Given the same topography of Alaska during the Holocene, we assumed that the wetland distribution kept the same throughout the Holocene. The inundation fraction was assumed to be the same within each grid through time and the land grids not covered by peatland were treated as uplands. We calculated the total area of modern Alaskan peatlands to be 302,410 km^2, which was within the range from 132,000 km^2 (Bridgham et al., 2006) to 596,000 km^2 (Kivinen and Pakarinen,

1981). The soil water pH data were extracted from Carter and Scholes (2000), and the elevation data were derived from Zhuang et al. (2007).

Our regional simulations considered the effects of basal ages on carbon accumulation. To obtain the spatially explicit basal age data for all peatlands grid cells, we first categorized the observed basal ages of peat samples from Gorham et al. (2012) into different time periods including 15-11 ka, 11-10 ka, 10-9 ka, and 9 ka-19th (Figure 3.1). For each time period, the areas dominated with different vegetation types were assigned with varying peatland basal ages. To do that, we examined the association of the field-measured peat basal ages and the reconstructed vegetation types from peat core data. For instance, we found that peatland initiations during 15-11 ka occurred in the regions that were dominated by alpine tundra at south, northwestern, and southeastern coast. We thus assign the different peatland basal ages for the grid cells according to their vegetation types for each time slice (Table 3.4).

Climate data were from ECBilt-CLIO model output (Timm and Timmermann, 2007) to minimize the difference from CRU data (He et al., 2014). Climate fields include monthly precipitation, monthly air temperature, monthly net incoming solar radiation, and monthly vapor pressure at resolution of $2.5° \times 2.5°$. We used the same time-dependent forcing atmospheric carbon dioxide concentration data for model input as were used in ECBilt-CLIO transient simulations from the Taylor Dome (Timm and Timmermann, 2007). The historical climate data used for the simulation through the 20th century were monthly CRU2.0 data (Mitchell et al., 2004).

3.2.5 Simulations and Sensitivity Test

Simulations for pixels located on the Kenai Peninsula from 15 to 5 ka were first conducted with the parameterized model. The peat-core data from four peatlands on the Kenai Peninsula, Alaska (Jones and Yu, 2010; Yu et al., 2010) (Table 5, also see Table 3 in Wang et al. (2016)) were used to compare with the simulations. The observed data include the peat depth, bulk density of both organic and inorganic matters at 1-cm interval, and age determinations. The simulated C accumulation rates represent the actual ("true") rates at different times in the past. However, the calculated accumulation rates from peat cores are considered as "apparent" accumulation rates, as peat would continue to decompose since the time of formation until present when the measurement was made (Yu, 2012). To facilitate comparison between simulated and observed accumulation rates, we converted the simulated "true" accumulation rates to "apparent" rates, following the approach by Spahni et al. (2013). That is, we summed the annual net C accumulation over each 500-year interval and deducted the total amount of C decomposition (equivalent to heterotrophic respiration in the model) from that time period, then dividing by 500 years.

Second, we conducted a transient regional simulation driven with monthly climatic data (Figure 3.2) from 15 ka to 2000 AD. The simulation was conducted assuming all grid cells were taken up by upland ecosystems to get the upland soil C spatial distributions during different time periods. We then conducted the second simulation assuming all grid cells were dominated by peatland ecosystems following Table 3 to obtain the distributions of peat SOC accumulation. Finally, we used the inundation fraction map to extract both uplands and peatlands and estimated the corresponding SOC stocks within each grid, which were then summed up to represent the Alaskan SOC stock. We also used the observed mean C content of 46.8% in peat mass and bulk

density of 166 ± 76 kg m^{-3} in Alaska (Loisel et al., 2014) to estimate peat depth distribution from the simulated peat SOC density (kg C m^{-2}).

Third, we conducted a series of extra simulations to further examine how uncertain climates and vegetation distribution affect our results. We used the original forcing data as the standard scenario and the warmer (monthly temperature $+5℃$) and cooler ($-5℃$) as other two scenarios while keeping the rest forcing data unchanged. Similarly, we used the original forcing data as the standard scenario and the wetter (monthly precipitation $+10$ mm) and drier (-10 mm) to test the effect from precipitation. To further study if vegetation distribution has stronger effects on SOC accumulation than climate in Alaska, we simply replaced *Sphagnum* spp.-black spruce (*Picea mariana*) bog/ peatland (SBP) with *Sphagnum* spp. poor fens (SP) and replaced the upland forests with tundra at the beginning of 15 ka. We then conducted the simulation under "warmer" and "wetter" conditions simultaneously as described before while keeping the vegetation distribution unchanged.

Table 3.1. Description of sites and variables used for parameterizing the core carbon and nitrogen module (CNDM).

Site[a]	Vegetation	Observed variables for CNDM parameterization	References
APEXCON	Moderate rich open fen with sedges (*Carex* sp.), spiked rushes (*Eleocharis* sp.), *Sphagnum* spp., and brown mosses (e.g., *Drepanocladus aduncus*)	Mean annual aboveground NPP in 2009; Mean annual belowground NPP in 2009; Aboveground biomass in 2009	Turetsky et al. (2008); Chivers et al. (2009); Kane et al. (2010)
APEXPER	Peat plateau bog with black spruce (*Picea mariana*), *Sphagnum* spp., and feather mosses		Churchill et al. (2011)

[a]The Alaskan Peatland Experiment (APEX) site is adjacent to the Bonanza Creek Experimental Forest (BCEF) site, approximately 35 km southwest of Fairbanks, AK. The area is classified as continental boreal climate with a mean annual temperature of -2.9℃ and annual precipitation of 269 mm, of which 30% is snow (Hinzman et al., 2006).

Table 3.2. Carbon pools and fluxes used for calibration of CMDM.

Annual Carbon Fluxes or Pools[a]	*Sphagnum* Open Fen		*Sphagnum*-Black Spruce Bog		References
	Observation	Simulation	Observation	Simulation	
NPP	445±260	410	433±107	390	Kuhry and Vitt (1996) Saarinen et al. (1996) Moore et al. (2002) Zhuang et al. (2002) Turetsky et al. (2008) Tarnocai et al. (2009) Churchill (2011)
Aboveground Vegetation Carbon	149-287		423		
Belowground Vegetation Carbon	347-669		987		
Total Vegetation Carbon Density	496-856	800	1410	1300	
Litter Fall Carbon Flux	300	333	300	290	
Methane Emission Flux	19.5	19.2	9.7	12.8	

[a] Units for annual net primary production (NPP) and litter fall carbon are $g\ C\ m^{-2}\ yr^{-1}$. Units for vegetation carbon density are $g\ C\ m^{-2}$. Units for Methane emissions are $g\ C-CH_4\ m^{-2}\ yr^{-1}$. The simulated total annual methane fluxes were compared with the observations at APEXCON in 2005 and SPRUCE in 2012. A ratio of 0.47 was used to convert vegetation biomass to carbon (Raich 1991).

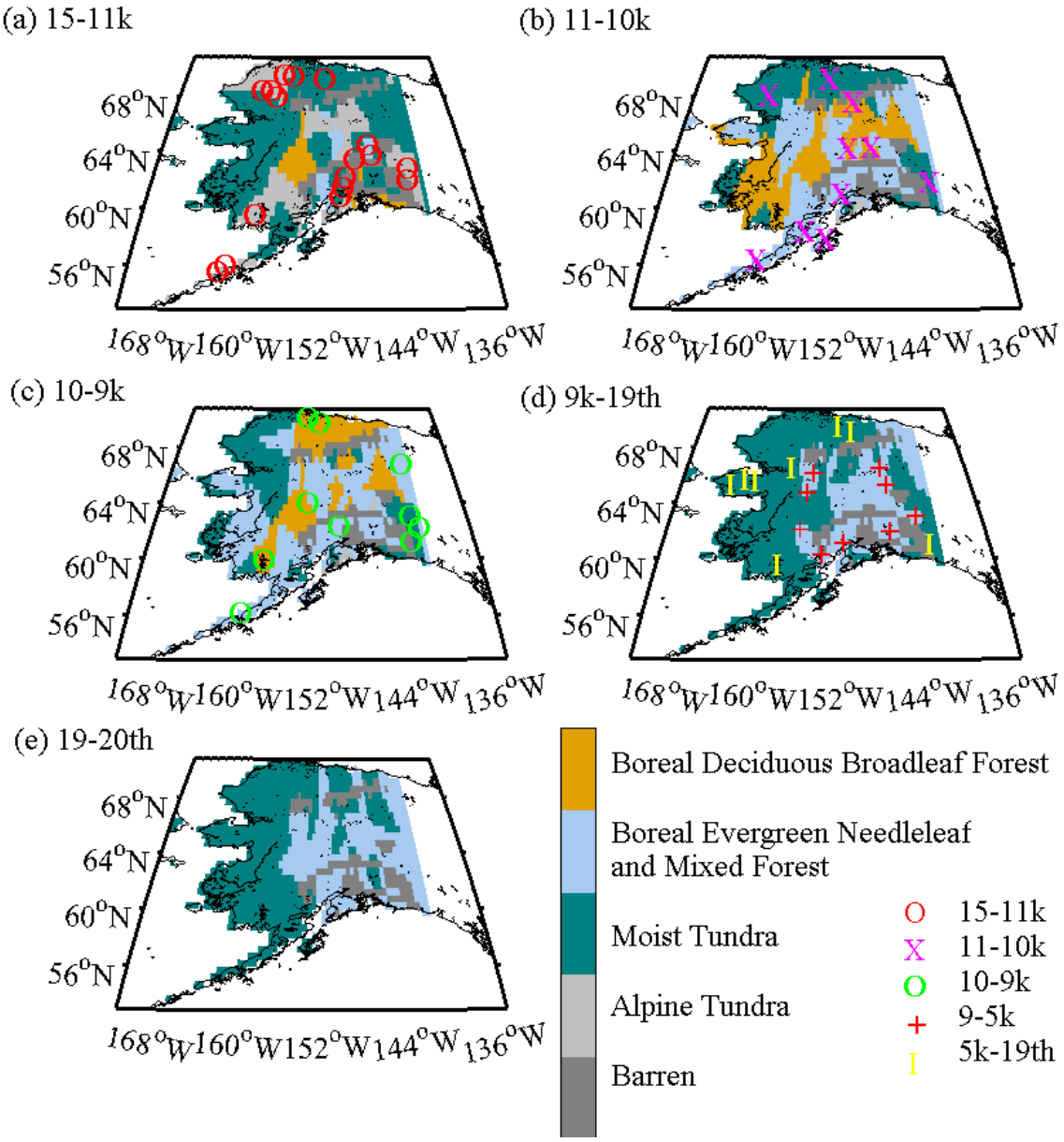

Figure 3.1. Alaskan vegetation distribution maps reconstructed from fossil pollen data during (a) 15-11 ka, (b) 11-10 ka, (c) 10-9 ka, (d) 9 ka -1900 AD, and (e) 1900-2000 AD (He et al., 2014). Symbols represent the basal age of peat samples ($n = 102$) in Gorham et al. (2012). Each symbol indicates 1-3 peat samples in the map. Peat samples with basal age 9-5k and 5k-19th are shown in map (d) as there is no change of vegetation distribution during 9k-19th. Barren refers to mountain range and large water body areas that can not be interpolated.

Table 3.3. Assignment of biomized fossil pollen data to the vegetation types in TEM (He et al., 2014).

TEM upland vegetation	TEM peatland vegetation	BIOMISE code
Alpine tundra		CUSH DRYT PROS
Moist tundra	*Sphagnum* spp. open fen	DWAR SHRU
Boreal evergreen needleleaf and mixed forest	*Sphagnum*-black spruce bog	TAIG COCO CLMX COMX
Boreal deciduous broadleaf forest		CLDE

Table 3.4. Relations between peatland basal age and vegetation distribution.

Peatland basal age	Vegetation types	Location in Alaska
15-11 ka	alpine tundra	south, northwestern, and southeastern coast
11-10 ka	moist tundra	south, north,
	boreal evergreen needleleaf forest	and southeastern coast
	boreal deciduous broadleaf forest	east central part
10-9 ka	moist tundra	south and north coast
	boreal evergreen needleleaf forest	central part
	boreal deciduous broadleaf forest	
9-5 ka	moist tundra	central part
	boreal evergreen needleleaf forest	
5 ka-1900 AD	moist tundra	west coast
	boreal evergreen needleleaf forest	

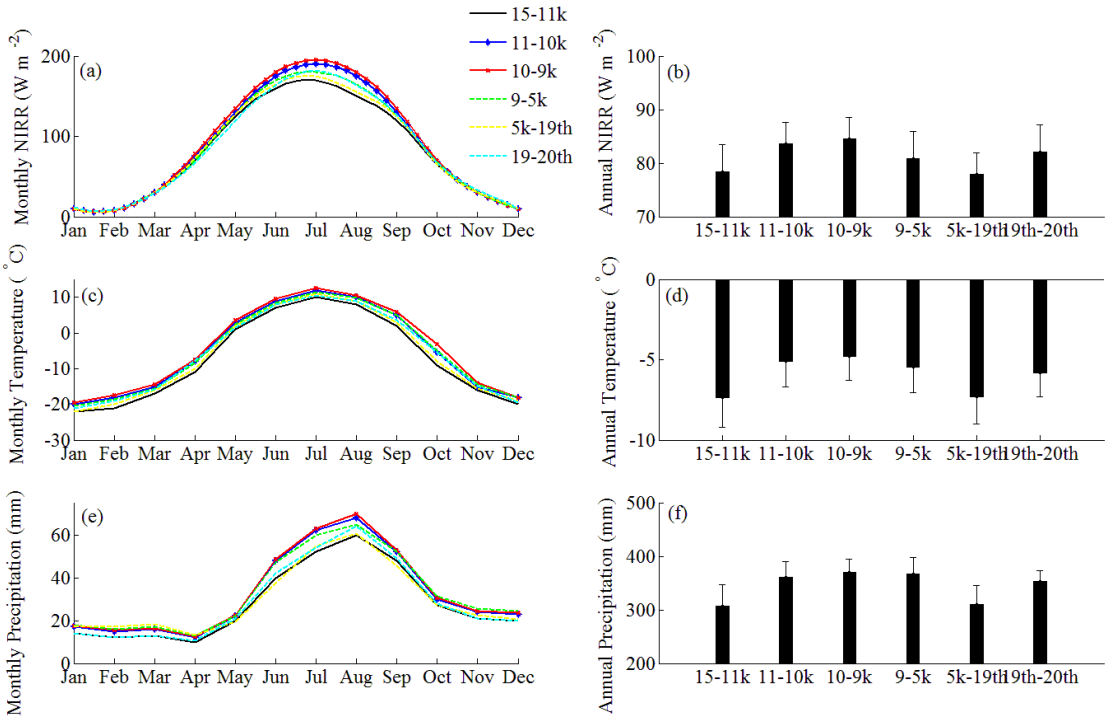

Figure 3.2. Simulated Paleo-climate and other input data from 15 ka to 2000 AD: (a) mean monthly and (b) mean annual net incoming solar radiation (NIRR, $W\ m^{-2}$), (c) mean monthly and (d) mean annual air temperature (℃), (e) mean monthly, and (f) mean annual precipitation (mm) (Timm and Timmermann, 2007; He et al., 2014).

3.3 Results and Discussion

3.3.1 Simulated Peatland Carbon Accumulation Rates at Site Level

Our paleo simulations showed a large peak of peat C accumulation rates at 11-9 ka during the HTM (Figure 3.3). The simulated "true" and "apparent" rates captured this primary feature in peat-core data at almost all sites (Jones and Yu, 2010; See Wang e al. (2016) Table 3 for sites details). We simulated an average of peat SOC "apparent" accumulation rate of 11.4 g C m^{-2} yr^{-1} from 15 to 5 ka, which was slightly higher than the observations at four sites (10.45 g C m^{-2} yr^{-1}). The simulated rate during the HTM was 26.5 g C m^{-2} yr^{-1}, up to five times higher than the rest of the Holocene (5.04 g C m^{-2} yr^{-1}). This corresponded to the observed average rate of 20 C m^{-2} yr^{-1} from 11.5 to 8.6 ka, which is, four times higher than 5 C m^{-2} yr^{-1} over the rest of the Holocene.

3.3.2 Vegetation Carbon

Model simulations showed an overall low vegetation C before the HTM (15-11 ka) (Figure 3.4a), paralleled to the relatively low annual and long-term NPP (Figures 5b and c). The lowest amount of C (~0.8 kg C m^{-2}) was stored in *Sphagnum*-dominated peatland. *Sphagnum*-black spruce peatland also had low vegetation C density (~1 kg C m^{-2}). Upland vegetation showed a generally higher C storage, among which boreal evergreen needleleaf forest ranked the first (~2 kg C m^{-2}). Highest NPP accompanied by highest vegetation carbon appeared during the HTM (11-9 ka) (Figures 3.4a and b). Lower annual C uptake along with lower C was found during mid- and late- Holocene (9 ka-19th), where peatland ecosystems exhibited the most obvious drops (Figures 3.4a and b).

In general, vegetation held about 2 Pg C before the HTM (Figure 3.5). Vegetation C in upland tundra ecosystems accounted for the most amount of total vegetation C. During the HTM,

Boreal evergreen needleleaf forest reached its highest and had an overwhelming proportion of total C. Similarly, a peak of total vegetation C appeared at the same time, averaging around 4.3 Pg C. Large decrease occurred at the mid-Holocene and a slight decline continued till the late-Holocene. We estimated a total 2.9 Pg C stored in modern Alaskan vegetation, with 0.4 Pg in peatlands and 2.5 Pg in non-peatlands. The uncertainties during the model calibration (Table 3.2) resulted in 0.3-0.6 Pg C and 2.2-3.1 Pg C in peatlands (see Wang et al. (2016) for model parameters) and non-peatland vegetation (see Tang and Zhuang (2008) for uncertainty analyses for upland vegetation), respectively. Our estimation of 2.5-3.7 Pg C stored in the Alaskan vegetation was lower than the previous estimate of 5 Pg (Balshi et al., 2007; McGuire et al., 2009), presumably due to the prior ranges of model parameters used from Tang and Zhuang (2008). Our overestimation of peatland area may also lead to a reduction of Alaskan non-peatland area.

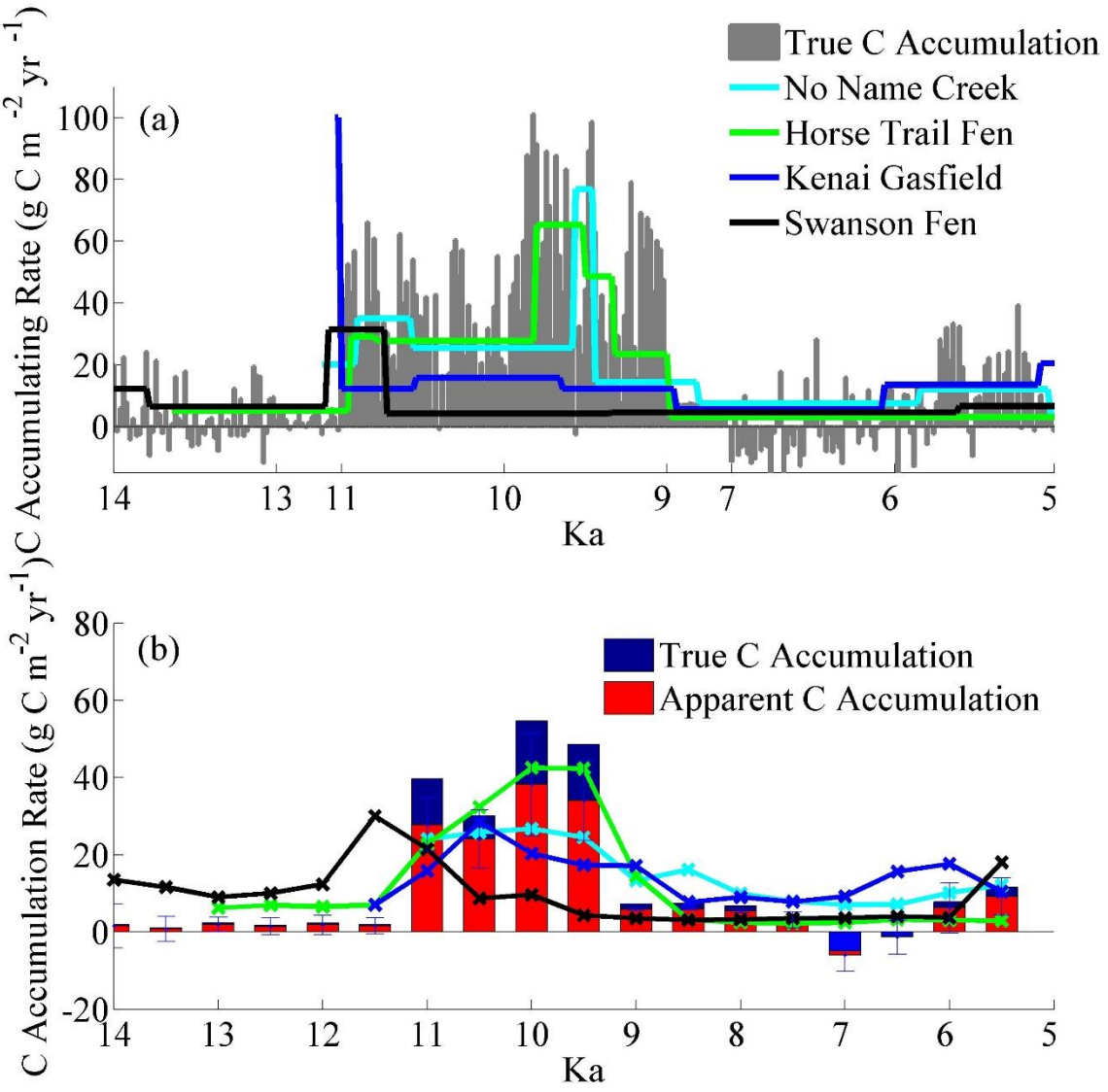

Figure 3.3. Simulated and observed carbon accumulation rates from 15 ka to 5 ka in 20-yr bins (a) and 500-yr bins with standard deviation (b) for No Name Creek, Horse Trail Fen, Kenai Gasfield, and Swanson Fen. Peat-core data were from Jones and Yu (2010).

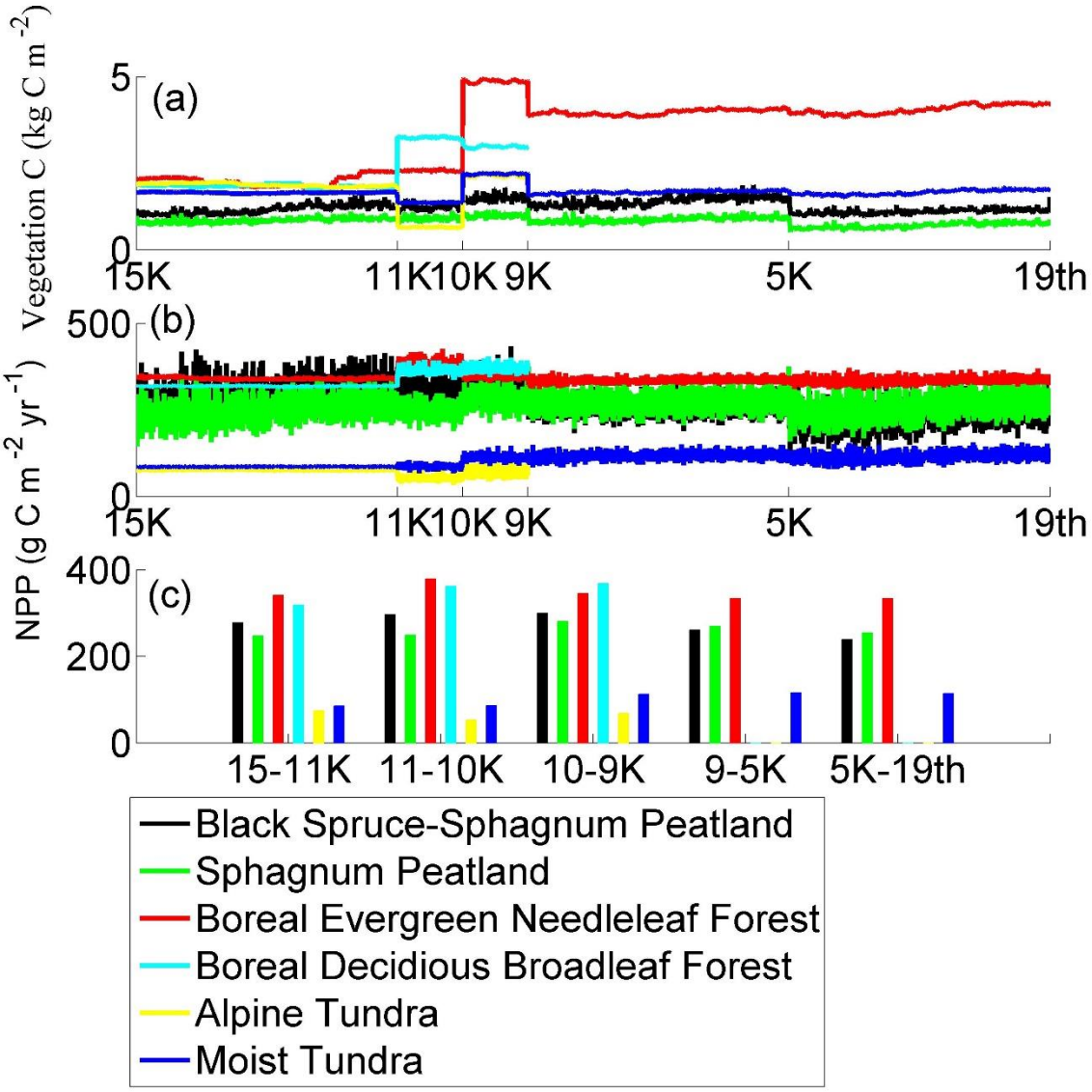

Figure 3.4. Simulated (a) mean vegetation carbon density (k$g\ C\ m^{-2}$) of different vegetation types, (b) annual NPP ($g\ C\ m^{-2}yr^{-1}$), and (c) long-term NPP ($g\ C\ m^{-2}yr^{-1}$).

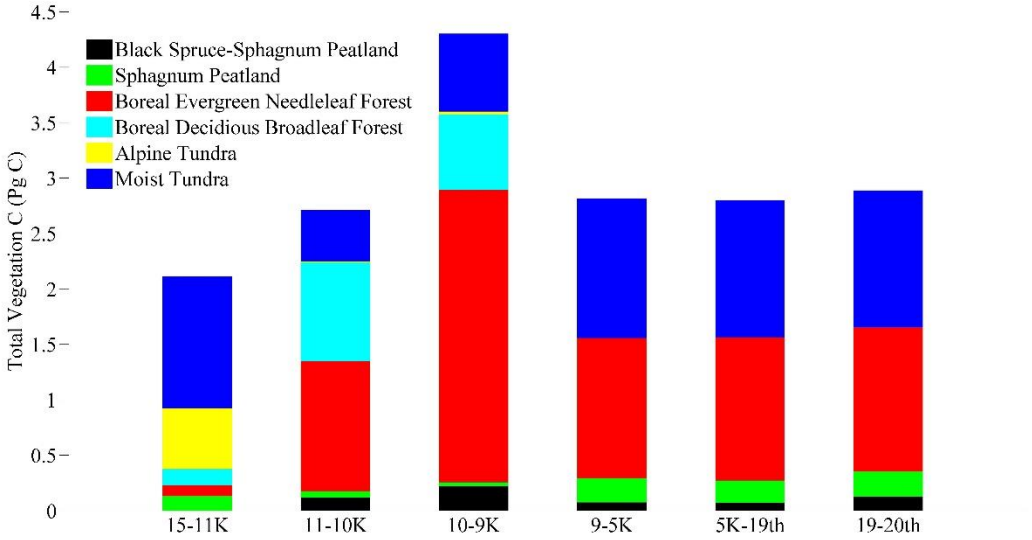

Figure 3.5. Total C (Pg C) stored in Alaskan vegetation for different time periods. Note no Boreal Deciduous Broadleef Forest after 9K.

3.3.3 Soil Carbon

Carbon storage in Alaskan non-peatland soils varied spatially (Figure 3.6). Moist tundra had the highest SOC density (12-25 kg C m^{-2}), followed by deciduous broadleaf forest (8-13 kg C m^{-2}) and evergreen needleleaf forest (3-8 kg C m^{-2}) through all time slices between 15 ka and 2000 AD. Dramatic changes of vegetation types have occurred in Alaska during different periods (Figure 3.1). Before the HTM (15-11 ka), the terrestrial ecosystem was dominated by tundra. Northwestern coast and eastern interior was covered by moist tundra. Southwestern Alaska and the interior south of the Brooks Range were dominated by alpine tundra (Figure 3.1a). The basal ages of peat samples from Gorham et al. (2012) suggested that peatlands were likely to form from the (alpine) tundra ecosystems, although patches of boreal deciduous broadleaf forest and boreal evergreen needleleaf and mixed forest appeared at the north of the Alaska Range. Initially, only *Sphagnum* open peatland (SP) existed, with less C (<10 kg C m^{-2})

sequestrated in the southeastern Brooks Range in comparison with southwestern and northwestern coastal parts (>15 kg C m^{-2}) (Figure 3.7a). Approximately 4.5× 10^5 km^2 area was covered by peatlands at the beginning of the HTM (~11 ka) (Figure 3.8). During the HTM (11-9 ka), boreal deciduous broadleaf and boreal evergreen needleleaf and mixed forests expanded (Figures 3.7b and c). Coastal tundra (moist wet tundra) covered north of the Brooks Range between 11 and 10 ka, where SP continued its expansion (Figure 3.7b). *Sphagnum*-black spruce forested peatland began forming in southwestern coast and eastern interior regions, with a rapid increase of total peatland area to about 13× 10^5 km^2 (Figure 3.8). At 10-9 ka, boreal deciduous forest expanded to north of the Brooks Range, making forest the dominant biome in Alaska (Figure 3.1c). Prevailing forest ecosystems indicated a large expansion of peatland, with SBP covering the interior Alaska (Figure 3.7c). During the mid-Holocene (9-5 ka), the terrestrial landscape generally resembled present-day ecosystems (Bigelow et al., 2003). Boreal evergreen needleleaf and mixed forest prevailed in southern and interior Alaska with tundra returned to north of the Brooks Range and western Alaska (Figures 3.1d and e). Although SP kept forming towards west, some areas dominated by SBP in interior Alaska ceased accumulating C (Figure 3.7d). At 5k-19th, almost all the peatlands have formed, with some interior regions exhibiting a C loss (Figure 3.7e). C accumulation increased again in the last century, averaging about 20 kg C m^{-2} kyr^{-1} (Figure 3.7f). We found that the distribution of SOC densities of both upland and peatland varied greatly depending on the vegetation distribution within each time slice, indicating that vegetation composition might be a major factor controlling regional C dynamics.

An average peat SOC "apparent" accumulation rate of 13 g C $m^{-2}yr^{-1}$ (2.3 Tg C yr^{-1} for the entire Alaska) was estimated from 15 ka to 2000 AD (Figure 3.9), lower than 18.6 g C $m^{-2}yr^{-1}$ as estimated from peat cores for northern peatlands (Yu et al., 2010), and slightly

higher than the observed rate of 13.2 g C $m^{-2}yr^{-1}$ from four peatlands in Alaska (Jones and Yu, 2010). A simulated peak occurred during the HTM with the rate 29.1 g C $m^{-2}yr^{-1}$ (5.1 Tg C yr^{-1}), which was slightly higher than the observed 25 g C $m^{-2}yr^{-1}$ for northern peatlands and ~20 g C $m^{-2}yr^{-1}$ for Alaska (Yu et al., 2010). It was almost four times higher than the rate 6.9 g C $m^{-2}yr^{-1}$ (1.4 Tg C yr^{-1}) over the rest of the Holocene, which corresponded to the peat core-based observations of ~5 g C $m^{-2}yr^{-1}$. The mid- and late Holocene showed much slower C accumulation at a rate approximately five folds lower than during the HTM. This corresponded to the observation of a six-fold decrease in the rate of new peatland formation after 8.6 ka (Jones and Yu 2010). The C accumulation rates increased abruptly to 39.2 g C $m^{-2}yr^{-1}$during the last century, within the field-measured average apparent rate range of 20-50 g C $m^{-2}yr^{-1}$ over the last 2000 years (Yu et al., 2010).

The SOC stock of northern peatlands has been estimated in many studies, ranging from 210 to 621 Pg (Oechel 1989; Gorham 1991; Armentano and Menges, 1986; Turunen et al., 2002; Yu et al., 2010; see Yu 2012 for a review). Assuming Alaskan peatlands were representative of northern peatlands and using the area of Alaskan peatlands (0.45×10^6 km^2; Kivinen and Pakarinen, 1981) divided by the total area of northern peatlnads (~4×10^6 km^2; Maltby and Immirzi 1993), we estimated a SOC stock of 23.6-69.9 Pg C for Alaskan peatlands. Our model estimated 27-48 Pg C (23.9 Pg C in SP and 13.5 Pg C in SBP) had been accumulated from 15 ka to 2000 AD (Figure 3.10), due to uncertain parameters (Table 3.2, see Wang et al. (2016) for model parameters). The uncertainty can also be resulted from peat basal age distributions and the estimation of total peatland area using modern inundation data as discussed above. By incorporating the observed basal age distribution to determine the expansion of peatland through time, we estimated that approximately 68% of Alaskan peatlands had formed by the end of the

HTM, similar to the estimation from observed basal peat ages that 75% peatlands have formed by 8.6 ka (Jones and Yu 2010).

The northern circumpolar soils were estimated to cover approximately 18.78×10^6 km^2 (Tarnocai et al., 2009). The non-peatland soil C stock was estimated to be in the range of 150-191 Pg C for boreal forests (Apps et al., 1993; Jobbagy and Jackson, 2000), and 60-144 Pg C for tundra in the 0-100 cm depth (Apps et al., 1993; Gilmanov and Oechel, 1995; Oechel et al., 1993). 1.24×10^6 km^2 non-peatland area was estimated from the total land area of Alaska (1.69×10^6 km^2). Therefore, Alaska non-peatland soil contained 17-27 Pg C by using the ratio of Alaskan over northern non-peatland. In comparison, we modeled 9-15 Pg C (within 1-meter depth), depending on the prior ranges of model parameters from Tang and Zhuang (2008).

The simulated modern SOC distribution (Figure 3.11c) was largely consistent with the study of Hugelius et al. (2014) (see Figure 3 in the paper). The model captured the SOC density on northern and southwestern coasts of Alaska with most grids >40 kg C m^{-2} on average. Those regions also showed high SOC density (>75 kg C m^{-2}), which was also exhibited in our result. East part and west coast had the lowest SOC densities, corresponding to the simulation result that most grids had SOC values between 20 and 40 kg C m^{-2}. We estimated an average peat depth of 1.9 ± 0.8 m considering the uncertainties within dry bulk densities. It was similar to the observed mean depth of 2.29 m for Alaskan peatlands (Gorham et al., 1991, 2012). Our estimates (Figure 12d) showed a relatively high correlation with the 64 observed peat samples, especially with higher depths (Figure 3.12) ($R^2 = 0.45$). The large intercept of the regression line (101 cm) suggested that the model might have not performed well in estimating the grids with low peat depths (<50 cm). The peat characteristics (e.g., bulk density) from location to location may differ

largely, even if within the same small region. Thus, it is difficult to capture the observed variations of peat depths as we used the averaged bulk density of whole Alaska.

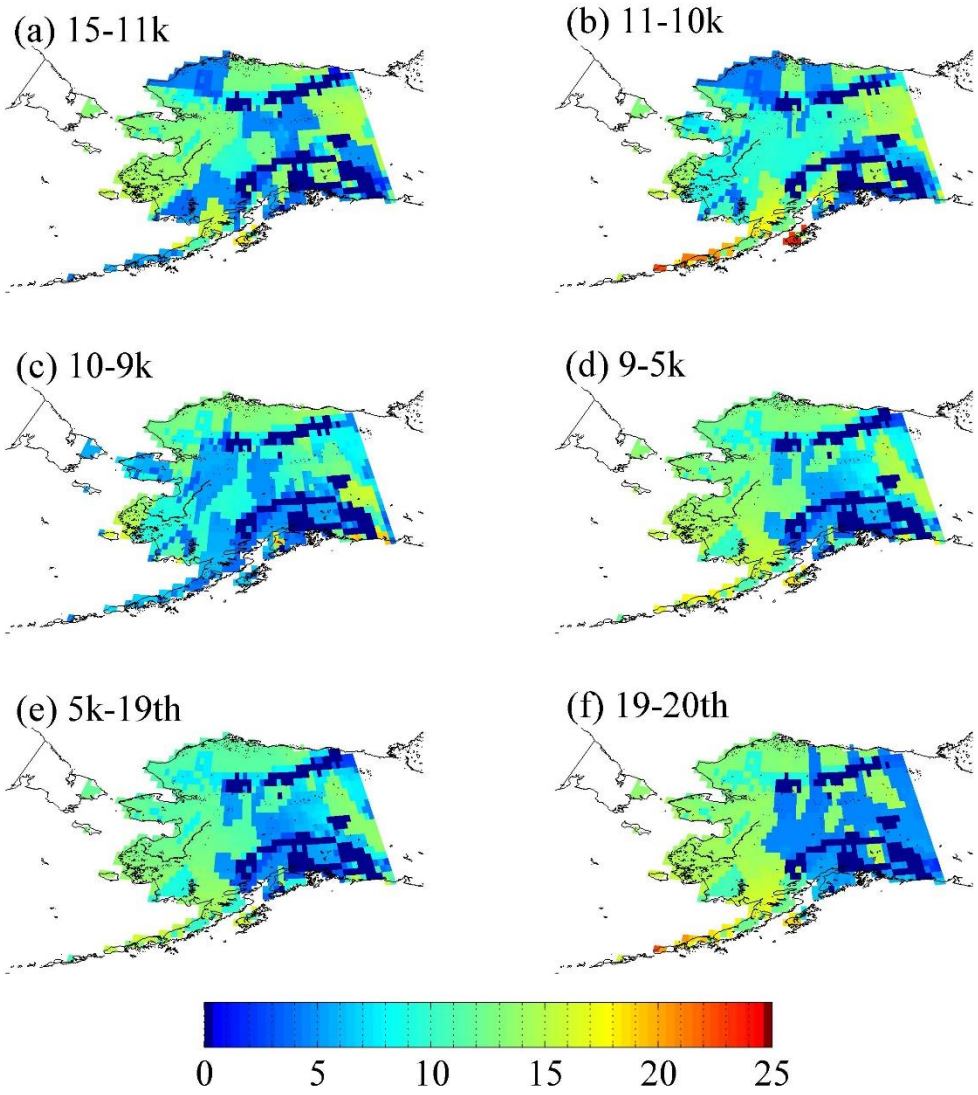

Figure 3.6. Average non-peatland (mineral) SOC density ($kg\ C\ m^{-2}$) during (a) 15-11 ka, (b) 11-10 ka, (c) 10-9 ka, (d) 9-5 ka, (e) 5 ka -1900 AD, and (f) 1900-2000 AD. The period of 9k-19th in Figure 3.1d is separated into 9-5k and 5k-19th.

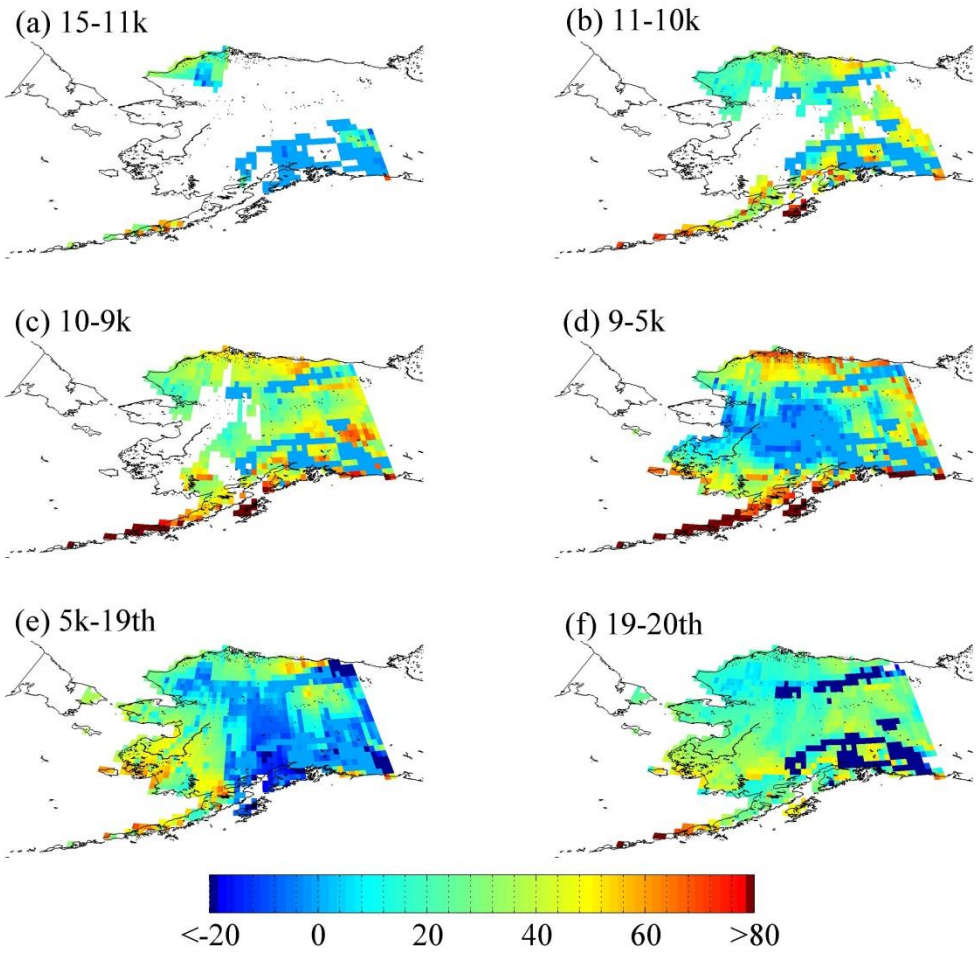

Figure 3.7. Peatland area expansion and peat soil C accumulation per 1000 years ($kg\ C\ m^{-2}\ kyr^{-1}$) during (a) 15-11 ka, (b) 11-10 ka, (c) 10-9 ka, (d) 9-5 ka, (e) 5 ka -1900 AD, and (f) 1900-2000 AD. The amount of C represents the C accumulation as the difference between the peat C amount in the final year and the first year in each time slice. The period of 9k-19th in Figure 2d is separated into 9-5k and 5k-19th.

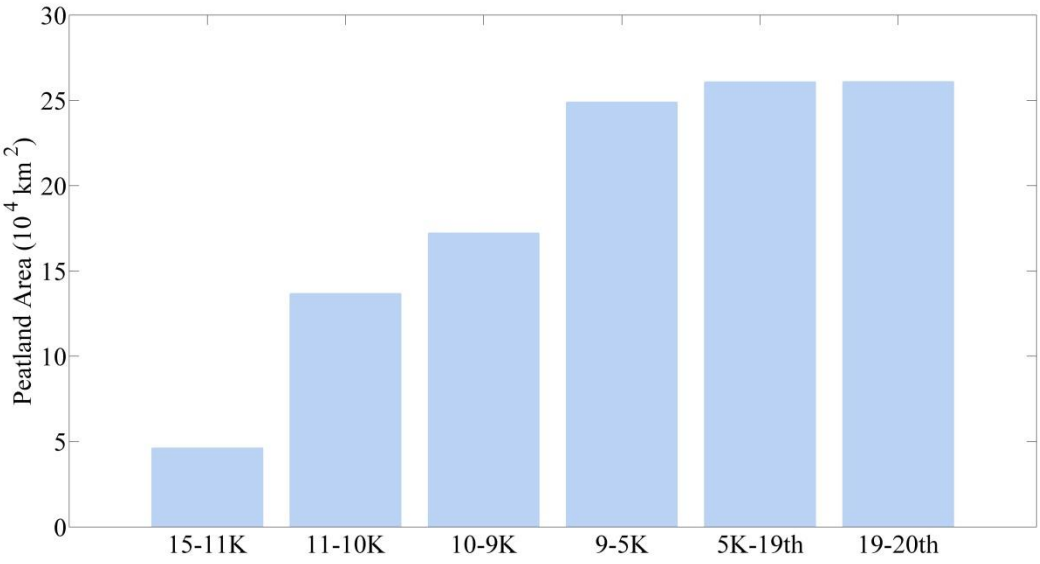

Figure 3.8. Total peatland expansion area ($10^4\ km^2$) in different time slices.

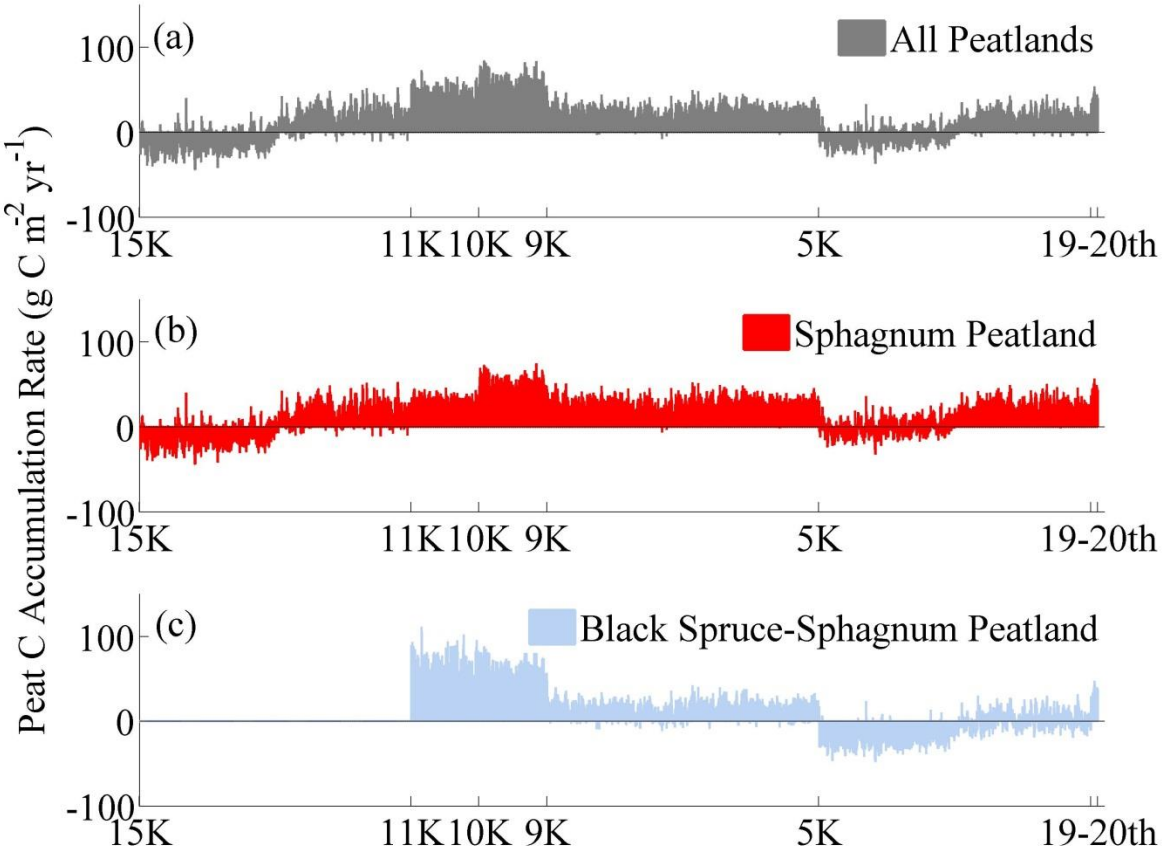

Figure 3.9. Bars of peatland mean C accumulation rates from 15 ka to 2000 AD for (a) weighted average of all peatlands, (b) Sphagnum open peatlands, and (c) Sphagnum-black spruce peatlands.

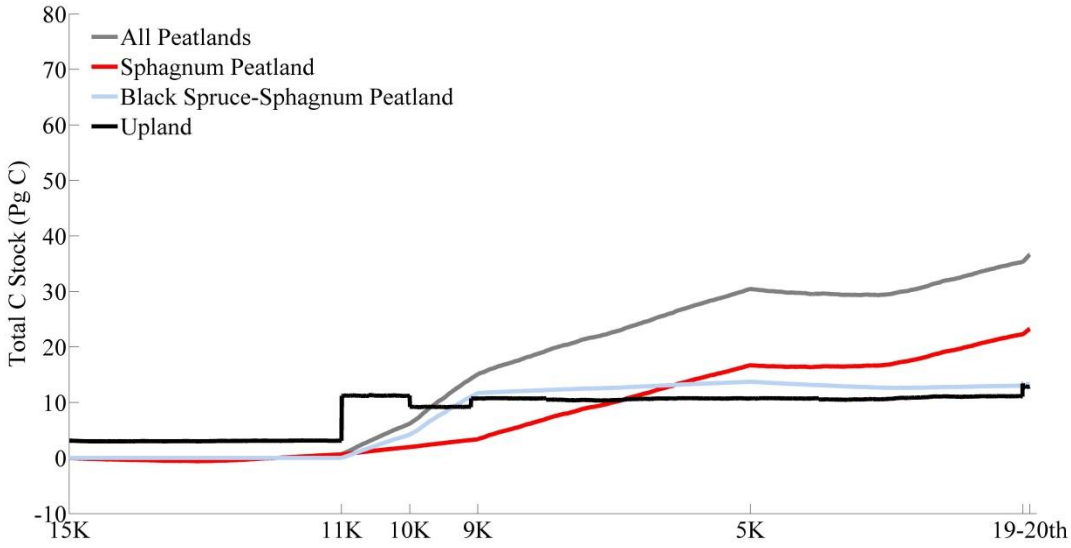

Figure 3.10. Total C stock accumulated from 15 ka to 2000 AD for all peatlands, Sphagnum open peatlands, Sphagnum-black spruce peatlands, and upland soils.

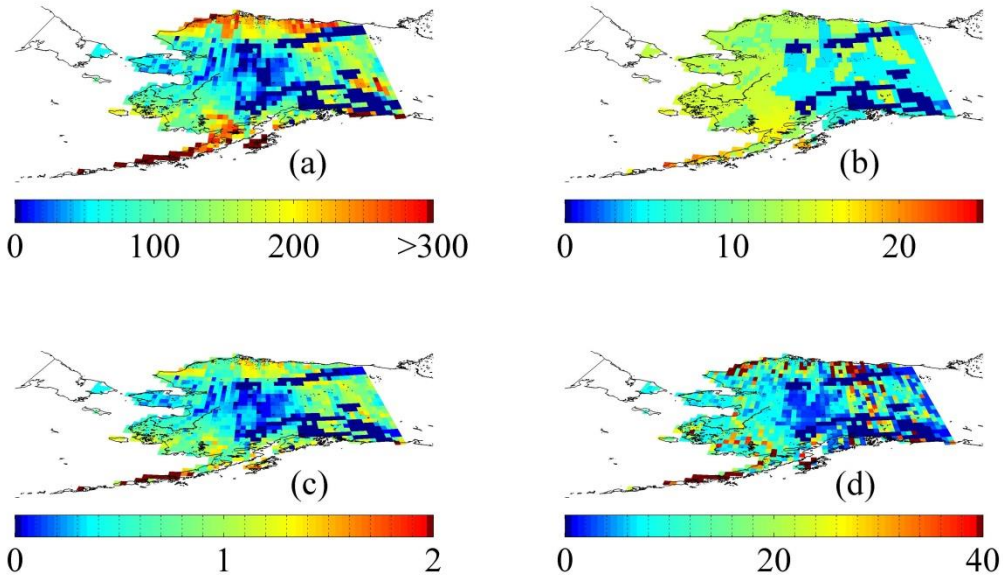

Figure 3.11. Spatial distribution of (a) total peat SOC density ($kg\ C\ m^{-2}$), (b) total mineral SOC density ($kg\ C\ m^{-2}$), (c) total peat depth (m), and (d) area-weighted total (peatlands plus non-peatlands) SOC density ($kg\ C\ m^{-2}$) in Alaska from 15 ka to 2000 AD.

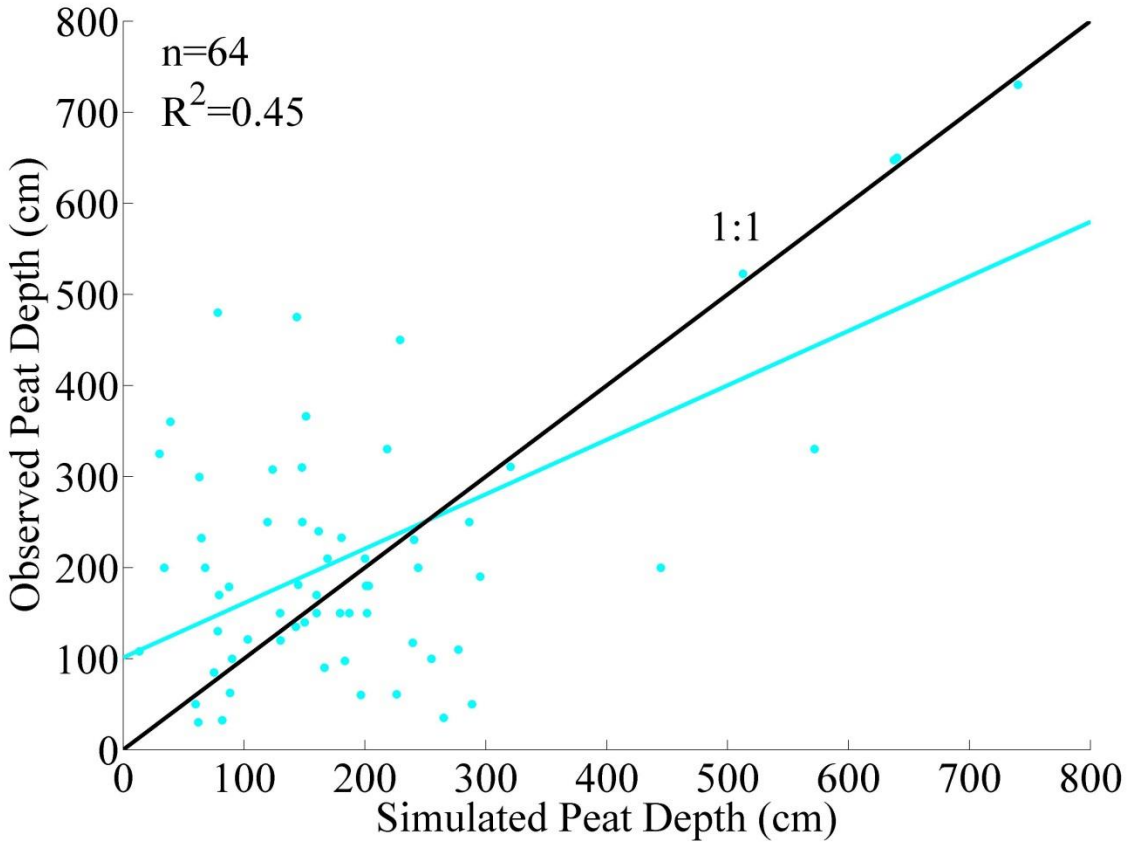

Figure 3.12. Evaluation of the simulation results: Field-based estimates and model simulations for peat depths in Alaska. The observed and simulated data are extracted from the same grids on the map. Linear regression line (cyan) is compared with the 1:1 line. The linear regression is significant (P<0.001, $n = 64$) with R^2 = 0.45, slope = 0.65, and intercept = 101.05 cm. The observations of >1000 cm are treated as outliers.

3.3.4 Effects of Climate on Ecosystem Carbon Accumulation

The simulated climate by ECBilt-CLIO model showed that among the six time periods, the coolest temperature appeared at 15-11 ka, followed by the mid- and late- Holocene (5 ka-1900 AD). Those two periods were also generally dry (Figure 3.2f). The former represented colder and drier climate before the onset of the Holocene and the HTM (Barber and Finney, 2000; Edwards et al., 2001). The latter represented post-HTM neo-glacial cooling, which has caused permafrost aggradation across northern high latitudes (Oksanen et al., 2001; Zoltai, 1995).

Despite the relatively large inter-annual NPP variation resulted from the annual fluctuations of the climate forcing (Figure 3.4b), the long-term NPP, vegetation C density and storage were highest during the HTM (Figures 3.4a and c). Annual C accumulation rates also reached the highest (Figures 3.4-3.10). The long-term variation of NPP has a similar pattern of the climate (see Figure 3.2 for climate variables), where higher NPP, along with higher vegetation C coincided with warmer temperatures and enhanced precipitation during the HTM, compared to other time periods. ECBilt-CLIO simulated a warmest summer and a prolonged growing season, leading to a stronger seasonality of temperature during the HTM (Kaufman et al., 2004, 2016), in line with the orbital-induced maximum summer insolation (Berger and Loutre, 1991; Renssen et al., 2009). The coincidence between the highest vegetation C uptake and SOC accumulation rates and the warmest summer and the wetter-than-before conditions indicated a strong link between those climate variables and C dynamics in Alaska. Enhanced climate seasonality characterized by warmer summer, enhanced summer precipitation and possibly earlier snow melt during the HTM accelerated the photosynthesis and subsequently increased NPP (Tucker et al., 2001; Kimball et al., 2004; Linderholm, 2006). As shown in our sensitivity test, annual NPP was increased by 40 and 20 $\mathrm{g\,C\,m^{-2}\,yr^{-1}}$ under the warmer and wetter scenarios, respectively (Figures 3.13a, b). Meanwhile, warmer condition could positively affect the SOC decomposition (Nobrega et al., 2007). However, it could be offset to a certain extent via the hydrological effect, as higher precipitation could raise the water-table position, allowing less space for aerobic heterotrophic respiration. Our sensitivity test results indicated that warmer and wetter conditions could lead to an increase of decomposition up to 35 and 15 $\mathrm{g\,C\,m^{-2}\,yr^{-1}}$, respectively (Figures 3.13c, d). We did not find a decrease in total heterotrophic respiration throughout Alaska from the higher precipitation. It was presumably due to a much

larger area of upland soils (1.3×10^6 km^2) than peatland soils (0.26×10^6 km^2), as higher precipitation would cause higher aerobic respiration in the unsaturated zone of upland soils, and consequently stimulated the SOC decomposition. The relatively low NPP and vegetation C density, along with the lower total soil C stocks were consistent with the unfavorable cool and dry climate conditions at 15-11 ka and during the mid- and late- Holocene. Statistical analysis indicated that temperature had the most significant effect on peat SOC accumulation rate, followed by the seasonality of NIRR (Wang et al., 2016). The seasonality of temperature, the interaction of temperature and precipitation, and precipitation alone also showed significance. The strong link between climate factors and C dynamics may explain the lower SOC accumulation during the neo-glacier cooling period (Marcott et al., 2013; Vitt et al., 2000; Peteet et al., 1998; Yu et al. 2010). The rapid peat SOC accumulation during the 20th century under warming and wetter climate may suggest a continuous C sink in this century, as concluded in Spahni et al. (2013). However, potential risk still exists as the rising temperature in the future may have positive effects on heterotrophic respiration (See Chapter 4 and Chapter 5) and simultaneously increase evapotranspiration and lower water table. This could increase aerobic decomposition and thus switch the Alaskan peatland from a C sink into a C source. The fate of Alaskan SOC stock and the biogeochemical cycling of the terrestrial ecosystems under future scenarios need further investigation.

3.3.5 Effects of Vegetation Distribution on Ecosystem Carbon Accumulation

Climate variables significantly affect C dynamics within each time slice. However, different vegetation distributions during various periods led to clear step changes, suggesting vegetation composition was likely to be another primary factor (Figures 3.5, 3.6, 3.7, and 3.10). As key parameters controlling C dynamics in the model (e.g., maximum rate of photosynthesis,

litter fall C, maximum rate of monthly NPP) are ecosystem type specific, vegetation distribution changes may drastically affect regional plant productivity and C storage. Our sensitivity test indicated that by replacing all vegetation types with forests, there was a total increase of 36.9 Pg in upland plus peatland soils. There was also an increase of 48.8 Pg C under warmer and wetter conditions, suggesting that both climate and vegetation distribution may have played important roles in carbon accumulation.

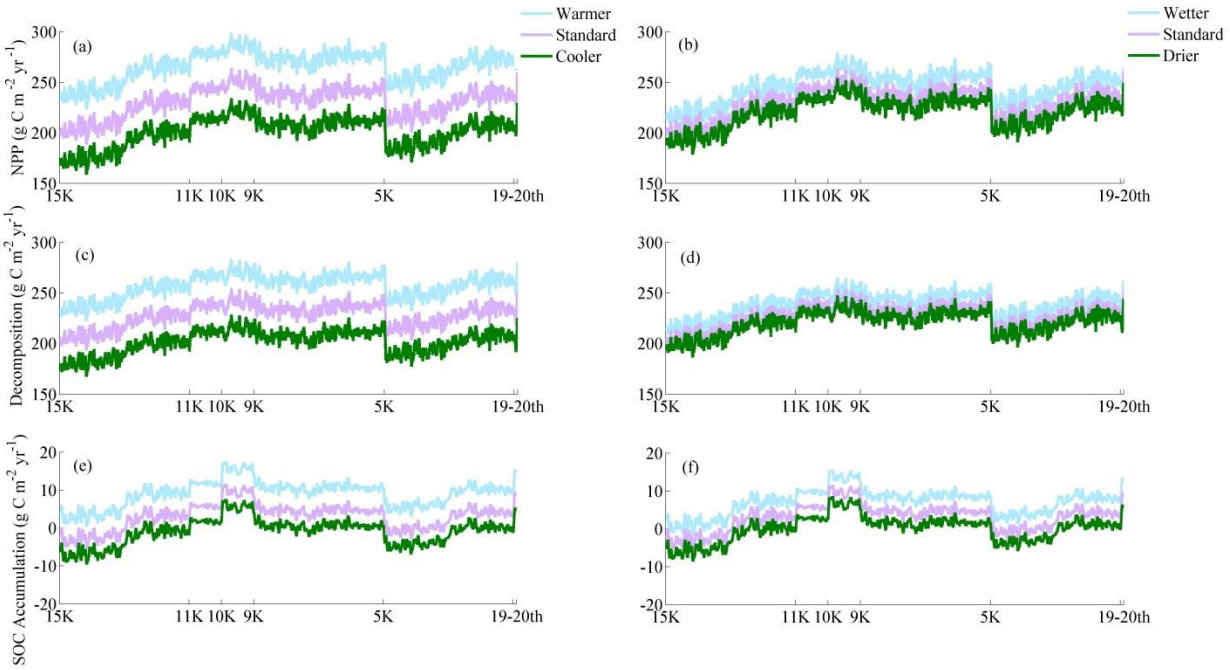

Figure 3.13. Temperature and precipitation effects on (a)(b) annual NPP, (c)(d) annual SOC decomposition rate (aerobic plus anaerobic), and (e)(f) annual SOC accumulation rate of Alaska. A 10-year moving average was applied.

3.4 Conclusions

We used a biogeochemistry model for both peatland and non-peatland ecosystems to quantify the C stock and its changes over time in Alaskan terrestrial ecosystems during the last 15,000 years. The simulated peat SOC accumulation rates were compared with peat-core data from four peatlands on the Kenai Peninsula in southern Alaska. The model well estimated the

peat SOC accumulation rates trajectory throughout the Holocene. Our regional simulation showed that 36-63 Pg C had been accumulated in Alaskan land ecosystems since 15,000 years ago, including 27-48 Pg C in peatlands and 9-15 Pg C in non-peatlands (within 1 m depth). We also estimated that 2.5-3.7 Pg C was stored in contemporary Alaskan vegetation, with 0.3-0.6 Pg C in peatlands and 2.2-3.1 Pg C in non-peatlands. The estimated average rate of peat C accumulation was 2.3 Tg C yr^{-1} with a peak (5.1 Pg C yr^{-1}) in the Holocene Thermal Maximum (HTM), four folds higher than the rate of 1.4 Pg C yr^{-1} over the rest of the Holocene. The 20th century represented another high SOC accumulation period after a much low accumulation period of the late Holocene. We estimated an average depth of 1.9 m of peat in current Alaskan peatlands, similar to the observed mean depth. The changes of vegetation distribution were found to be the major control on the spatial variations of SOC accumulation in different time periods. The warming in the HTM characterized by the increased summer temperature and increased seasonality of solar radiation, as well as the higher precipitation might have played an important role in the high C accumulation.

Acknowledgment. We acknowledge the funding support from a NSF project IIS-1027955 and a DOE project DE-SC0008092. We also acknowledge the SPRUCE project to allow us use its data. Data presented in this paper are publicly accessible: ECBilt-CLIO Paleo-simulation (http://apdrc.soest.hawaii.edu/datadoc/sim2bl.php), CRU2.0 (http://www.cru.uea.ac.uk/data). Model parameter data and model evaluation process are in Wang et al. (2016). Other simulation data including model codes are available upon request from the corresponding author (qzhuang@purdue.edu).

CHAPTER 4. A POTENTIAL SHIFT FROM A CARBON SINK TO A SOURCE IN AMAZONIAN PEATLANDS UNDER A CHANGING CLIMATE[3]

4.1 Introduction

Tropical peatlands cover ~441,025 km^2 and store a large quantity (88.6 Pg C) of soil organic carbon (SOC) (Page et al., 2002, 2004, 2011; Rieley et al., 2008). These ecosystems occupy ~11% of the global peatland area and account for 15-19% of the total global peat SOC stock[3]. Tropical peatlands are mainly distributed in Southeast Asia (~56%, 247,778 km^2), and South and Central America (~23%, 107,486 km^2). Recently, additional 145,500 km^2 of tropical peatlands containing 30.6 Pg C was discovered in central Congo basin, Africa (Dargie et al., 2017). Given their significant C stocks, studying their responses to past climatic trends and to the future climate change is of global importance (Guzmán Castillo, 2007; Lähteenoja et al., 2009a, 2011).

To date, most studies on the role of tropical peatlands in the global C cycle have focused on Indonesian peatlands, which have been acting during the last decades as a considerable C source to the atmosphere resulting from anthropogenic activities (e.g., land exploitation and fires) (Rieley and Page., 2005; Maltby et al., 1993; Miettinen et al., 2011). Few studies have focused on the Amazon basin, where peatlands remain nearly intact, and have been a long-term C sink (Lähteenoja et al., 2009a, 2009b, 2011; Draper et al., 2014). The 120,000 km^2 Pastaza-Marañón foreland basin (PMFB) located in Peru is the most extensive peatland complex in the Amazon basin, with up to 7.5 m thick peat deposits. The basal ages vary from 0.67 to 8.9 ka (1 ka=1000 cal years before present) and the peat SOC accumulation rates range from 26 to 195

[3]**Wang, S**., Zhuang, Q., Lähteenoja, O., Draper, F., and Cadillo-Quiroz, H, Potential shift from a carbon sink to a source in Amazonian peatlands under a changing climate, Proceedings of the National Academy of Sciences Nov 2018, 201801317; DOI: 10.1073/pnas.1801317115, 2018.

g C m^{-2} yr^{-1} (Lähteenoja et al., 2011, 2012). It is a subsiding foreland basin, resulting from the Cenozoic uplift of the Andes Mountains (Dumont et al., 1990, 1991; Räsänen et al., 1990, 1992) and characterized by meandering (more than 100 m in a year (Kalliola et al., 1992)) and avulsions of rivers (abrupt changes in the location of river stretches (Smith et al., 1989; Guimberteau et al., 2013)). Waterlogged conditions due to high precipitation and low lying topography provide a favorable environment for peat accumulation (Lähteenoja et al., 2012; Draper et al., 2014). By measuring peat characteristics at several peatland sites within the basin, and using Landsat TM images, Lähteenoja et al (2012) estimated a peatland area of 21,929 km^2 with SOC stock of 3.116 Pg (0.837-9.461 Pg) for the central parts of the PMFB. Further, by incorporating multi-sensor remote sensing and adding more peat core data, Draper et al (2014) mapped the distribution of peatland and non-peatland ecosystems in the PMFB and estimated a peatland area of 35,600$\pm$2133 km^2 with 3.14 Pg C (0.44−8.15 Pg) stored in the vegetation and peat deposits of the whole basin.

According to most climate models, mean air temperature of South America is projected to increase by 1.8-5.1℃ for the PMFB by the end of this century depending on different future scenarios (Guimberteau et al., 2013; Marengo et al., 2012; Sánchez et al., 2015; Zulkafli et al., 2016). Annual precipitation is projected to increase by up to 500 mm, although a large uncertainty exists. The strong dependence of C dynamics on climate suggests that warming in the 21st century may turn the peatlands in the PMFB from a long-term C sink into a source (Guzmán Castillo, 2007; Lähteenoja et al., 2009a; Rieley and Page, 2005; Cox et al., 2004). However, this potential change has not been quantified or modelled in any way in previous studies. Nearly all models focusing on the future C dynamics of the Amazon basin have been applied to non-peatland ecosystems (Tian et al., 1998, 2000; Li et al., 2007; Cleveland et al.,

2015; Rowland et al., 2015; Restrepo-Coupe et al., 2017; Powell et al., 2013; Delbart et al., 2010; Schulman et al., 1999) with the exception of Li et al (2007).

Process-based models offer an alternative approach to quantifying peatland C dynamics and providing insights for future projection (Frolking et al., 2010; Spahni et al., 2013; Kleinen et al., 2012; Wang et al., 2016a, 2016b). Recently, a peatland terrestrial ecosystem model (P-TEM) was developed for both peatland and non-peatland ecosystems by combining a hydrology module (HM), a soil thermal module (STM), a methane dynamics module (MDM), and a C and nitrogen dynamics module (CNDM) (Wang et al., 2016a). P-TEM has been evaluated and used for estimating C stocks across the Alaskan landscape since the last deglaciation. Here, we parameterize and evaluate the P-TEM for tropical peatlands and model the C dynamics of the peatlands in the Pastaza-Marañón foreland basin, Peruvian Amazonia (Figure 4.1) from 9 ka to 2014 AD. The model parameters were optimized using published peat, vegetation and remote-sensing data for the PMFB from Lähteenoja et al (2012) and Draper et al (2014) as well as other published sources (Tables 4.1 and 4.2). The model was then used to 1) quantify past C accumulation from 12 ka to 2014 AD in peatlands, and 2) predict the future trends of C accumulation under different climate scenarios in the 21st century in peatland and non-peatland ecosystems within the PMFB.

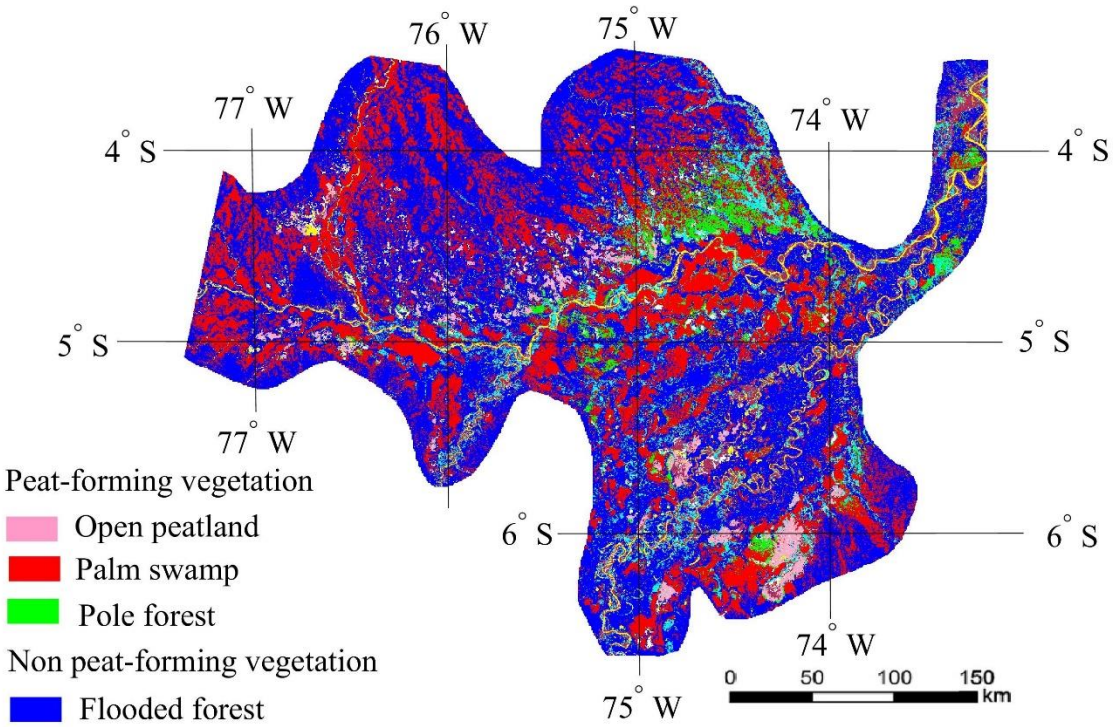

Figure 4.1. Distribution of peat- and non peat-forming vegetation in the PMFB at the resolution of 90 m×90 m. The map was resized to 1.69 km×1.69 km. Colors represent vegetation types: open peatland (pink), palm swamp (red), pole forest (green), and flooded forest (dark blue). Yellow represents open water and light blue represents other. See the Figures 1 and 4 of Draper et al (2014) for original map.

Table 4.1. NPP and vegetation C stocks in Amazonia used for parameter optimization of P-TEM. Values in the columns "Measurement" refer to values taken from literature, whereas values in the columns "Simulation" refer to the averaged values from all selected plausible parameter sets after the initial Monte Carlo simulations.

Annual NPP or stocks[a]	Pole forest		Palm swamp		Open peatland[e]		Flooded forest		Ref
	Measurement	Simulation	Measurement	Simulation	Measurement	Simulation	Measurement	Simulation	
Aboveground NPP	985-1087[3]	-	1041-1279[8]	-	-	-	1041-1279[8]	-	[1]*ref. 13*
Belowground NPP									[2]*ref. 14*
Total NPP	362-448[3]	-	353-434[3,c]	-	-	-	353-434[3,c]	-	[3]*ref. 15*
									[4]*ref. 16*
	1347-1535[3]	1382	1394-1713	1424	-	125	1394-1713	1404	[5]*ref. 17*
Aboveground vegetation C density	5200-7160[1,4]	-	9320-10860[1,4]	-	-	-	9320-10860[1,4]	-	[6]*ref. 18*
									[7]*ref. 19*
									[8]*ref. 20*
Belowground vegetation C density	2080-28645[5,6,b]	-	3728-4344[2,d]	-	-	-	3728-4344[2,d]	-	[9]*ref. 21*
Total vegetation C density	7280-10020	9098	13048-15204	14861	-	1003	13048-15204	14153	
Leaf area index (LAI)	3.3[8]	3.0	4.2-4.4[8]	4.4	-	1.0	5.2-5.8[3]	5.4	

[a] Units for annual net primary production (NPP) are g C m^{-2} yr^{-1}. Units for above/belowground/total vegetation C density are g C m^{-2}. A ratio of 0.473 was used to convert vegetation biomass to carbon[7,9]. [b] A ratio of 0.39 was used to obtain belowground biomass given aboveground live biomass for Amazonian pole forest[5]. [c] A ratio of 0.34 was used to obtain the belowground NPP given aboveground NPP for palm swamp and flooded forest[3]. [d] A ratio of 0.41 was used to obtain the belowground biomass given aboveground live biomass for palm swamp and flooded forest[2]. [e]Open peatland has no available field measurement of NPP and vegetation C.

ref 13: Baker et al., 2004; ref 14: Goodman et al., 2013; ref 15: Del Aguila-Pasquel et al., 2014; ref 16: Draper et al., 2014; ref 17: Houghton et al., 2001; ref 18: Malhi et al., 2011; ref 19: Martin and Thomas, 2011; ref 20: Nebel et al., 2001; ref 21: McGuire et al., 1992

Table 4.2. Description of the model parameters and their final values after optimization via (1) Initial Monte Carlo simulations, and (2) Second step Monte Carlo simulations and Bayesian inference. The values are the mean values with 1.96 standard deviation from the posterior distributions after the optimization. T_{min}, T_{optmin}, T_{optmax}, T_{opt}, and T_{max} were the same for other types of vegetation based on the optimization for pole forest.

Variables	Description	Unit	Pole forest	Palm swamp	Open peatland	Flooded forest	Ref
C_V	Initial[a] organic C density in vegetation	g m^{-2}	16935±2580	16983±2249	16671±1528	16671±1528	*ref. 1*
C_{S1}	Initial[a] organic C density in soil	g m^{-2}	9476±1031	9476±1031	9476±840	10204±1251	*ref. 11*
C_{max}	Maximum rate of C assimilation through photosynthesis	g m^{-2} $month^{-1}$	1089±142	1283±128	104±3	1263±109	*ref. 21*
CFALL	Proportion of vegetation C loss as litterfall	g g^{-1} $month^{-1}$	0.010945±0.001	0.010679±0.004	0.010664±0.001	0.008969±0.002	*ref. 22*
C_{VLmax}	Maximum canopy leaf C density	g m^{-2}	454±20	654±26	100±9	754±45	*ref. 23*
K_d	Aerobic heterotrophic respiration at 0℃	g g^{-1} $month^{-1}$	0.013617±0.0005	0.020023±0.001	0.00594±0.0003	0.004823±0.0005	*ref. 24*
T_{min}	Minimum temperature for GPP[b]	℃	10.0±1.5	10.0±1.5	10.0±1.5	10.0±1.5	
T_{optmin}	Minimum optimum temperature for GPP	℃	21.9±2.2	21.9±2.2	21.9±2.2	21.9±2.2	
T_{optmax}	Maximum optimum temperature for GPP	℃	32.7±2.9	32.7±2.9	32.7±2.9	32.7±2.9	
T_{opt}	Optimum temperature for GPP	℃	27.3±1.9	27.3±1.9	27.3±1.9	27.3±1.9	
T_{max}	Maximum temperature for GPP	℃	37.0±3.1	37.0±3.1	37.0±3.1	37.0±3.1	

[a] Initial values are the default values of vegetation C and SOC in the first time step during the simulation. [b] GPP: gross primary production.

ref 1: Wang et al., 2016a; ref 11: Tang and Zhuang 2009; ref 21: McGuire et al., 1992; ref 22: Tang and Zhuang 2008; ref 23: Zhuang et al., 2002; ref 24: Lähteenoja et al., 2009a

4.2 Methods

4.2.1 The peatland biogeochemistry model

In P-TEM, peat SOC accumulation is determined by the difference between NPP and aerobic and anaerobic respiration R_H at a monthly step. Parameters in P-TEM were first optimized with data of annual C fluxes and stocks in the Amazon basin taken from literature (Table 4.1) in order to obtain the prior distribution of the parameter space for peatland ecosystems. Specifically, site-level measurements of tree biomass from Amazonian peatlands (Draper et al., 2014) were used to compare with model simulations to optimize parameters. Due to the lack of NPP measurements, NPP values used in the model are field measurements from neighboring white-sand forests (for pole forest peatlands) and seasonally flooded forests (for palm swamp peatlands and flooded forests) (Table 4.1). Second, a Bayesian approach was used to optimize parameters (Table 4.2) with Monte Carlo ensemble simulations driven by the extracted paleo climate data at five peatland sites (Figures 4.2 and 4.3).

The distribution of vegetation types was taken from Draper et al (2014) at a resolution of 90 m×90 m and was resized to 1.69 km×1.69 km. Vegetation types in the region include three peat-forming vegetation types (pole forest (PF), palm swamp (PS), and open peatland (OP, peatland lacking closed canopy)) and a non-peat forming type (flooded forest (FF)) (Figure 4.1). OP was assumed to have minimal NPP and vegetation biomass during the simulation.

4.2.1.1 Peat Soil Organic Carbon Accumulation

Peat soil organic carbon (SOC) accumulation is determined by the net primary production (NPP) and aerobic and anaerobic respiration[1] based on the core C and nitrogen dynamic module for upland ecosystems (Zhuang et al., 2003). The net ecosystem production (NEP) for the peatland ecosystem is calculated at a monthly step:

$$\text{NEP} = \text{NPP} - R_H - R_{CH_4} - R_{CWM} - R_{CM} - R_{COM}$$

where NPP represents the monthly net primary production. R_H represents the monthly aerobic respiration related to the variability of water table depth, soil moisture, soil temperature, and soil organic C. R_{CH_4} represents the monthly methane emission after methane oxidation. R_{CWM} represents the CO_2 emission due to methane oxidation (Zhuang et al., 2015). R_{CM} represents the CO_2 release accompanied with the methanogenesis (Tang et al., 2010). R_{COM} represents the CO_2 release from other anaerobic processes (e.g., fermentation and terminal electron acceptor reduction) (Keller and Bridgham, 2007).

4.2.1.2 Net Primary Production (NPP)

Gross primary production (GPP) is defined as the total assimilation of CO_2-C by plants, excluding photorespiration. GPP is modeled as a function of the irradiance of photosynthetically active radiation (PAR), atmospheric CO_2 concentrations, moisture availability, mean air temperature, the relative photosynthetic capacity of the vegetation, and nitrogen availability (see Raich et al (1991) for details of the formulas below):

$$\text{GPP} = (C_{max})\frac{PAR}{k_i + PAR}\frac{C_i}{k_c + C_i} f(PHENOLOGY) f(FOLIAGE) f(T) f(NA)$$

where C_{max} is the monthly maximum rate of C assimilation by the entire plant canopy under optimal environmental conditions (g m^{-2} $month^{-1}$); PAR is the irradiance of photosynthetically active radiation at canopy level (J cm^{-2} day^{-1}); k_i is the irradiance at which C assimilation proceeds at one-half its maximum rate; C_i is the concentration of CO_2 inside leaves (mL L^{-1}); k_c is the internal CO_2 concentration at which C assimilation proceeds at one-half its maximum rate. $f(PHENOLOGY)$ is monthly leaf area relative to leaf area during the month of maximum leaf area and depends on monthly estimated evapotranspiration. $f(FOLIAGE)$ is a scaler function that

ranges from 0.0 to 1.0 and represents the ratio of canopy leaf biomass relative to maximum leaf biomass. T is monthly air temperature and NA is nitrogen availability. The function $f(NA)$ models the limiting effects of plant nitrogen status on GPP.

Moisture limitations on CO_2 assimilation is modeled by the modifying the conductance of leaves to CO_2 diffusion. The mean monthly moisture availability is the degree to which environmental demands for water are met by rainfall and available soil moisture. This is expressed as the ratio of actual evapotranspiration (*EET*) to potential evapotranspiration (*PET*). We assume that the relationship between CO_2 concentration inside stomatal cavities (C_i) and in the atmosphere (C_a) is proportional to relative moisture availability:

$$G_V = 0.1 + (\frac{0.9EET}{PET})$$

and

$$C_i = G_V C_a$$

where G_V is relative canopy conductance, a unitless multiplier that accounts for changes in leaf conductivity to CO_2 resulting from changes in moisture availability. When moisture is not limiting, G_V is close to 1.0 and CO_2 inside leaves will be close to ambient CO_2.

Temperature effect on GPP is modeled as a multiplier on potential GPP, with a maximum value of 1 at the optimum temperature and lower values at suboptimal temperatures:

$$f(T) = \frac{(T - T_{min})(T - T_{\max})}{(T - T_{min})(T - T_{max}) - \left(T - T_{opt}\right)^2}$$

where $f(T)$ is the unitless multiplier on GPP and T is the mean monthly air temperature (℃).

The phenological model was developed for simulating the changes seasonal changes in the vegetation's capacity to assimilate C. It models relative changes in the photosynthetic capacity of

mature vegetation (*KLEAF*) from estimated actual evapotranspiration (*EET*) and the previous month's photosynthetic capacity:

$$f(PHENOLOGY)_j = a\left(\frac{EET_j}{EET_{max}}\right) + b\left(f(PHENOLOGY)_{j-1}\right) + c$$

$$f(PHENOLOGY)_j = 1$$

$$(\text{if } f(PHENOLOGY)_j > 1)$$

$$f(PHENOLOGY)_j = \frac{f(PHENOLOGY)_t}{f(PHENOLOGY)_{max}}$$

$$(\text{if } f(PHENOLOGY)_j < 1)$$

The time step j is one month; EET_{max} is the maximum *EET* occurring during any month; $a, b,$ and c are regression-derived parameters.

Plant (autotrophic) respiration (R_A) is the total respiration (excluding photorespiration), including all CO_2 production from the various processes of plant maintenance, nutrient uptake, and biomass construction. R_A is the sum of maintenance respiration (R_m), and growth respiration (R_g):

$$R_A = R_m + R_g$$

The maintenance respiration is modeled as a direct function of plant biomass (C_V).We assume that increasing temperatures increase maintenance respiration logarithmically with a Q_{10} of 2 over all temperatures:

$$R_m = K_r(C_V)e^{0.0693T}$$

where K_r is the respiration rate of the vegetation per unit of biomass carbon at 0℃ ($\text{g g}^{-1}\ \text{month}^{-1}$), and T is the mean monthly air temperature (℃). Growth or construction respiration R_g is estimated to be 20% of the difference between GPP and R_m:

$$\text{NPP}'_t = \text{GPP}_t - R_{mt}$$

$$R_{gt} = 0.2\mathrm{NPP'_t}$$

where NPP′ is the potential net primary production assuming that the conversion efficiency of photosynthate to biomass is 100% and *t* refers to the monthly time step.

Net primary production (NPP) is the difference between GPP and autotrophic respiration (R_{At}):

$$\mathrm{NPP_t} = \mathrm{GPP_t} - R_{At}$$

NPP is calibrated to correctly estimate annual NPP since monthly observed NPP do not exist for most vegetation types from the field measurements.

Nitrogen availability influences GPP individually by influencing the relative allocation of effort toward C vs. nitrogen uptake (Ac). See Raich et al (1991) for details in Carbon-Nitrogen interaction model.

4.2.1.3 Aerobic Respiration Related to Water Table Depth (R_H)

SOC aerobic respiration related to the variability of water table depth (R_H) is calculated as:

$$R_H = K_d C_{s1} f(M_V) e^{0.069 H_T} \frac{WTD}{LWB}$$

where M_V represents the mean monthly soil water content (percentage of saturation) in the peat unsaturated zone above the water table depth (*WTD*). K_d is a logarithm of heterotrophic rate at 0℃. H_T is the mean monthly temperature of the soil above the lowest water table boundary (Granberg et al., 1999) (*LWB*, a fixed parameter, the soil below which is set saturated). The SOC between *LWB* and soil surface (C_{s1}) in the transient simulation is obtained after a 2000-year equilibrium run.

$f(M_V)$ is a non-linear function defining the influence of soil moisture on decomposition:

$$B = \left(\frac{M^{m1} - M_{opt}^{m1}}{M_{opt}^{m1} - 100^{m1}} \right)^2$$

$$f(M_V) = (0.8 M_{sat}^{B}) + 0.2$$

where $m1$ is a parameter defining the skewness of the curve. M_{opt} is the soil moisture content at which $f(M_V)$ is maximum (1.0). M_{sat} is a parameter that determines the value of $f(M_V)$ when the soil pore space is saturated with water.

The peatland soil is modeled as a two-layer system. The soil layers above the *LWB* are divided into 1 cm sublayers, where peat soil characteristics in the upper peat are constant above 7 cm peat depth and change linearly in the section interval of 1 cm below the *WTD*. The *WTD* is estimated based on the total amount of water content above the LWB within the upper two soil layers. Using the calculated *WTD*, the water content at each 1 cm above the *WTD* can be determined after solving the water balance equations.

4.2.1.4 R_{CH_4}, R_{CWM}, R_{CM}, and R_{COM}

R_{CH_4} represents the monthly methane emission after methane oxidation (see Zhuang et al (2004) for details):

$$R_{CH_4} = M_P - M_O$$

where M_P is the monthly methane production /methanogenesis and M_O is the monthly methane oxidation.

M_P is modeled as an anaerobic process that occurs in the saturated zone of the soil profile. It is calculated as the integration of the hourly methanogenesis ($M_P(z,t)$) at each 1-cm layer:

$$M_P = \int_{t=1}^{24\times30} \int_{z=1}^{100} M_P(z,t)\, dtdz$$

where

$$M_P(z,t) = M_{G0} f\big(S_{OM}(z,t)\big) f\big(M_{ST}(z,t)\big) f\big(pH(z,t)\big) f(R_X(z,t))$$

M_{G0} is the ecosystem-specific maximum potential production rate; $f\big(S_{OM}(z,t)\big)$ is a multiplier that enhances methanogenesis with increasing methanogenic substrate availability, which is a

function of net primary production of the overlying vegetation; $f\left(M_{ST}(z,t)\right)$ is a multiplier that enhances methanogenesis with increasing soil temperatures. $f\left(pH(z,t)\right)$ is a multiplier that diminishes methanogenesis if the soil-water pH is not optimal (i.e., pH=7.5). $f(R_X(z,t))$ is a multiplier that describes the effects of the availability of electron acceptors which is related to redox potential on methanogenesis.

M_O is modeled as the integration of hourly methane oxidation rate ($M_O(z,t)$) at each 1-cm layer:

$$M_O = \int_{t=1}^{24\times30} \int_{z=1}^{100} M_O(z,t)\, dtdz$$

where

$$M_O(z,t) = O_{MAX} f\left(C_M(z,t)\right) f\left(T_{SOIL}(z,t)\right) f\left(E_{SM}(z,t)\right) f(R_{OX}(z,t))$$

O_{MAX} is the ecosystem-specific maximum oxidation coefficient; $f\left(C_M(z,t)\right)$ is a multiplier that enhances methanotrophy with increasing soil methane concentrations; $f\left(T_{SOIL}(z,t)\right)$ is a multiplier that enhances methanotrophy with increasing soil temperatures; $f\left(E_{SM}(z,t)\right)$ is a multiplier that diminishes methanotrophy if the soil moisture is not at an optimum level; and $f(R_{OX}(z,t))$ is a multiplier that enhances methanotrophy as redox potentials increase.

R_{CWM} is the CO_2 emission due to methane oxidation; R_{CM} is the CO_2 release accompanied with methanogenesis. We assume the same amount of CO_2 is released along with the methane production (M_P). R_{COM} is the CO_2 release from other anaerobic processes. We assume R_{COM}: R_{CH_4} to be 5.

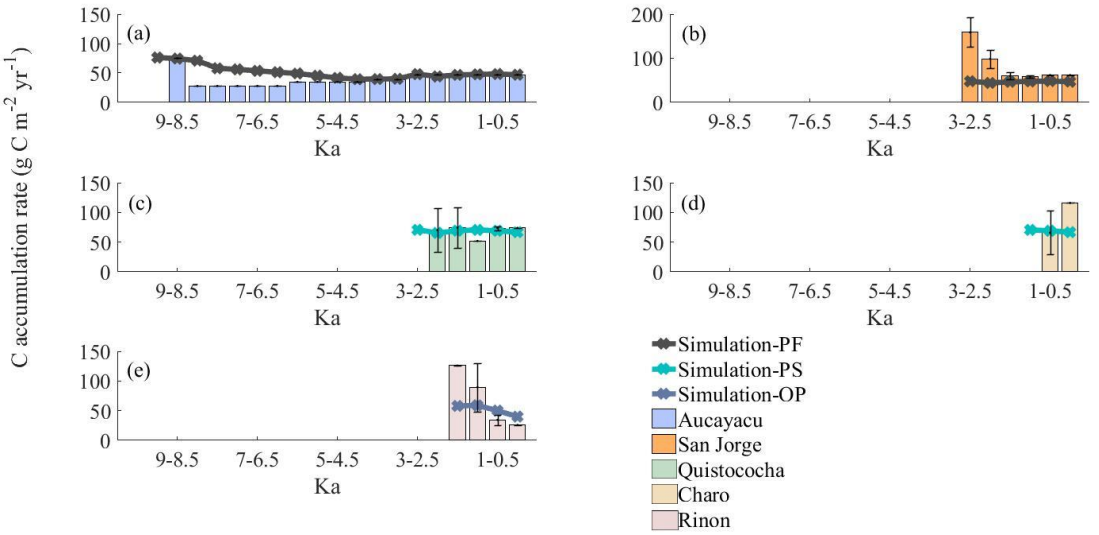

Figure 4.2. Comparison between simulated (this study) and measured (Lähteenoja et al., 2009a, 2012) SOC accumulation rates of pole forest (PF) at (a) Aucayacu, and (b) San Jorge; palm swamp (PS) at (c) Quistococha, and (d) Charo; and open peatland (OP) at (e) Riñón in 500 year bins from 10 ka to 2014 AD. Colors of lines represent simulations for different vegetation types using different parameters. Note that the starting ages of the model regional transient simulations are: 4 ka for PF, 2 ka for PS, and 1.6 ka for OP.

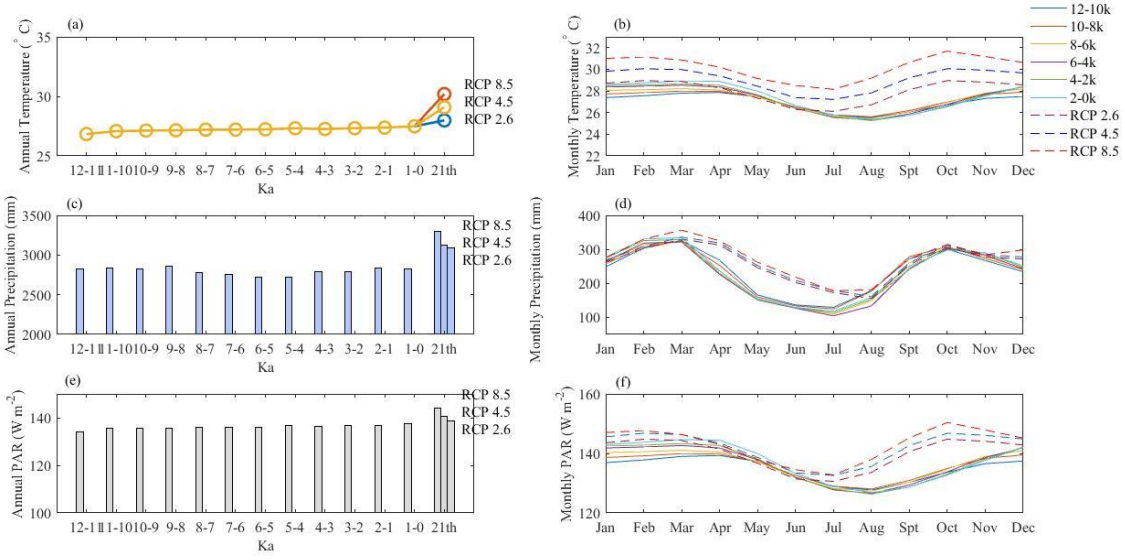

Figure 4.3. Climate forcing of annual (a) temperature, (c) precipitation, (e) photosynthetically active radiation (PAR) and monthly mean (b) temperature, (d) precipitation, and (f) PAR for PMFB (Carlson et al., 2012; Mitchell et al., 2004; Change, 2014).

4.2.2 Model Parameterization

4.2.2.1 Initial Monte Carlo Simulations

The initial Monte Carlo simulations were conducted to obtain the proper prior range of the parameter space for peatland ecosystems based on the original parameter space for upland ecosystems:

(1) We applied the Latin Hypercube Sampler (LHS) (Iman et al., 1988). Each random variable θ_1, …, θ_k was divided into 5000 nonoverlapping intervals based on their uniform distributions with equal probability. One value from each interval was selected randomly based on the equal probability. 5000 values drawn for θ_1 was paired with 5000 values drawn for θ_2 and so forth. We repeated the same process until 5000 sets of *k* tuples were generated.

(2) We then drove the model using the climate data (Figure 4.3) from 1900 to 1990 AD. We averaged the simulated monthly C fluxes and pools (aboveground NPP, annual belowground NPP, annual total NPP, aboveground vegetation carbon, belowground vegetation carbon, and total vegetation carbon) to annual values and then averaged them from 1900 to 1990 AD. We selected the plausible parameter set based on which the simulated annual C fluxes and pools are within the uncertainty ranges of the field measurements (Table 4.1).

(3) The selected plausible parameter sets based on the initial Monte Carlo ensemble simulations were used as priors for peatland ecosystems.

4.2.2.2 Second Step Monte Carlo Simulations and Bayesian Inference

The Bayes' framework is:

$$\mathrm{P}(\boldsymbol{\theta}|\mathbf{V}) \propto \mathrm{P}(\mathbf{V}|\boldsymbol{\theta})\mathrm{P}(\boldsymbol{\theta})$$

where $\mathrm{P}(\boldsymbol{\theta}|\mathbf{V})$ is the posterior after the Bayesian inference conditioned on the available field measurements $\mathbf{V}$. $\boldsymbol{\theta}$ is the matrix of the parameters for adjustment. $\mathbf{V}$ is the difference matrix

between the Monte Carlo simulations and the corresponding field measurements. P($\boldsymbol{\theta}$) is the prior distribution for peatland ecosystems obtained from the initial Monte Carlo ensemble simulations. P($\mathbf{V}|\boldsymbol{\theta}$) is the likelihood function, which is calculated as the function of the difference between Monte Carlo simulations and available field measurements.

We assume the monthly field measurement data are independent from month-to-month and the field measurement data follow the following error distribution (Thiemann et al., 2001):

$$p_i(v_{ti}|\sigma_{ti},\beta_i,\theta) = \omega(\beta_i)\sigma_{ti}^{-1}\exp(-c(\beta_i)\left|\frac{v_{ti}}{\sigma_{ti}}\right|^{2/(1+\beta_i)})$$

The error term follows a normal distribution when $\beta_i = 0$; a double exponential distribution when $\beta_i = 1$; a uniform distribution when β_i approaches -1. Variance σ_{ti} was assumed to be a constant during the time period $t_{i-1} < t < t_i$.

$c(\beta_i)$ and $\omega(\beta_i)$ are defined as:

$$c(\beta_i) = \left\{\frac{\Gamma\left[\frac{3(1+\beta_i)}{2}\right]}{\Gamma\left[\frac{1+\beta_i}{2}\right]}\right\}^{\frac{1}{1+\beta_i}}$$

$$\omega(\beta_i) = \frac{\left\{\Gamma\left[\frac{3(1+\beta_i)}{2}\right]\right\}^{\frac{1}{2}}}{(1+\beta_i)\left\{\Gamma\left[\frac{1+\beta_i}{2}\right]\right\}^{\frac{3}{2}}}$$

We further assume that the error term follows the following distribution:

$$p(\boldsymbol{V}|\boldsymbol{\sigma},\boldsymbol{\beta},\boldsymbol{\theta}) = \prod_{i=1}^{N}\prod_{t=1}^{T}\omega(\beta_i)\sigma_{ti}^{-1}exp(-c(\beta_i)\left|\frac{v_{ti}}{\sigma_{ti}}\right|^{2/(1+\beta_i)})$$

$$\propto \exp[-\sum_{i=1}^{N}c(\beta_i)\sum_{t=1}^{T}\left|\frac{v_{ti}}{\sigma_{ti}}\right|^{2/(1+\beta_i)}]$$

where $\boldsymbol{\sigma}$ and $\boldsymbol{V}$ are matrices with a size of $T \times N$. $\boldsymbol{\beta}$ is a vector with size of N,

we get the likelihood function:

$$p(\boldsymbol{V}|\boldsymbol{\beta},\boldsymbol{\theta}) \propto \prod_{i=1}^{N}[\sum_{t=1}^{T}|v_{ti}|^{\frac{2}{1+\beta_i}}]\hat{}(\frac{1}{2}-T)(1+\beta_i)$$

We again applied the LHS algorithm to draw 3 ×1000 sets of parameters from the prior distributions for three different peatland ecosystems (pole forest, palm swamp, and open peatland) obtained from the previous Monte Carlo simulations. The observational data/ field measurement data are peat SOC accumulation rates for pole forest (PF) at (a) Aucayacu, and (b) San Jorge; palm swamp (PS) at (c) Quistococha, and (d) Charo; and open peatland (OP) at (e) Riñón in 500-year bins from 10 ka to 2014 AD. We then averaged the simulated monthly SOC accumulation rates at those sites into 500-year bins and compared them with the field measurement data. We next applied the Sampling Importance Resampling (SIR) technique (Skare et al., 2003) to calculate the importance ratio of each parameter set drawn iteratively and construct the posterior distributions for the model parameters. At last, the highest plausible parameter sets contain 3 ×50 parameters based on the calculated importance ratio out of 1000 from their prior distributions.

4.2.3 Climate Data

The climate forcing data for historic simulations include temperature, precipitation, photosynthetically active radiation (PAR), vapor pressure at a monthly step and CO_2 at an annual step from 12 ka to 1990 AD, simulated by CCSM3 (TraCE-21ka) at a spatial resolution of 3.75° ×3.75°. Climate forcing data for modern simulations is from Climate Research Unit (CRU2.0) at a monthly step from 1990 to 2014 AD at a resolution of 0.5° ×0.5°. For future simulations, we applied the Representative Concentration Pathway (RCP) 2.6 (mean annual temperature in the PMFB has the smallest increase (by ~0.5 ℃), mean annual precipitation increases by ~260 mm, and CO_2 increases by ~80 ppm at 2050 AD and decreases by ~30 ppm at

2100 AD), RCP 4.5 (by ~1.5 ℃, ~290 mm, and CO_2 increases by ~150 ppm at 2100 AD), and RCP 8.5 (by ~2.7 ℃, ~350 mm, and ~600 ppm at 2100 AD) at a monthly step from 2014 to 2100 AD at 0.5° ×0.5° as possible future climate scenarios. The CRU data together with the modern digital elevation data at 1.69 km×1.69 km were input into interpolation software ANUSPLIN4.4. We then downscaled the paleo-climate data (TraCE-21ka, 3.75° ×3.75°) and the RCP data (0.5° ×0.5°) based on the spatial variations of the interpolated CRU data (1.69 km×1.69 km) by assuming that the spatial variations of CRU to be the same as that of paleo and RCP data.

4.2.4 Model Application and Uncertainty Analysis

A 500-year run was conducted for each peatland ecosystem type ahead of the basal age using parameters of non peat-forming FF to determine the initial SOC within the upper 1 m mineral soil underlying the peat deposit. The model was first run from 12 ka to 2014 AD for validation at five peatland sites (Figure 4.2). The simulated SOC accumulation rates of PS, OP, and PF were firstly compared with measured SOC accumulation rates annually in 500-year bins (Lähteenoja et al., 2009a, 2012). Second, we applied the model to a regional simulation with interpolated monthly paleo-climate data for the PMFB. We averaged all the measured basal ages of each peatland type to determine the mean basal age of each peatland ecosystem type (Table 4.3). Basal ages at sites where they have not been measured were calculated using mean SOC accumulation rates, bulk density, peat depth and C content of each peatland ecosystem type derived from Lähteenoja et al (2009a) and Draper et al (2014), following the equations in Lähteenoja et al (2009a). We conducted the simulation from 1 ka to 2014 AD for FF. Finally, we conducted the simulations for future projection using the interpolated RCP 2.6, RCP 4.5 and RCP 8.5. A series of simulations were conducted to examine the effects of the spatial variation of climate and the posterior distribution of the parameter on the estimated C accumulation rates and

stocks. Twenty sets of parameters were randomly drawn from the posterior parameter space. All pixels in the study area were then assigned with the same climate forcing data which were random combinations between temperature and precipitation.

To quantify the uncertainty ranges of the regional C stock simulations resulting from both the parameterization and the climate spatial interpolation, 20 sets of parameters were randomly drawn from the posterior distributions respectively for three different peatland ecosystem types (PF, PS, and OP). Based on the randomly selected parameters, all pixels in the study area were assigned with the same climate forcing data which were random combinations between temperature and precipitation, both within their uncertainty ranges from interpolation (mean temperature (25-29℃) and precipitation (2200-2900 mm) (Figure 4.4)). We next conducted the regional simulation to obtain the uncertainty ranges of the simulated C stocks.

Table 4.3. Description of peatland sites used for establishing basal ages for pole forest, palm swamp, and open peatland. The basal ages were taken from Lähteenoja et al (2009a) and Lähteenoja et al (2012), whereas the other values were from the online supplementary material (table 1) of Draper et al (2014).

Site	Long (°W)	Lat (°S)	Basal age (cal year BP)	Mean bulk density (g cm^{-3})	Mean peat thickness (m)	Mean C content (%)	Mean basal age (cal year BP)
Pole forests							~4000
Aucayacu (forested)	74.384	3.935	8870±110	0.108	4.63	49	
San Jorge (*M. flexuosa* palm swamp and forested)	73.189	4.058	2945±65	0.112	2.92	44	
Roca Fuerte (forested)	74.823	4.436	5170±120	0.073	3.82	52	
Palm swamps							~2000
Quistococha (*M. flexuosa* palm swamp and forested)	73.318	3.837	2335±15	0.095	2.44	47	
Charo (Mixed *M. flexuosa* palm swamp)	73.254	4.270	672±12.5	-	1.26	-	
Buena Vista del Maquia (*M. flexuosa* palm swamp)	74.720	6.207	-	0.088	1.21	38	
San Roque (*M. flexuosa* palm swamp)	74.622	4.540	7705±35	0.161	3.53	42	
Open peatlands							~1600
Riñón (open savanna)	74.001	4.900	1615±75	0.06	3.55	49	
Maquía (open, scattered *M. flexuosa* palm swamp)	74.808	6.323	1975±30	0.074	3.88	44	

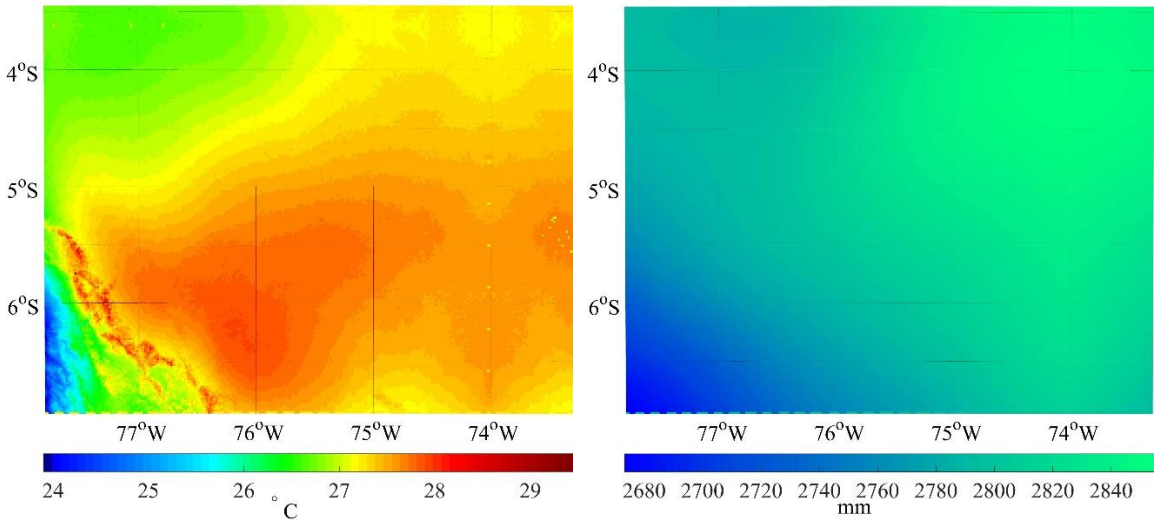

Figure 4.4. Interpolated (a) mean temperature and (b) mean annual precipitation distribution from 4 ka to 2014 AD of the study area.

4.3 Results and Discussion

4.3.1 Past C Accumulation

The annual comparison between model simulation and measurements (Lähteenoja et al., 2012) at a temporal resolution of a year at the thickest and largest Amazonian peatland site (Aucayacu site) reveals that our model captures the historic peat SOC accumulation rates (Figure 4.5a) and the peat depth profile (Figure 4.5b) for most simulation periods, but overestimates the rates between 8 and 6 ka. Simulated total depth reaches 8 m (ranging 6-12 m), slightly higher than the measured 7.5 m. The correlation between simulations and measurements using 500-year bins at multiple sites with different vegetation types indicates that the model well estimates SOC accumulation trajectories at millennial time scales (Figure 4.2). The model underestimates the rates between 3 and 2 ka at San Jorge, and between 0.5 and 0 ka at Charo. Although the model underestimates the rates between 2 and 1.5 ka at Rinon (an open peatland site), the starting basal age for the regional transient simulation for the open peatlands is at 1.6 ka. As indicated by the mean basal age applied in the model, pole forest (PF) has a longer SOC accumulation period

than palm swamp (PS) and open peatland (OP) in general (Figure 4.2), with peat initiation of PF around 2000 years ahead of PS and OP peat initiation.

Our simulation suggests there were strong relationships between peat C dynamics and climatic change. Temporally, temperature and photosynthetically active radiation (PAR) rose slightly over the whole period (Figure 4.3a and e), whereas annual precipitation decreased before 4 ka and subsequently increased (Figure 4.3c). Under increasingly warmer and drier conditions before 4 ka, the historic SOC accumulation rate declined at the Aucayacu site. It started to increase concurrently with the wetter conditions after 3.5 ka (close to 4 ka), despite continuing warming. Overall, the historic SOC accumulation rates of the Aucayacu peat core followed the historic pattern of the precipitation change (Figure 4.3c). This suggests that higher rainfall might have accelerated while warming and drought might have decelerated peat SOC accumulation at millennial time scales.

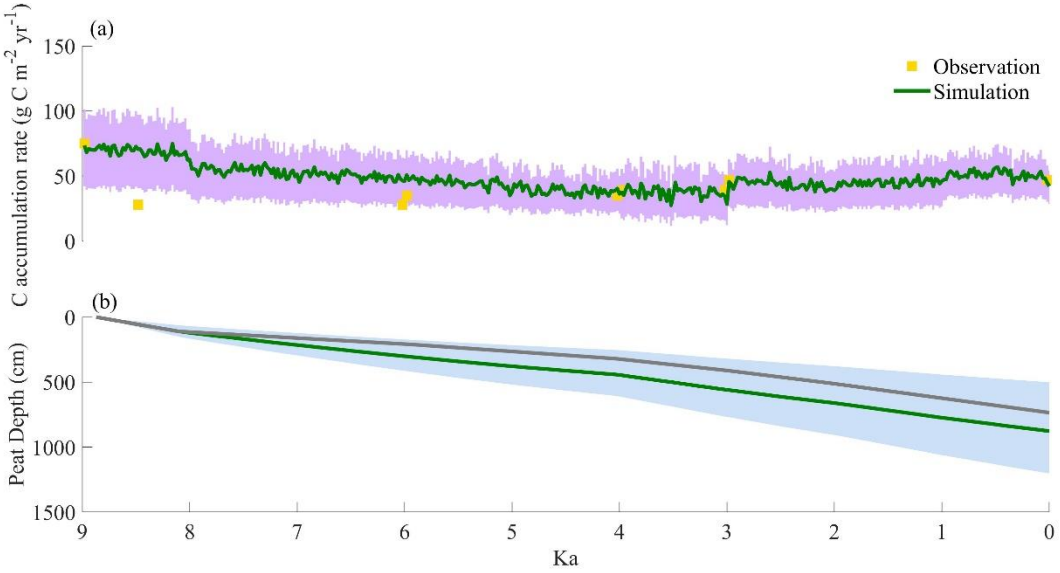

Figure 4.5. Comparison between simulation and measurement at the Aucayacu site. (a) SOC accumulation rates and (b) peat depth. Shaded areas represent the range due to uncertainties from the posterior distributions of the parameters after the parameterization. 0 cm at ~9 ka indicates no peat accumulation.

Spatially, this relationship between the peat SOC accumulation and climate was indicated by the patterns of the peat SOC densities distribution and mean historic temperature and precipitation within the PMFB (Figures 4.6 and 4.4). We find that the highest peat SOC density region fell in the northeast with the highest precipitation and relatively low temperature. The secondary highest peat SOC region was located in the northwest with moderate precipitation but the lowest temperature. The lowest peat SOC zone fell within the southwest where the lowest precipitation and highest temperature coincided. This, again, suggests that higher precipitation increased whereas higher temperature reduced peat SOC accumulation at regional scales.

The climatic effects on the long-term peat SOC accumulation in the PMFB can be explained by our simulated C fluxes and hydrological factors. Peat accumulated SOC where the rate of soil C input was higher than the decomposition (Loisel et al., 2012). Soil C input from litters was largely controlled by and was proportional to plant net primary productivity (NPP). Soil decomposition was modeled as heterotrophic respiration (R_H) (Yu et al., 2009). Increasing temperature and PAR stimulated the plant C uptake by increasing NPP. However, warming might have created favorable conditions for microbial decomposition (Nobrega et al., 2007). Warming also increased the evapotranspiration, decreasing water table, thereby reducing anaerobic respiration and increasing aerobic respiration (Hobbie et al., 2000). Increasing precipitation had a positive effect on NPP. It also lifted the water table and decreased R_H. This, in turn, enhanced peat C accumulation. In our previous study for the northern (Alaskan) peatlands (Wang et al., 2016b), under the warmer conditions, the stimulation of NPP exceeded the stimulation of R_H, thereby increasing SOC accumulation in northern peatlands during the Holocene Thermal Maximum (HTM). Similarly, we find that R_H within 1 m depth followed the increasing trend of temperature with a decrease at 4 ka when precipitation increased (Figure 4.7).

This suggests that warmer condition in the PMFB enhances R_H while wetter condition decreases R_H. The volumetric soil moisture (VSM) (Figure 4.7c) and water table (Figure 4.7d) started decreasing at 8 ka as precipitation became lower. At the same time, R_H kept increasing under such drier condition. Interestingly, when climate became wetter at ~4 ka (Figure 4.3c), the VSM abruptly increased. The water table also stopped dropping and showed an increase pattern. Meanwhile, R_H started decreasing. This again suggests that higher precipitation may decrease R_H and thus slows the peat SOC decomposition by increasing the soil moisture and raising the water table. As warming continued, the continuing increase of VSM and water table resulting from the wetter condition became slight, presumably due to the enhanced evapotranspiration from warming.

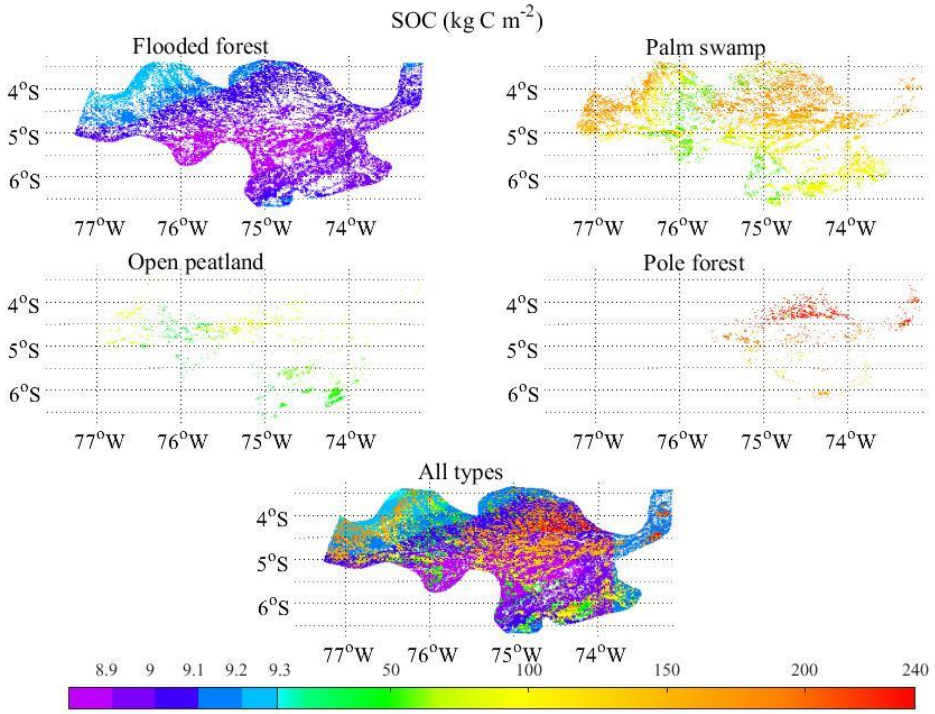

Figure 4.6. Current (2014 AD) SOC density of flooded forest, palm swamp, open peatland, pole forest and their combination in the PMFB.

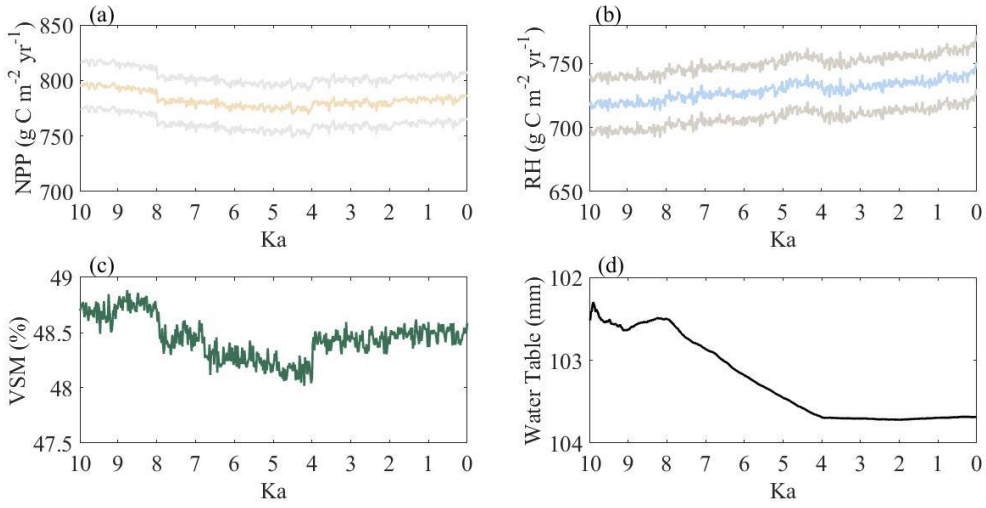

Figure 4.7. Simulated (a) net primary production (NPP), (b) heterotrophic (aerobic+anaerobic) respiration (R_H), (c) volumetric soil moisture (VSM), and (d) water-table depth (WTD) at Aucayacu from 10 ka to 2014 AD (based on averages of 20 years). Grey lines in (a) and (b) indicate the upper and lower uncertainty range resulting from the Bayesian inference.

To examine how temperature and precipitation have impacted NPP in this region. The attributions of these two key drivers and soil water content to NPP for both historical periods and the 21st century were analyzed with the Analysis of Variance table (ANOVA) and the F-test of the multi-variate linear regression between annual mean NPP and climate variables. For the historical simulation at Aucayacu site, we find that, although higher precipitation and higher temperature increase the NPP (Tables 4.4 and 4.5), those two factors have limited effects presumably because the temperature exceeds the optimum temperature for photosynthesis and soil water content is already suitable for plant growth. The variable with the highest importance is VSM, indicating the hydrological condition plays the most important role in determining the NPP. Such hydrological condition is modeled by various factors including the temperature, precipitation, solar radiation and others such as soil porosity, soil layers characteristics that are described in our previous hydrological modeling studies (Wang et al., 2016a).

Our historical simulations at Aucayacu and in the PMFB suggest that NPP was consistent with the temporal patterns of precipitation and VSM (Figure 4.3). The spatial correlations between NPP, vegetation C density, and mean historic precipitation were detected (SI Appendix, Figures 4.4b and 4.8) when observing each peatland vegetation type separately. Pixels with higher vegetation C density and NPP fell within the northeastern wetter region while lower vegetation C density and NPP pixels were in the southwestern drier region. Our explanation is that during the historical period, the point where NPP will no longer positively respond to the increasing precipitation and VSM has not been reached. Still, the wetter condition stimulates the SOC accumulation by increasing NPP and decreasing R_H. However, for the simulations under three future climate scenarios (Table 4.6), we find that the F values of the precipitation started decreasing as the precipitation continued to be higher from RCP 2.6 to 8.5. This suggests that precipitation becomes less and less important in the future for NPP as it increases, based on the existing suitable hydrological condition.

Table 4.4. Analysis of variance table (ANOVA) of the multi-variate linear regression between annual mean NPP and climate variables for the historical simulation at Aucayacu site.

Source	Sum of Squares	Degree of Freedom	F-value	Pr (>F)
Annual Temperature (℃)	15.785142	1.0	18.117638	2.095649e-05
Annual Precipitation (mm)	18.340884	1.0	21.051029	4.526578e-06
Annual Volumetric Soil Moisture (VSM, %)	372.013772	1.0	426.984481	6.340108e-93
Temperature×Precipitation	17.451831	1.0	20.030605	7.705596e-06
Residual	8708.226683	9995.0		

Table 4.5. The coefficients, standard errors, and the 95% confident intervals of the parameters in the regression model (without feature normalization).

	Coefficient	Standard Error	95% CI
Intercept	-67.9910	23.792	**(**-114.628, -21.354)
Annual Temperature (℃)	3.7166	0.873	**(**2.005, 5.428)
Annual Precipitation (mm)	0.4696	0.102	**(**0.269, 0.670)
Annual Volumetric Soil Moisture (VSM, %)	0.6014	0.029	**(**0.544, 0.658)
Temperature×Precipitation	-0.0168	0.004	**(**-0.024, -0.009)

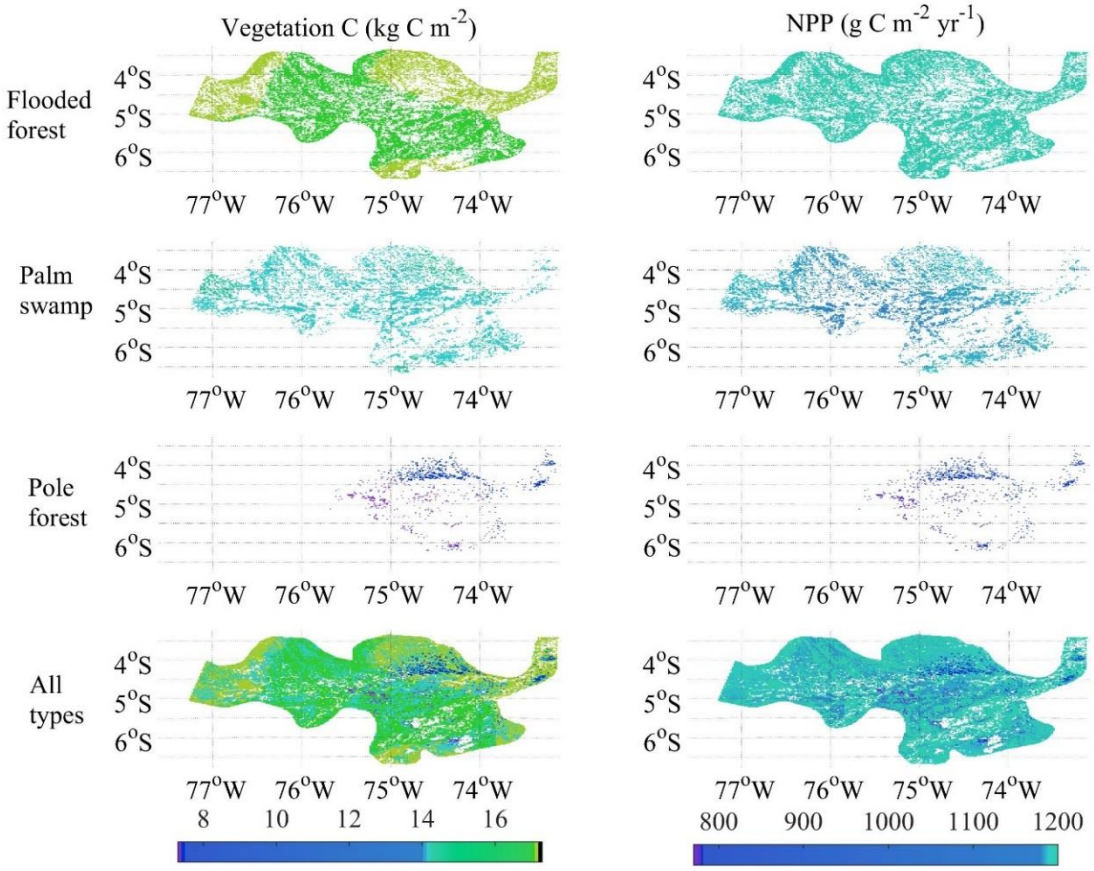

Figure 4.8. Current (2014 AD) vegetation C (above+belowground) density and mean historic NPP of flooded forest, palm swamp, pole forest and their combination in the PMFB. NPP is the average from 4 ka to 2014 AD. Open peatlands with minimal vegetation C and NPP are not shown.

Table 4.6. Analysis of variance table (ANOVA) of the multi-variate linear regression between annual mean NPP and climate variables (Annual temperature and precipitation) in RCP 2.6, RCP 4.5, and RCP 8.5 scenarios. F-value indicates the importance of each climate variable.

Scenarios	Source	F-value
RCP 2.6	Annual Temperature (℃)	15.498204
	Annual Precipitation (mm)	17.902754
RCP 4.5	Annual Temperature (℃)	12.099724
	Annual Precipitation (mm)	11.833428
RCP 8.5	Annual Temperature (℃)	7.323143
	Annual Precipitation (mm)	8.410239

In our model, GPP is a function of atmospheric CO_2 concentrations in addition to physical variables. The CO_2 effects is modeled with a Michaelis-Menten equation considering

CO_2 concentrations inside leaves which is assumed to be directly proportional to atmospheric CO_2 concentrations when stomata are fully open. When moisture is a limiting factor, the limitation on CO_2 assimilation is modeled by the modifying the conductance of leaves to CO_2 diffusion. The moisture availability is expressed as the ratio of actual evapotranspiration (*EET*) to potential evapotranspiration (*PET*). The relationship between CO_2 concentration inside stomatal cavities (C_i) and in the atmosphere (C_a) is proportional to relative moisture availability:

$$G_V = 0.1 + (\frac{0.9EET}{PET})$$

$$C_i = G_V C_a$$

where G_V is a unitless multiplier that accounts for changes in leaf conductivity to CO_2 resulting from changes in moisture availability. When there is sufficient water in soils, *EET* will not be limited by water, which will reach its maximum value, GV is close to 1. This suggests that inside of leaves CO_2 will be close to ambient CO_2. When the ecosystem has sufficient precipitation, GPP and NPP will not respond to increasing precipitation.

At northern high latitudes, in addition to CO_2 fertilization effects, warming also enhances photosynthesis, stimulating plant productivity (NPP) and thus increasing SOC accumulation (Yu et al., 2009; Davidson and Janssens, 2006; Jones and Yu, 2010; Yu et al., 2010). In contrast, warming in the tropical regions generally led to temperatures above the optimum level for photosynthesis (Jenkinson et al., 1991; Cox et al., 2002), which is also suggested by the ANOVA analysis (SI Appendix, Tables 4.4 and 4.6) as increasing temperature in the future has less and less positive effects on NPP. Increasing temperature accelerates R_H, however, at the same time. The less sensitivity of NPP versus R_H to warming might ultimately result in the SOC loss in the PMFB under warmer conditions.

4.3.2 Current C stocks

Overall, model simulations of current peatland C stocks are comparable to the field measurements (Draper et al., 2014). Specifically, PF has the SOC density of 1900 $Mg\ C\ ha^{-1}$, consistent with the field measurements (800-2200 $Mg\ C\ ha^{-1}$, SI Appendix, Fig S6a)[13]. PS has the next highest SOC density (1100 $Mg\ C\ ha^{-1}$), which is sufficiently within the measured range of 300-1390 $Mg\ C\ ha^{-1}$. The SOC density of OP is 535 $Mg\ C\ ha^{-1}$, also within the measured 392-1492 $Mg\ C\ ha^{-1}$. The high SOC density of PF corresponds to the longer SOC accumulation period compared to the other types (Figures 4.2a, b and 4.9a). Our simulations are even closer to the field measurements[13] when vegetation C density was examined (Figure 4.9b). The simulated lowest vegetation C density was in PF (86 $Mg\ C\ ha^{-1}$) and within the measured range of 80-100 $Mg\ C\ ha^{-1}$.

The model estimates a total SOC of 3.922 (2.208~5.777) Pg in the PMFB including 3.519 (1.833~5.344) Pg in the peatland soils, which is higher than the measured total peat SOC, 2.844 Pg (Table 4.7). The simulated vegetation C stock of 1.104 (1.097~1.137) Pg with 0.34 (0.338~0.369) Pg on the PMFB peatlands is also higher than the measured value (0.293 Pg C). Our model may overestimate the soil and vegetation C stocks. The uncertainty of the simulated C stocks is mainly due to the spatial variations of the interpolated mean temperature (25-29℃) and precipitation (2200-2900 mm).

Our uncertainty analysis suggests that the uncertainty of the simulated past C accumulation rates was mainly due to parameters, spatial variations of climate variables (Figure 4.4), and the uncertain peat basal ages (Table 4.3). Specifically, using the mean peat basal age by averaging the basal ages of peat samples for each peatland type is a top uncertainty source. The

variation of peat characteristics (e.g., bulk density, C content, peat depth) and limited number of samples are also sources of the uncertainty.

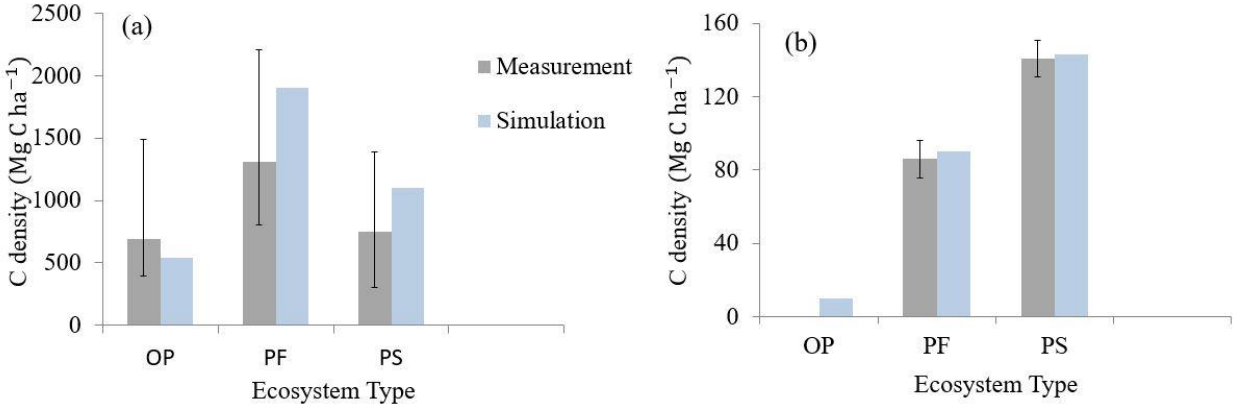

Figure 4.9. Simulated density of (a) SOC and (b) vegetation C for pole forest (PF), palm swamp (PS), and open peatland (OP) versus field measurements of[4]. A ratio of 0.473 was used to convert vegetation biomass to C (Raich et al., 1991; Martin and Thomas, 2011). A ratio of 0.39 was used to obtain belowground biomass given aboveground live biomass for PF (Houghton et al., 2001). A ratio of 0.41 was used to obtain the belowground biomass given aboveground live biomass for PS (Goodman et al., 2013). OP has no measurement of vegetation C density.

Table 4. 7. Simulated and field-measured total C stocks of SOC and vegetation C for pole forest, palm swamps, open peatlands, non-peatland (flooded forest), and the totals in the PMFB. Values in the columns "Measurement" refer to values from Draper et al (2014), whereas values in the columns "Simulation" refer to the results obtained from the P-TEM. The uncertainty ranges of the "simulation" are from the uncertainty of the parameterization plus the uncertainty from the climate data interpolation.

Ecosystem type		Area (km^2)		Soil organic C (Pg)		Vegetation C (Pg)		Total C stock (Pg)	
		Simulation	Measurement	Simulation	Measurement	Simulation	Measurement	Simulation	Measurement
Pole forest	Mean	2909	3686	0.511	0.494	0.0216	0.030	0.532	0.524
	Range	-	±810	0.269-0.646	0.110-1.131	0.0215-0.0218	0.009-0.074	0.316-0.723	0.138-1.174
Palm swamps	Mean	25069	27732	2.779	2.073	0.318	0.263	3.097	2.336
	Range	-	±1101	1.459-4.376	0.012-5.738	0.316-0.349	0.138-0.355	1.775-4.725	0.268-5.997
Open peatlands	Mean	3915	4181	0.229	0.277	~0	0	0.229	0.277
	Range	-	±222	0.105-0.322	0.034-0.974	~0	0	0.105-0.322	0.034-0.974
Non-peatland	Mean	47429	-	0.403	-	0.764	-	1.167	-
	Range	-	-	0.375-0.433	-	0.759-0.768	-	1.134-1.201	-
Total (peatlands)	Mean	31893	35600	3.519	2.844	0.34	0.293	3.859	3.137
	Range	-	±2133	1.833-5.344	-	0.338-0.369	-	2.171-5.713	0.440-8.145
Total (peatlands+non-peatland)	Mean	79322	-	3.922	-	1.104	-	5.026	-
	Range	-	-	2.208-5.777	-	1.097-1.137	-	3.305-6.914	-

4.3.3 Future Projection

Under the RCP 2.6 scenario, the SOC accumulation rate in all ecosystem types within the PMFB decreases from current 16 (9~24) to 7.9 (4.3~12.2) g C m^{-2} yr^{-1} and the SOC accumulation rate in the peatlands dramatically decreases from 56 (29~85) to 23 (15~32) g C m^{-2} yr^{-1} (Table 4.8). The PS exhibits the biggest drop from 65 to 26 g C m^{-2} yr^{-1}. Spatially, the majority of pixels within the PMFB have positive SOC accumulation and vegetation C change, but some areas with PS have SOC loss (Figures 4.10 and 4.11). Overall, 0.067 (0.037~0.108) Pg SOC, including 0.06 (0.03~0.1) Pg SOC in the peatlands, will be accumulated in the PMFB by the end of the 21st century under moderately warmer and wetter conditions of this climate scenario (Table 4.8). There will be 0.0148 Pg C accumulated in vegetation, including 0.0048 Pg C in peatland vegetation.

Under the RCP 8.5 scenario, the SOC accumulation rate declines from 16 to -53 (-67~-41) C m^{-2} yr^{-1} and the rate in peatlands declines from 56 to -123 (-152~-91) C m^{-2} yr^{-1}. Again, the highest decline of the rate is for PS, from 65 to -135 g C m^{-2} yr^{-1}. The pixels with SOC and vegetation C loss dominate the region (Figures 4.10 and 4.11). Under this climate scenario, the PMFB will act as a C source of 0.413 (0.319~0.518) Pg C by 2100 AD. Peatlands will lose 0.31 (0.23~0.38) Pg C compared with 0.1 Pg C loss from non-peatland ecosystems. Vegetation will lose 0.07 Pg C, including 0.02 Pg C from peatland vegetation. Among all peatland ecosystem types, PS could be severely affected by the climate due to its large area within the PMFB and within the whole Amazon Basin (Ruokolainen et al., 2001). It must be taken into account that the tendency of the model to overestimate the current soil and vegetation C stocks in the PMFB might affect these values to some extent.

Under the intermediate RCP 4.5 scenario, the SOC accumulation rate declines from 16 to -19 $\mathrm{C\ m^{-2}\ yr^{-1}}$ and the SOC accumulation rate in peatlands declines from 56 to -45 $\mathrm{C\ m^{-2}\ yr^{-1}}$. Peatlands will lose 0.12 Pg C compared with 0.034 Pg C from non-peatlands.

Three extra simulations were conducted as sensitivity tests to examine the effects of potential drier climate in the PFMB on SOC accumulation rates. We assume that (1) The future precipitation will decrease 5% in our study region over the century, but holding air temperature change as in the original RCP 2.6; (2) The future precipitation will decrease 10% but holding air temperature change as in RCP 4.5; (3) The future precipitation will decrease 15% but holding air temperature change as in RCP 8.5. The precipitation was manually decreased at monthly step for each grid cell from 2014 to 2100 AD to achieve the certain percentage total reduction at the end of 2100 AD. Our simulations show that the C accumulations are +0.027 (0.02~0.068), -0.203 (-0.349~-0.167), and -0.594 (-0.731~-0.51) Pg C under the three sensitivity simulations. These extra simulations suggest that the slightly drier condition will decrease but will not have significant effects on the C accumulation in this region.

The modeled current C stocks agree with the field observations at the Aucayacu site, which is a PF site. However, instead of PF, PS is the dominant peatland type in the study area and its SOC accumulation rates at Charo site is underestimated. Thus, using PS as representative peatland types for regional simulations under future climate scenarios may evolve uncertainty due to the underestimation during the parameterization.

Table 4.8. Current soil organic C accumulation rates, soil and vegetation C stocks and their changes in the PMFB from 2014 to 2100 AD in RCP 2.6 and RCP 8.5 scenarios (see RCP 4.5 in Future Projection section in the main text). Current soil organic accumulation rates are mean rates and uncertainty ranges over the simulation periods till 2014 AD and total rates are area-weighted means. The uncertainty ranges of the "simulation" are from the uncertainty of the parameterization plus the uncertainty from the climate data interpolation. "+" and "-" in soil organic C and vegetation C columns indicate C accumulation and loss in the from 2014 AD to 2100 AD. "-5%" and "-15%" in sensitivity tests indicate 5% and 15% annual precipitation reduction by 2100 AD under RCP 2.6 and RCP 8.5.

Ecosystem type		**Soil C accumulation rates (g C m^{-2} yr^{-1})**			**Soil organic C (Pg)**			**Vegetation C (Pg)**		
		Current	RCP 2.6	RCP 8.5	Current	RCP 2.6	RCP 8.5	Current	RCP 2.6	RCP 8.5
Pole forest	Mean	15.02	11.88	-89.95	0.511	+0.003	-0.023	0.022	+0.0004	-0.0021
	Range	7.9-18.9	6.3-14.5	-135.3,-56.7	0.269-0.646	0.0016-0.0037	-0.035,-0.015	0.0215-0.0218		
Palm swamps	Mean	64.69	26.09	-135.23	2.779	+0.052	-0.264	0.318	+0.0044	-0.02
	Range	34-101.8	15.2-43.9	-160.4,-102	1.459-4.376	0.03-0.09	-0.313,-0.199	0.316-0.349		
Open peatlands	Mean	29.53	14.69	-63.84	0.229	+0.005	-0.022	~0	~0	~0
	Range	13.5-41.5	8-17.3	-98.2,-40.9	0.105-0.322	0.0027-0.0059	-0.034,-0.014	~0		
Non-peatland	Mean	0.1	1.64	-25.22	0.403	+0.007	-0.104	0.764	+0.01	-0.0482
	Range	0.09-0.11	1.54-1.76	-32.8,-22.1	0.375-0.433	0.0066-0.0075	-0.136,-0.091	0.759-0.768		
Total (peatlands)	Mean	55.98	23.42	-122.7	3.519	+0.06	-0.309	0.34	+0.0048	-0.0221
	Range	29.1-85	14.9-31.5	-151.7,-90.5	1.833-5.344	0.03-0.1	-0.382,-0.228	0.338-0.369		
Peatlands+non-peatland	Mean	16.08	7.89	-53.25	3.922	+0.067	-0.413	1.104	+0.0148	-0.0703
	Range	9.1-23.7	4.3-12.2	-66.82,-41.2	2.208-5.777	0.037-0.108	-0.518,-0.319	1.097-1.137		
Sensitivity tests		**Soil C accumulation rates (g C m^{-2} yr^{-1})**			**Soil organic C (Pg)**			**Vegetation C (Pg)**		
		Current	-5%	-15%	Current	-5%	-15%	Current	-5%	-15%
Peatlands	Mean	55.98	13.92	-163.13	3.519	+0.03	-0.425	0.34	+0.0043	-0.0257
	Range	29.1-85	8.9-18.86	-205.1,-146	1.833-5.344	0.01-0.6	-0.544-0.398	0.338-0.369		
Peatlands+non-peatland	Mean	16.08	4.45	-76.75	3.922	+0.027	-0.594	1.104	+0.0124	-0.0758
	Range	9.1-23.7	2.3-7.91	-94.33,-65.8	2.208-5.777	0.02-0.068	-0.731,-0.51	1.097-1.137		

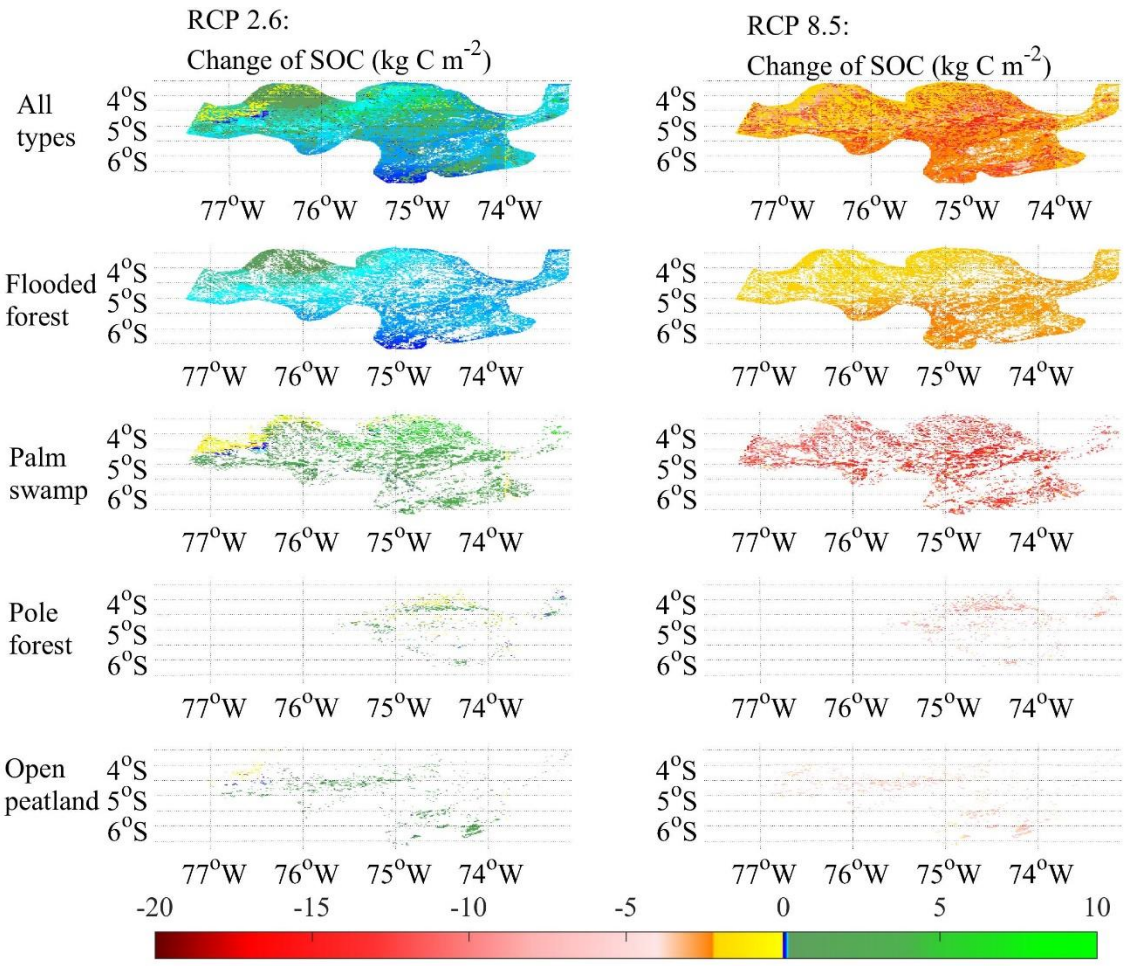

Figure 4.10. Changes of SOC density from 2014 to 2100 AD under RCP 2.6 and RCP 8.5 future climate scenarios in flooded forest, palm swamp, pole forest, open peatland, and their combination in the PMFB. Blue and green represent the SOC accumulation. Yellow and red represent the SOC loss.

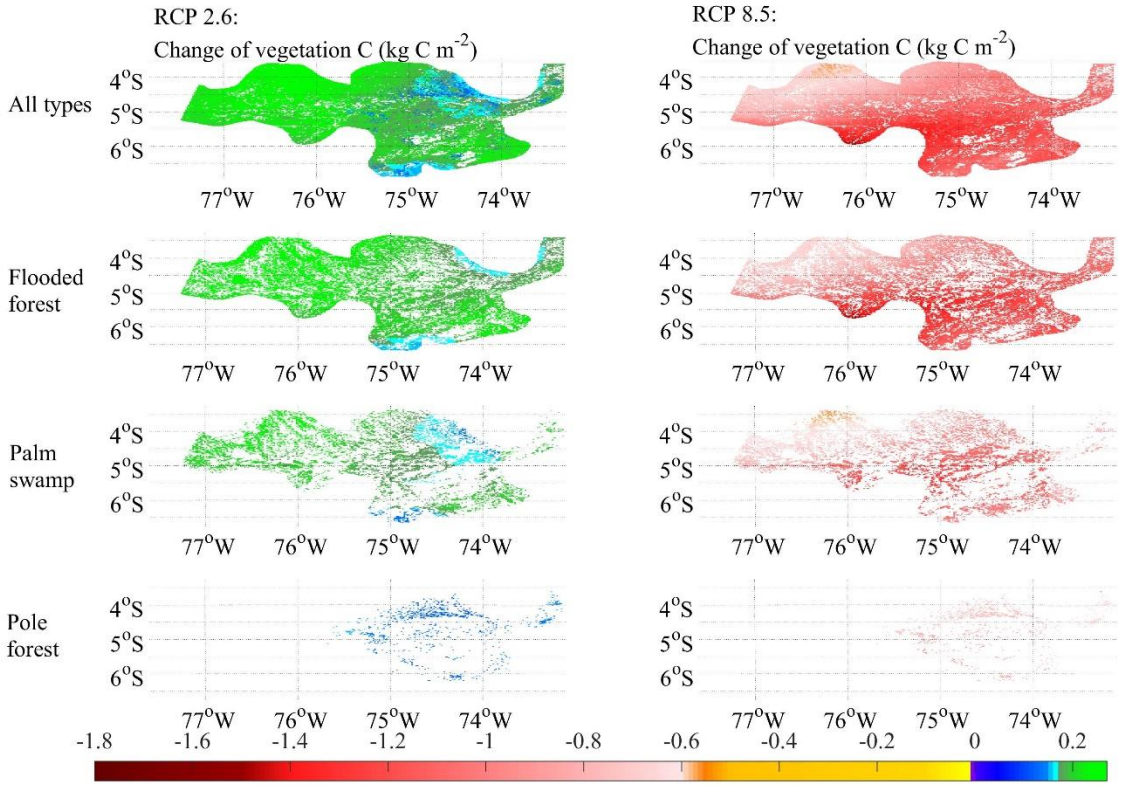

Figure 4.11. Changes of vegetation C (above+belowground) density from 2014 to 2100 AD under RCP 2.6 and RCP 8.5 future climate scenarios of flooded forest, palm swamp, pole forest, and their combination in the PMFB. Open peatlands with minimal vegetation C and NPP are not shown. Blue and green represent the vegetation C accumulation. Yellow and red represent the vegetation C loss.

4.4 Conclusions

In conclusion, the warming in the 21st century may weaken the C sink function of the Amazonian peatlands in the PMFB or may entirely switch them from a long-term carbon sink into a source, depending on the severity of the warming. The same has also been predicted for the Amazonian rainforest in general. The vegetation and SOC density changes (future total C stock changes divided by the corresponding areas of peatlands and non-peatland) were calculated to compare with other studies. Our model estimation of vegetation C change for the non-peatland (mainly flooded forest) ecosystem in the 21st century (+0.23~-1.17 kg C m^{-2}) is well within the range of other studies (+0.6~-1.2 kg C m^{-2}) on the future vegetation C change from Amazonian rainforest dieback (Table 4.9) (Cox et al., 2004; Rammig et al., 2010). Our estimation of SOC change for the non-peatland ecosystem in the 21st century (+0.18~-3.35 kg C m^{-2}) is also comparable to -3.88 kg C m^{-2} from other studies (Cox et al., 2004; Rammig et al., 2010). Further, we find that the ratio of SOC density changes for peatlands and non-peatland ecosystems in the next 100 years ranges from 3.9 to 5.8 (Table 4.9). This indicates that future warming is likely to affect the Amazonian peatlands more dramatically than non-peatland ecosystems, although the total area of peatlands is much smaller than that of non-peatland ecosystems within the PMFB (31000 km^2 vs. 47000 km^2). The high vulnerability of peatland ecosystems to future climate is presumably due to its large amount of existing SOC stock (3.5 Pg C) compared with non-peatland ecosystems (0.4 Pg C). Another possible reason is that, in addition to the non-linear function defining the volumetric soil moisture (VSM) effect on heterotrophic respiration within the unsaturated zone, there is also a linear relation between water-table depth and aerobic respiration in the model. Future warming increases evapotranspiration that subsequently decreases VSM and increases aerobic respiration for both peatland and non-peatland ecosystems. For peatlands, it further lowers the water table which, in turn, increases aerobic respiration. This

suggests that peatland ecosystems may suffer larger SOC decomposition under the changing climate and may help explain its vulnerability. In addition, increased land use change, expansion of commercial agriculture, transport infrastructure, and hydropower development form a threat to the persistence of the considerable C stock (Roucoux et al., 2017). The most carbon dense ecosystems of the whole Amazon basin may turn into C sources.

Acknowledgements: Author Contributions: Qianlai Zhuang and Sirui Wang conceived and designed the study; Sirui Wang, Outi Lähteenoja and Freddie Draper processed the data; Sirui Wang and Qianlai Zhuang drafted the paper; All authors contributed to the revision of the paper.

Table 4.9. Comparison between our model simulation of vegetation C density change and SOC density change in the 21st century for peatlands and non-peatland and other model simulations for forest dieback (non-peatland vegetation C and SOC density change) in northwestern Amazonia areas. The density changes are the total C stock changes (Table 4.8) divided by the corresponding area (Table 4.7) of peatlands and non-peatland ecosystems.

Models	Ecosystem type	Vegetation C density change (kg C m^{-2})	SOC density change (kg C m^{-2})	Ref
LPJmL	Non-peatland	+0.6~-1.2	~	*Ref. 26*
HadCM3 coupled with HadOCC and TRIFFID	Non-peatland	-9.49	-3.88	*Ref. 27*
P-TEM (RCP 2.6 and RCP 8.5)	Non-peatland	-0.45 (+0.23~--1.13)	**-1.55** (+0.18~-3.28)	
	Peatland	-0.34 (+0.19~-0.86)	**-6** (+3.15~-15.2)	
			$\frac{\textbf{Peatland}}{\textbf{Non peatland}} = \mathbf{3.9}$	
P-TEM (precipitation -5% and -15%)	Non-peatland	-0.49 (+0.19~-1.17)	**-1.61** (+0.13~--3.35)	
	Peatland	-0.42 (+0.17~--1)	**-9.31** (+1.89~-20.5)	
			$\frac{\textbf{Peatland}}{\textbf{Non peatland}} = \mathbf{5.8}$	

Ref 26: Cox et al., 2004; Ref 27: Rammig et al., 2010

CHAPTER 5. QUANTIFYING PEAT SOIL CARBON ACCUMULATION IN NORTH AMERICA DURING THE LAST 12,000 YEARS[4]

5.1. Introduction

Among all terrestrial ecosystems, peatlands form the largest reservoir of Soil Organic Carbon (SOC). Global peatlands cover approximately 3% (4 million km^2) of the land area on the planet, but sequester 400-600 Pg C (1 Pg C = 10^{15} g C) (Gorham, 1991, 1995; Clymo, 1998; Yu et al., 2010; Maltby and Immirzi, 1993). Peatlands accumulate carbon mainly because waterlogged soils decrease their carbon decomposition through anaerobic respiration. This favorable hydrological condition along with other climate factors allow carbon to accumulate in peatland ecosystems during the past several thousand years (Gorham et al., 2012; MacDonald et al., 2006; Jones and Yu, 2010; Turunen et al., 2002). As a result, northern peatlands have stored 200-455 Pg C (Harden et al., 1992; Kivinen and Pakarinen, 1981). Tropical and subtropical peatlands account for 15-19% (~88 Pg C) of the global peatlands SOC stock (Page et al., 2004, 2011).

Northern peatlands are largely located in Canada, Russia, Alaska and Fennoscandian countries (Lappalainen, 1996; Turunen et al., 2002) and have been acting as a long-term carbon dioxide (CO_2) sink and methane (CH_4) source during the Holocene period (Bridgham et al., 2006; Jones and Yu, 2010). As warming has been projected to continue in the 21st century, particularly in northern high-latitudes (IPCC, 2014), the climate trend could potentially modify, or shift the balance between peat SOC production and decomposition in the future (Frolking et al., 2011; Turunen et al., 2002; McGuire et al., 2009). Recent studies have focused on the mechanism of the responses of peatland carbon accumulation to climate change in the northern high-latitude regions using long-term carbon dating and modeling approaches (Dorrepaal et al.,

[4]**Wang, S**., Zhuang, Q., Aires, F., Prigent, C., Yu, Z., Keller, J., and Bridgham, S., Quantifying peat soil carbon accumulation in North America during the last 12,000 years, 2019 (To be submitted to JGR-Biogeoscience).

2009; Charman et al., 2013; Yu et al., 2009, 2012; Davidson and Janssens, 2006; Christensen and Christensen, 2007; Wang et al., 2016a, 2016b). Warming may lead to a greater Net Primary Productivity (NPP) and subsequently enhance peat SOC accumulation, but may also lead to an enhanced soil decomposition and evapotranspiration (Hobbie et al., 2000; Loisel et al., 2012; Yu et al., 2009). In contrast to the view that warming may slow the peat SOC accumulation (Dorrepaal et al., 2009), recent studies focusing on the peat SOC accumulation during the Holocene have indicated that higher temperature may stimulate the carbon accumulation at millennial timescales over the northern peatlands (Wang et al., 2016a, 2016b; Jones and Yu, 2010, Loisel et al., 2014). Other climate factors such as the seasonality of Photosynthetically Active Radiation (PAR), the seasonality of temperature, annual precipitation and the growing season length may also play an important role in controlling the carbon dynamics in northern peatlands (Jones and Yu, 2010; He et al., 2014; Wang et al., 2016a, 2016b).

Tropical and subtropical peatlands are mainly distributed in Southeast Asia (~56%, Page et al., 2004, 2011), and South and Central America (~23%, Lähteenoja et al., 2009a, 2009b). They are largely restricted to poorly drained coastal regions and inland fluvial plains (Gore, 1983; Maltby and Immirzi, 1993; Lähteenoja and Page, 2011). High evapotranspiration rate resulting from the warm air temperature could limit the waterlogged conditions and warm subsurface temperature increases the carbon decomposition, limiting the formation of peatlands in tropical and subtropical regions (Gore, 1983; Chapin et al., 2002; Davidson et al., 2000; Trumbore et al., 1996). Recent research suggests that the prevailing climate (Wang et al., 2018) along with the autogenic processes of peatlands (transition from minerotrophic to ombrotrophic conditions, Lähteenoja and Page, 2011) could be important factors affecting the tropical peat formation in the Amazon basin. Specifically. Wang et al (2018) suggests that warming

accelerates peat SOC loss while increasing precipitation stimulates peat SOC accumulation at millennial timescales. Under warmer and presumably wetter conditions over the 21st century, tropical peatlands are more likely to switch from a carbon sink to a carbon source. Further, SOC accumulation could also be largely controlled by non-climate factors such as the transition from minerotrophic to ombrotrophic conditions induced by the form and thickness of the peat deposit, and the active lateral migration of rivers (Lähteenoja and Page, 2011; Lähteenoja et al., 2012).

Studies have been conducted to advance the understanding of the peat carbon dynamics resulting from the climate and geological factors (Turunen et al., 2002; Roulet et al., 2007; Yu et al., 2009; Lähteenoja et al., 2009a, 2009b, 2012; Swindles et al., 2014; Kelly et al., 2017; Roucoux et al., 2013). However, the interaction between peat carbon accumulation and the climate change still remains difficult to assess (Loisel et al., 2012, 2014). The main reasons are: (1) the understanding of the mechanism of peatland responses to climate change is limited (Frolking et al., 2011; Loisel et al., 2014; Belyea, 2009), (2) there are data gaps and large uncertainties in regional peat SOC stocks using field measurements (Yu, 2012), and (3) few modeling studies have focused on peatland carbon dynamics (but see Spahni et al., 2013; Frolking et al., 2010; Kleinen et al., 2012).

In this study, a peatland terrestrial ecosystem model (P-TEM) was developed by coupling a hydrological module (HM), a soil thermal module (STM), a methane module (MDM), and a carbon and nitrogen module (CNDM) (Wang et al., 2016a,b, 2018). P-TEM has been parameterized and applied to estimate the regional peat carbon accumulation rates and current stocks in Alaska (northern peatlands) and in the Amazon basin (tropical peatlands) over the past several thousand years. Here, we parameterize and evaluate the model using long-term peat accumulation rate data at multiple sites in Alaska, Canada, the northern conterminous USA, and

the Florida Everglades. The model was then applied to simulate the peat SOC accumulation in the past 12,000 years and quantify the current peat SOC stocks in North America.

5.2. Methods

5.2.1 Model Framework

5.2.1.1 Peat Soil Organic Carbon Accumulation Rate

Peat SOC accumulation rate is determined by NPP and aerobic and anaerobic respiration based on the core carbon and nitrogen dynamic module (CNDM, Zhuang et al., 2003; Wang et al., 2016a). The net ecosystem production (NEP) for the peatland ecosystem is calculated at a monthly step:

$$\mathrm{NEP} = \mathrm{NPP} - R_H - R_{CH_4} - R_{CWM} - R_{CM} - R_{COM} \quad (1)$$

NPP is the monthly net primary production. R_H is the monthly aerobic respiration related to the variability of the water table depth, soil moisture, soil temperature, and soil organic C. R_{CH_4} is the monthly methane emission after methane oxidation. R_{CWM} represents the CO_2 emission due to methane oxidation (Zhuang et al., 2015). R_{CM} represents the CO_2 release related to the methanogenesis (Tang et al., 2010). R_{COM} represents the CO_2 release from other anaerobic processes (e.g., fermentation and terminal electron acceptor reduction, Keller and Bridgham, 2007).

5.2.1.2 Net Primary Production (NPP)

Gross primary production (GPP, see Raich et al. 1991 for details) is defined as the total assimilation of CO_2-C by plants, excluding photorespiration. GPP is modeled as a function of the irradiance of photosynthetically active radiation (PAR), atmospheric CO_2 concentrations, moisture

availability, mean air temperature, the relative photosynthetic capacity of the vegetation, and nitrogen availability:

$$\text{GPP} = (C_{max})\frac{PAR}{k_i+PAR}\frac{C_i}{k_c+C_i}f(PHENOLOGY)f(FOLIAGE)f(T)f(NA) \quad (2)$$

where C_{max} is the monthly maximum rate of C assimilation by the entire plant canopy under optimal environmental conditions (g m^{-2} $month^{-1}$); PAR is the irradiance of photosynthetically active radiation at canopy level (J cm^{-2} day^{-1}); k_i is the irradiance at which C assimilation proceeds at one-half its maximum rate; C_i is the concentration of CO_2 inside leaves (mL L^{-1}); k_c is the internal CO_2 concentration at which C assimilation proceeds at one-half its maximum rate. $f(PHENOLOGY)$ is monthly leaf area relative to leaf area during the month of maximum leaf area and depends on monthly estimated evapotranspiration (Raich et al., 1991). $f(FOLIAGE)$ is a scaling function that ranges from 0.0 to 1.0 and represents the ratio of canopy leaf biomass relative to maximum leaf biomass. T is monthly air temperature and NA is nitrogen availability. The function $f(NA)$ models the limiting effects of plant nitrogen status on GPP.

Plant (autotrophic) respiration (R_A, see Raich et al. 1991 for details) is the total respiration (excluding photorespiration), including all CO_2 production from the various processes of plant maintenance, nutrient uptake, and biomass construction. R_A is the sum of maintenance respiration (R_m), and growth respiration (R_g):

$$R_A = R_m + R_g \quad (3)$$

The maintenance respiration is modeled as a direct function of plant biomass (C_V).We assume that increasing temperatures increase maintenance respiration logarithmically with a Q_{10} of 2 over all temperatures:

$$R_m = K_r(C_V)e^{0.0693T} \quad (4)$$

where K_r is the respiration rate of the vegetation per unit of biomass carbon at 0℃ ($\mathrm{g\,g^{-1}\,month^{-1}}$), and T is the mean monthly air temperature (℃). Growth or construction respiration R_g is estimated to be 20% of the difference between GPP and R_m:

$$\mathrm{NPP'_t} = \mathrm{GPP_t} - R_{mt} \quad (5)$$

$$R_{gt} = 0.2\mathrm{NPP'_t} \quad (6)$$

where NPP′ is the potential net primary production assuming that the conversion efficiency of photosynthate to biomass is 100% and *t* refers to the monthly time step.

Net primary production (NPP) is the difference between GPP and autotrophic respiration (R_{At}):

$$\mathrm{NPP_t} = \mathrm{GPP_t} - R_{At} \quad (7)$$

where NPP is calibrated to correctly estimate annual NPP since monthly observed NPP do not exist for most vegetation types from the field measurements.

5.2.1.3 Aerobic Respiration Related to Water Table Depth (R_H)

SOC aerobic respiration related to the variability of water table depth (R_H) is calculated as:

$$R_H = K_d C_{s1} f(M_V) e^{0.069 H_T} \frac{WTD}{LWB} \quad (8)$$

where M_V represents the mean monthly soil water content (percentage of saturation) in the peat unsaturated zone above the water table depth (*WTD*). K_d is a logarithm of heterotrophic rate at 0℃. H_T is the mean monthly temperature of the soil above the lowest water table boundary (*LWB*, a fixed parameter, the soil below which is set saturated, Granberg et al., 1999). The SOC between *LWB* and soil surface (C_{s1}) in the transient simulation is obtained after a 2000-year equilibrium run.

5.2.1.4 R_{CH_4}, R_{CWM}, R_{CM}, and R_{COM}

R_{CH_4} represents the monthly methane emission after methane oxidation (see Zhuang et al (2004) for details):

$$R_{CH_4} = M_P - M_O \qquad (9)$$

where M_P is the monthly methane production /methanogenesis and M_O is the monthly methane oxidation.

M_P is modeled as an anaerobic process that occurs in the saturated zone of the soil profile. It is calculated as the integration of the hourly methanogenesis ($M_P(z,t)$) at each 1-cm layer:

$$M_P = \int_{t=1}^{24\times30} \int_{z=1}^{100} M_P(z,t)\, dtdz \qquad (10)$$

where

$$M_P(z,t) = M_{G0} f\big(S_{OM}(z,t)\big) f\big(M_{ST}(z,t)\big) f\big(pH(z,t)\big) f(R_X(z,t)) \quad (11)$$

M_{G0} is the ecosystem-specific maximum potential production rate. $f\big(S_{OM}(z,t)\big)$ is a multiplier that enhances methanogenesis with increasing methanogenic substrate availability, which is a function of net primary production of the overlying vegetation. $f\big(M_{ST}(z,t)\big)$ is a multiplier that enhances methanogenesis with increasing soil temperatures. $f\big(pH(z,t)\big)$ is a multiplier that diminishes methanogenesis if the soil-water pH is not optimal (i.e., pH=7.5, a constant in the model). $f(R_X(z,t))$ is a multiplier that describes the effects of the availability of electron acceptors which is related to redox potential on methanogenesis.

M_O is modeled as the integration of hourly methane oxidation rate ($M_O(z,t)$) at each 1-cm layer:

$$M_O = \int_{t=1}^{24\times30} \int_{z=1}^{100} M_O(z,t)\, dtdz \qquad (12)$$

where

$$M_O(z,t) = O_{MAX} f\big(C_M(z,t)\big) f\big(T_{SOIL}(z,t)\big) f\big(E_{SM}(z,t)\big) f(R_{OX}(z,t)) \qquad (13)$$

O_{MAX} is the ecosystem-specific maximum oxidation coefficient; $f\big(C_M(z,t)\big)$ is a multiplier that enhances methanotrophy with increasing soil methane concentrations; $f\big(T_{SOIL}(z,t)\big)$ is a multiplier that enhances methanotrophy with increasing soil temperatures; $f\big(E_{SM}(z,t)\big)$ is a multiplier that diminishes methanotrophy if the soil moisture is not at an optimum level; and $f(R_{OX}(z,t))$ is a multiplier that enhances methanotrophy as redox potentials increase.

R_{CWM} is the CO_2 emission due to methane oxidation; R_{CM} is the CO_2 release accompanied with methanogenesis. We assume the same amount of CO_2 is released along with the methane production (M_P). R_{COM} is the CO_2 release from other anaerobic processes. We assume R_{com}/R_{CH4}=5.

5.2.2 Model Parameterization

Key parameters of the individual modules, including HM, STM, and MDM have been parameterized in our previous studies of northern peatlands and tropical peatlands (see Wang et al., 2016a, 2018 for details). Here, we re-adjusted those key parameters (Table 5.1) based on the annual C fluxes and pools at multiple sites of northern and subtropical peatlands. We first conducted the initial Monte Carlo simulations to get the proper prior range of the parameter space for peatland ecosystems based on the original parameter space obtained from the parameterization in our previous studies. Annual C fluxes and pools taken from two sites in Alaska (APEXCON and APEXPER) were used to obtain the prior distribution for northern peatlands during the initial parameterization (Table 5.2). Annual C fluxes and pools taken from the large Shark River Slough (SRS) basin and the Taylor River/C-111/Florida Bay Basin (TS/Ph) in South Florida were used to obtain the prior distribution for subtropical peatlands in the Great Everglades and other coastal regions (Table 5.2). A Latin Hypercube Sampler (Iman et al., 1988) was applied to draw 5000 sets

of parameters from their uniform distributions. The model was then driven by the climate data (Figure 5.1) from 1900 to 1990 AD. We averaged the simulated monthly C fluxes and pools (aboveground NPP, annual belowground NPP, annual total NPP, aboveground vegetation carbon, belowground vegetation carbon, and total vegetation carbon) to annual values and then averaged them from 1900 to 1990 AD. All parameter sets were selected based on which the simulated annual C fluxes and pools are within the uncertainty ranges of the field measurements (Table 5.3). The prior distribution of *Sphagnum* open fen and *Sphagnum* black spruce bog were then merged to represent the prior distribution for northern peatlands. Similarly, the prior distribution of sawgrass swamp and mangrove tree island were merged to represent the prior distribution for subtropical peatlands.

To select the highest plausible sets of parameters, a Bayes' framework was applied (see Tang and Zhuang (2009) for details):

$$P(\boldsymbol{\theta}|\mathbf{V}) \propto P(\mathbf{V}|\boldsymbol{\theta})P(\boldsymbol{\theta}) \quad (14)$$

where $P(\boldsymbol{\theta}|\mathbf{V})$ is the posterior after the Bayesian inference conditioned on the available field measurements $\mathbf{V}$. $\boldsymbol{\theta}$ is the matrix of the parameters for adjustment. $\mathbf{V}$ is the difference matrix between the Monte Carlo simulations and the corresponding field measurements. $P(\boldsymbol{\theta})$ is the prior distribution for peatland ecosystems obtained from the initial Monte Carlo ensemble simulations. $P(\mathbf{V}|\boldsymbol{\theta})$ is the likelihood function, which is calculated as the function of the difference between Monte Carlo simulations and available field measurements. We again applied the LHS algorithm to draw 1000 sets of parameters from the prior distributions obtained from the previous Monte Carlo simulations. The observational data/ field measurement data are peat SOC accumulation rates in Alaska, Canada, north conterminous USA, and South Florida (subtropical regions), USA (Table 5.4) in 500-year bins from their basal ages to 2014 AD. We then averaged the simulated

monthly SOC accumulation rates at those sites into 500-year bins and compared them with the field measurement data. We next applied the Sampling Importance Resampling (SIR) technique (Skare et al., 2003) to draw 50 highest plausible parameter sets as the posterior distributions. Finally, we grouped the posterior distributions obtained from different sites into 5 different groups based on their latitudes (subtropical region, latitude 40º-45º, latitude 45º-49º, latitude 49º-60º, and latitude 60º-72º). We next averaged the posterior parameter space of each site within the corresponding group (Table 5.4).

5.2.3 Regional Simulations and Uncertainty Quantification

Basal ages were calculated by averaging the basal ages from all peatland sites from Loisel et al (2014) and MacDonald et al (2006) (see Figure 1 in MacDonald et al (2006) for basal age distribution of northern peatlands). The averaged basal age for northern peatlands in Canada, Alaska, and northern conterminous USA is 12 ka (1 ka = 1000 years before present) and the averaged basal age for subtropical peatlands in North America is 4 ka. Northern peatlands were grouped into 4 sub-regions by their latitudes (e.g., latitude 40º-45º, latitude 45º-49º, latitude 49º-60º, and latitude 60º-72º) based on the peatland distribution map taken from Yu et al (2010). The peatland map was then downscaled into 0.5º by 0.5º resolution (Figure 5.2). Regional simulations were conducted within each group by applying the averaged parameter sets from their posterior distributions from the corresponding group (see Table 5.4 for averaged parameter sets from their posterior distribution for each group). The total peat SOC stocks of North America were calculated by multiplying the current peat SOC density by the corresponding inundation percentage at each pixel (Figure 5.2, see Aires et al (2017) for inundation distribution). The inundation map is assumed to be static over the simulation period (12 ka till 2014 AD) by averaging the annual variations within each grid (1993 to 2007). A 500-year run was conducted for peatland ecosystem

ahead of the basal age using parameters of non-peatland ecosystems to determine the initial SOC within the upper 1 m mineral soil underlying the peat deposit. The parameters used for the 500-year initial simulation were taken from Wang et al (2016b) for northern soils and Wang et al (2018) for subtropical soils.

The uncertainty of the estimated total peat SOC stocks in North America resulting from the parameterization was quantified. 20 sets of parameters were randomly drawn from the posterior distributions respectively from each latitude group. Based on the randomly selected parameters, all pixels in the study area were assigned with the same climate forcing data (Figure 5.1).

Table 5.1. Description of the model parameters and their final values after optimization via (1) Initial Monte Carlo simulations, and (2) Second step Monte Carlo simulations and Bayesian inference. The values are the mean values with 1.96 standard deviation from the posterior distributions for each latitude group after the optimization. T_{min}, T_{optmin}, T_{optmax}, T_{max}, D_{moss}, D_{org}, and P_{tot} were prescribed.

Variables	Description	Unit	Latitude 60º-72º	Latitude 49º-60º	Latitude 45º-49º	Latitude 40º-45º	Subtropical
C_V	Initial[a] organic C density in vegetation	g m^{-2}	633.45±108	633.45±108	633.45±108	633.45±108	13671.05±1291
C_S	Initial[a] organic C density in soil	g m^{-2}	11859.75±1542	11859.75±1542	11859.75±1542	11859.75±1542	12204.04±1636
C_{max}	Maximum rate c assimilation through photosynthesis	g m^{-2} $month^{-1}$	586.35±54	1260.99±121	912.78±78	1300.99±153	859.42±65
CFALL	Proportion of vegetation C los litterfall	g g^{-1} $month^{-1}$	0.036±0.009	0.028±0.007	0.03±0.008	0.038±0.009	0.031±0.008
C_{VLmax}	Maximum canop leaf C density	g m^{-2}	124.02±11	129.37±13	128.32±13	126.34±13	454.5±22
K_d	Aerobic heterotrophic respiration at 0°	g g^{-1} $month^{-1}$	0.011±0.0005	0.012±0.0005	0.0097±0.0003	0.012±0.0005	0.012±0.0005
T_{min}	Minimum temperature for GPP[b]	℃	-1.0	-1.0	-1.0	0.0	10.0
T_{optmin}	Minimum optim temperature for GPP	℃	5.5	5.5	14.0	17.0	21.9
T_{optmax}	Maximum optin temperature for GPP	℃	20.0	20.0	25.0	30.9	32.7
T_{max}	Maximum temperature for GPP	℃	22.0	22.0	30.0	34.0	37.0
D_{moss}	Thickness of mo layer	cm	10.0	10.0	10.0	10.0	10.0
D_{org}	Thickness of organic layer ab *LWB*	cm	20.0	20.0	20.0	20.0	20.0
LWB	Lowest water-ta boundary	cm	30.0±5.2	30.0±5.2	30.0±5.2	30.0±5.2	30.0±5.2
P_{tot}	Total porosity o two layers	%	94, 88	95, 88	95, 83	95, 88	98, 90

Table 5.2. Description of sites in northern peatlands and subtropical peatlands and variables used for parameterizing the carbon fluxes and pools in core carbon and nitrogen module (CNDM).

Site[a]	Vegetation	Observed variables for CNDM parameterization	References
APEXCON	Moderate rich open fen with sedges (*Carex* sp.), spiked rushes (*Eleocharis* sp.), *Sphagnum* spp., and brown mosses (e.g., *Drepanocladus aduncus*)	Mean annual aboveground and belowground NPP in 2009; Aboveground biomass in 2009	Chivers et al. (2009) Turetsky et al. (2008) Kane et al. (2010) Churchill et al. (2011)
APEXPER	Peat plateau bog with black spruce (*Picea mariana*), *Sphagnum* spp., and feather mosses		
SRS-3 SRS-4 TS/Ph-3 TS/Ph-6	Fresh water marshes dominated by sawgrass (*Cladium jamaicense*)	Mean annual aboveground and below ground NPP in 2004; Aboveground and belowground biomass in 2004	Ewe et al. (2006) Juszli et al. (2006) Castañeda-Moya et al. (2013)
SRS-4 SRS-5 SRS-6 TS/Ph-6 TS/Ph-7 TS/Ph-8	Freshwater mangrove forests (*C. jamaicense-Eleocharis sp. and scrub R. mangle-C. erectus, Avicennia germinans and L. racemosa*) that dot the tree islands	Mean annual aboveground and below ground NPP in 2004; Aboveground and belowground biomass in 2004	

[a]The Alaskan Peatland Experiment (APEX) site is adjacent to the Bonanza Creek Experimental Forest (BCEF) site, approximately 35 km southwest of Fairbanks, AK. (Hinzman et al., 2006). The large Shark River Slough (SRS) basin discharge is channeled via Shark River. The Taylor River/C-111/Florida Bay Basin (TS/Ph) drains southeast Everglades National Park and is a much smaller basin that drains into a considerably larger estuarine and subtidal area. A ratio of 0.47 was used to convert vegetation biomass to carbon for northern peatlands (Raich 1991). Annual NPP of sawgrass and mangrove were converted from biomass to carbon based on plant carbon content. Sawgrass biomass 48% carbon and mangrove 44% carbon.

Table 5.3. Carbon fluxes and pools stocks in northern and subtropical peatlands used for parameter optimization of P-TEM. Values in the columns "Observation" refer to values taken from literature, whereas values in the columns "Simulation" refer to the averaged values from all selected plausible parameter sets after the initial Monte Carlo simulations.

Annual Carbon Fluxes or Pools[a]	*Sphagnum* Open Fen		*Sphagnum* Black Spruce Bog		References
	Observation	Simulation	Observation	Simulation	
NPP	445±260	410	433±107	390	Turetsky et al. (2008), Churchill (2011)
Aboveground Vegetation Carbon	149-287		423		Saarinen et al. (1996)
Belowground Vegetation Carbon	347-669		987		Moore et al. (2002)
Total Vegetation Carbon Density	496-856	800	1410	1300	Zhuang et al. (2002)
Litter Fall Carbon Flux	300	333	300	290	Tarnocai et al. (2009)
Methane Emission Flux	19.5	19.2	9.7	12.8	Kuhry and Vitt (1996)
	Sawgrass swamp		Mangrove tree island		
	Observation	Simulation	Observation	Simulation	
Aboveground NPP	213±18				Ewe et al. (2006) Juszli et al. (2006) Castañeda-Moya et al. (2013)
Belowground NPP	213±49				
Total NPP	426±67	416	993	904	
Aboveground Vegetation Carbon	348±120		2888		
Belowground Vegetation Carbon	685±110		1632		
Total Vegetation Carbon Density	1033±230	984	4520	4139	

[a] Units for annual net primary production (NPP) and litter fall carbon are $g\ C\ m^{-2}\ yr^{-1}$. Units for vegetation carbon density are $g\ C\ m^{-2}$. Units for methane emissions are $g\ C-CH_4\ m^{-2}\ yr^{-1}$. The simulated total annual methane fluxes were compared with the observations at APEXCON in 2005 and SPRUCE in 2012. The observed aboveground and belowground NPP, and observed aboveground and belowground vegetation carbon are the mean values from SRS and TS/Ph sites.

Table 5.4. Description of sites in Canada, Alaska, northern conterminous US, and subtropical regions in the USA used for optimizing the model parameters from their prior distributions. Sites were grouped into different latitude regions.

Site name	Location	Peatland type	Latitude	Longitude	Basal age (cal yr BP)	References
		Subtropical Region				Hu et al. (1994) Lavoie and Richard (2000) Gorham et al. (2003) Booth et al. (2004) Camill et al. (2009) Yu et al. (2010) Jones et al. (2014) Charman et al. (2015) Wang et al. (2016a) Wang et al. (2016b) Beilman, unpubl
02-05-21-5 02-05-21-2	South Florida, USA	Sawgrass swamp, ridge and slough	25º17'N	80º53'W	4,500	
98-4-23 00-8-7-1	South Florida, USA	Mangrove tree island	25º17'N	80º53'W	3,000	
			Latitude 40º-45º			
Caribou Bog	Maine, USA	Bog	45ºN	69ºW	12,500	
Sidney Bog	Maine, USA	Bog	44.39ºN	69.79ºW	11,000	
Petite Bog	Canada	Bog	45.1ºN	63.94ºW	11,000	
			Latitude 45º-49º			
FRON-2	Canada	Bog	45.97ºN	71.13ºW	12,500	
South Rhody	Upper Michigan, USA	Bog	46.55ºN	86.07ºW	10,559	
Denbigh	North Dakota, USA	Fen	48.22ºN	100.5ºW	12,455	
MAL-2	Canada	Bog	47.6ºN	70.97ºW	10,500	
			Latitude 49º-60º			
Sundance Fen	Canada	Fen	53.58ºN	116.75ºW	11,000	
Patuanak	Canada	Internal Lawn	55.85ºN	107.68ºW	9,000	
Joey Lake	Canada	Bog	55.47ºN	98.15ºW	8,500	
JBL3	Canada	Bog	52.87ºN	89.93ºW	8,000	
Nordan's Pond Bog	Canada	Bog	53.6ºN	49.17ºW	9,000	
Slave Lake Bog	Canada	Bog	55.01ºN	114.09ºW	10,500	
			Latitude 60º-72º			
Kenai Gasfield	Alaska, USA	Fen	60.45ºN	151.25ºW	11,408	
Horse Trail Fen	Alaska, USA	Fen	60.42ºN	150.9ºW	13,000	
No Name Creek	Alaska, USA	Fen	60.63ºN	151.08ºW	11,526	
Swanson Fen	Alaska, USA	Fen	60.79ºN	150.83ºW	14,225	

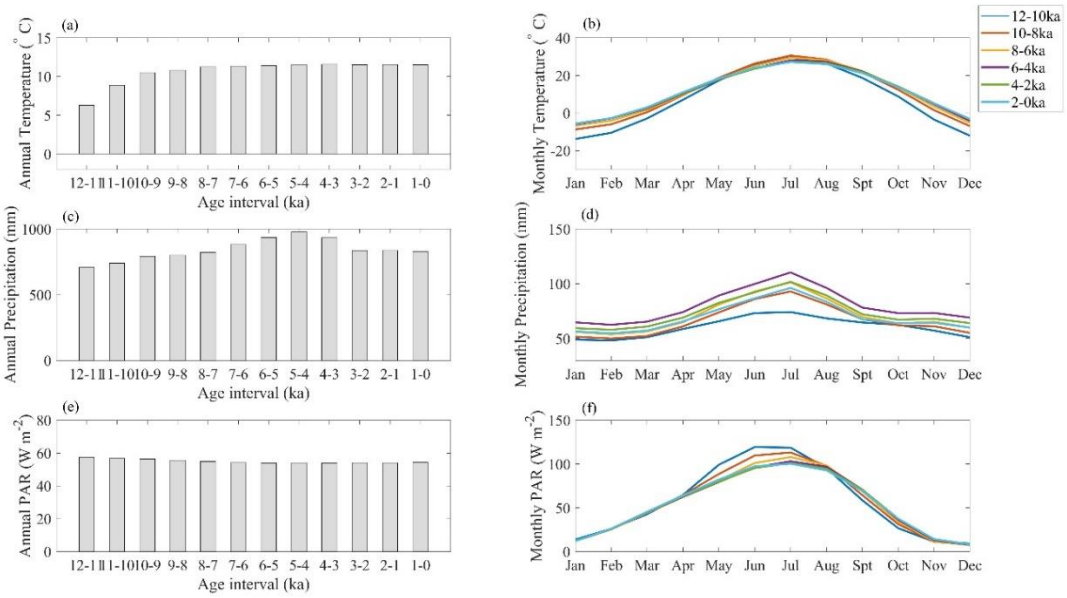

Figure 5.1. Climate forcing of annual (a) temperature, (c) precipitation, (e) photosynthetically active radiation (PAR) and monthly mean (b) temperature, (d) precipitation, and (f) PAR for North America.

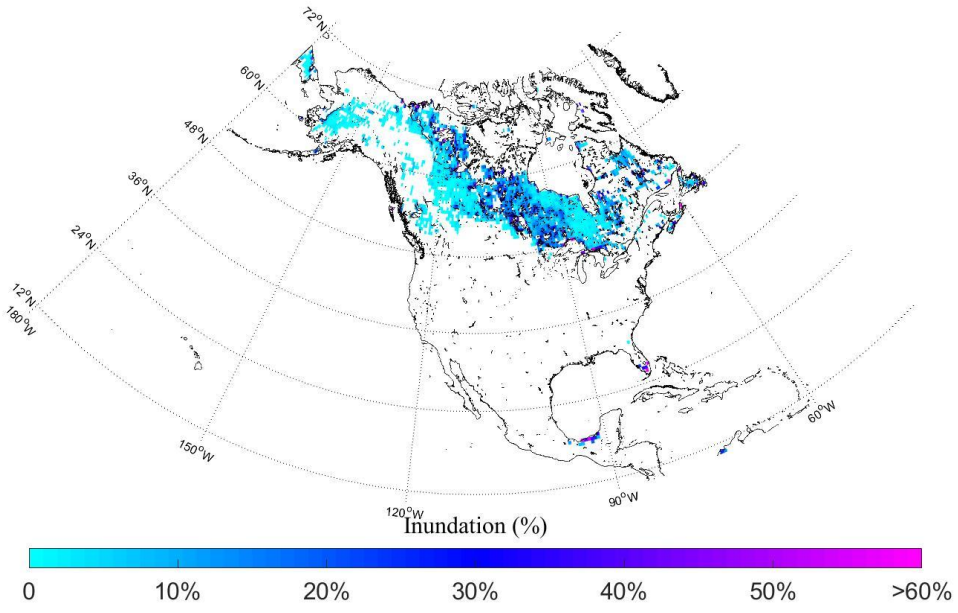

Figure 5.2. Mean inundation (%) for the peatlands in North America (northern peatlands and subtropical peatlands) at the P-TEM resolution of 0.5º by 0.5º (Aires et al., 2017). Blank areas in the map indicate non-peatland.

5.3. Results and Discussion

5.3.1 Site-level Evaluation

Peat soil organic carbon accumulation (SOC) rates were simulated at multiple sites individually to adjust and evaluate the model performance. In the region of latitude 60º-72º that covers Alaska and northern Canada, the simulations of 4 sites in Alaska in 500-year bins showed a large variation from 15 ka to 5 ka (Figure 5.3, see figures in Wang et al (2016a) for details). The large peak of SOC accumulation rates at 11 ka-9 ka (during the Holocene Thermal Maximum (HTM)) and the secondary peak at 6 ka-5 ka were captured with the magnitudes well estimated at No Name Creek and Horse Trail Fen sites. Overall, the simulated trend of SOC accumulation rates was consistent with the curves from the observation from the four sites. The R^2 coefficient between the simulation and observation was 0.88 for Horse Trail Fen, 0.87 for No Name Creek, 0.38 for Gasfiled and -0.05 for Swanson Fen. The negative correlation at Swanson Fen may result from the time shifted between the simulated accumulation peak in the late HTM and the observed peak in the early HTM (Wang et el., 2016a). In the region of latitude 49º-60º that covers the main area of Canada, the 500-year bins indicated a largest peak at 9 ka-8 ka at both Nordan's Pond Bog and Slave Lake Bog sites (Figure 5.4). This time period was consistent with the high SOC accumulation rate peak that occurred during the late HTM at four sites in Alaska. The largest peak at Sundance Fen and Joey Lake Bog sites shifted to 8.5 ka-8 ka, while the peak at Patuanak Bog site shifted to 7.5 ka-7 ka. No peak was observed at JBL3 Bog site. The magnitudes of the largest peaks at the sites in latitude 49º-60º were in the range of 55 to 90 $\mathrm{g\,C\,m^{-2}\,yr^{-1}}$, comparable to the largest peaks at the sites in latitude 60º-72º, indicating similar long-term peat SOC accumulation pattern in northern peatlands. P-TEM captured the largest peaks at all sites but underestimated the SOC accumulation rates in magnitude. At Sundance Fen

site, the modeled primary peak shifted 1 ka (Figure 5.4). The observed pattern of SOC accumulation rates also showed a secondary peak of accumulation at 1.5 ka -2014 AD (0 ka), with the magnitudes varied from 10 to >100 g C m^{-2} yr^{-1}. P-TEM underestimated the magnitude at Sundance Fen and patuanak Bog sites while overestimated the magnitude at Joey Lake Bog, JBL3 Bog, Nordan's Pond Bog, and Slave Lake Bog sites. The R^2 coefficient between the simulation and observation was 0.43 for Patuanak Bog, 0.44 for Joey Lake Bog, 0.46 for Sundance Fen, 0.61 for JBL3 Bog, 0.77 for Nordan's Pond Bog, and 0.84 for Slave Lake Bog. In the region of latitude 45º-49º and latitude 40º-45º in the northern conterminous USA, the observed long-term peat SOC accumulation rates at most sites again showed significant peaks at late HTM (10 ka-9 ka) and early-to-mid Holocene (9 ka-7.5 ka) (Figures 5.5 and 5.6). The magnitudes of the peaks range from 35 to 95 g C m^{-2} yr^{-1}, comparable to the regions of latitude 49º-60º and latitude 60º-72º (Figures 5.3 and 5.4). Caribou Bog site had the most significant increase of accumulation rate while no obvious peak was observed at South Rhody and FRON-2 Bog sites. The model captured all the primary peaks overall. SOC accumulation peaks at Caribou Bog, Denbigh Fen, and MAL-2 Bog sites were underestimated by the simulation. P-TEM accurately simulated the peaks at FRON-2 Bog, Sidney Bog, and Petite Bog sites. Similarly, a secondary peak of SOC accumulation rate was observed at all sites at 1 ka to 2014 AD (0 ka). The model simulated this secondary peak well at most of the sites. The R^2 coefficient between the simulation and observation was 0.55 for MAL-2 Bog, 0.7 for Denbigh Fen, 0.74 for FRON-2 Bog, 0.82 for South Rhody in the region of latitude 45º-49º. The R^2 was 0.75 for Petite Bog, 0.78 for Sidney Bog, and 0.84 for Caribou Bog in the region of latitude 40º-45º.

In the subtropical region within North America, observed long-term peat SOC showed a large variation between sawgrass (< 10 g C m^{-2} yr^{-1}) peatland and tree island peatland (70-200

g C m^{-2} yr^{-1}) (Figure 5.7). SOC accumulation rates in 250-year bins showed similar pattern at 02-05-21-5 and 02-05-21-2 sites with most of the rates below 10 g C m^{-2} yr^{-1}. Tree island peatland at 98-4-23 site had much higher accumulation rates in 100-years bins after 1.1 ka when the transition from sawgrass to tree island was assumed according to the observation (Jones et al., 2014). Peaks at all three sites were observed after 0.5 ka and were captured but largely underestimated by the model (Figure 5.7). The R^2 was 0.45 for 02-05-21-5, 0.49 for 02-05-21-2, and 0.8 for 98-4-23.

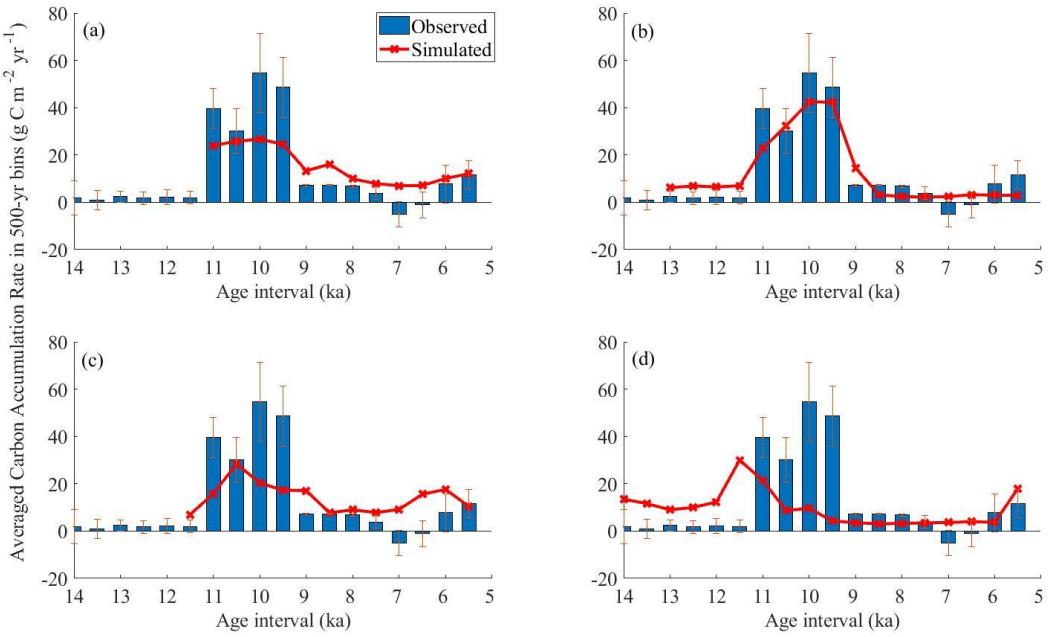

Figure 5.3. Simulated and observed carbon accumulation rates from 14.5 ka to 5 ka in 500-year bins in latitude 60º-72º for (a) No Name Creek; (b) Horse Trail Fen; (c) Kenai Gasfield; and (d) Swanson Fen (see Figure 4 in Wang et al (2016a)).

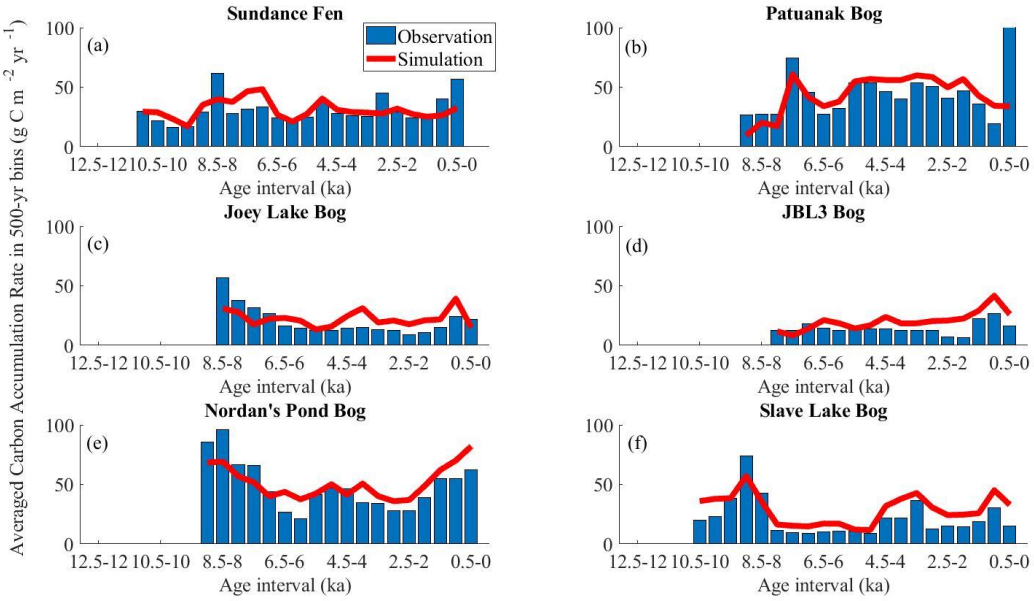

Figure 5.4. Simulated and observed carbon accumulation rates from 12.5 ka to 2014 AD (0 ka) in 500-year bins in latitude 49º-60º for (a) Sundance Fen; (b) Patuanak Bog; (c) Joey Lake Bog; (d) JBL3 Bog; (e) Nordan's Pond Bog; and (f) Slave Lake Bog. Only the comparisons within the time period with available observed data were conducted.

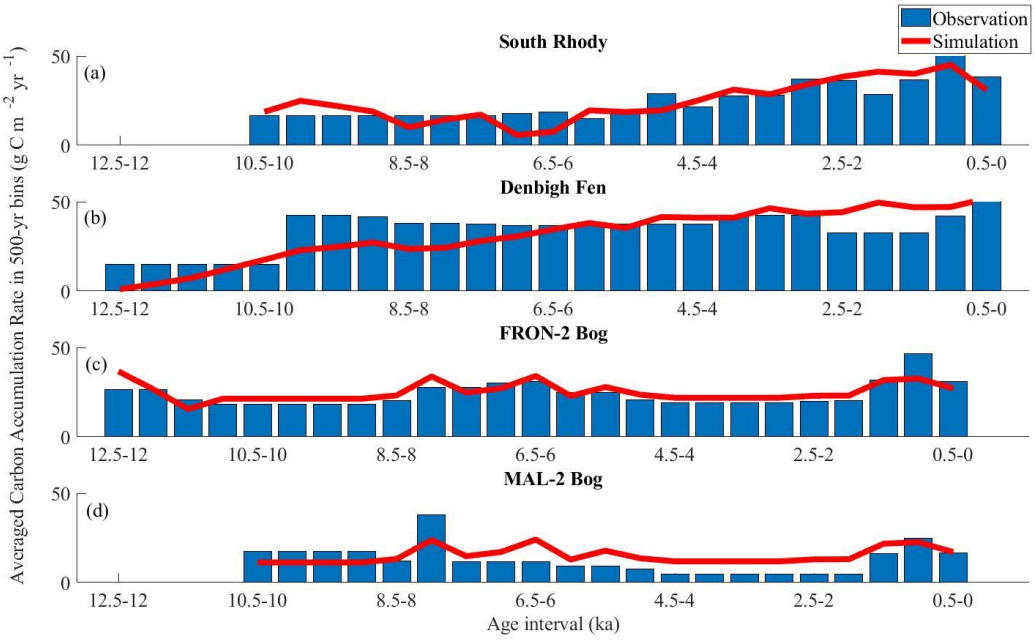

Figure 5.5. Simulated and observed carbon accumulation rates from 12.5 ka to 2014 AD (0 ka) in 500-year bins in latitude 45º-49º for (a) South Rhody; (b) Denbigh Fen; (c) FRON-2 Bog; and (d) MAL-2 Bog. Only the comparisons within the time period with available observed data were conducted.

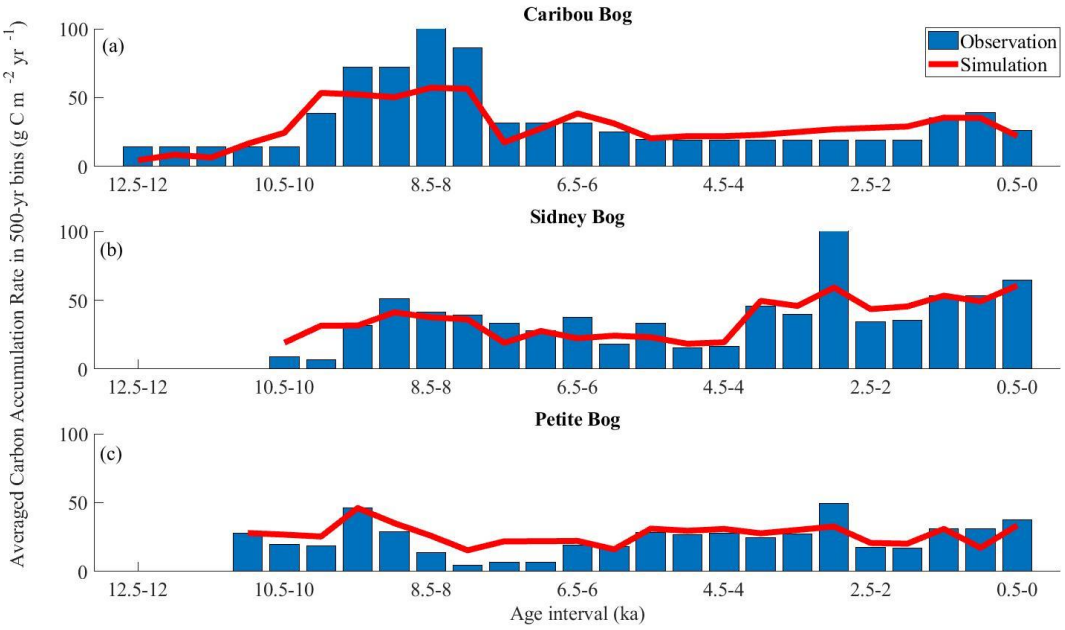

Figure 5.6. Simulated and observed carbon accumulation rates from 12.5 ka to 2014 AD (0 ka) in 500-year bins in latitude 40º-45º for (a) Caribou Bog; (b) Sidney Bog; and (c) Petite Bog. Only the comparisons within the time period with available observed data were conducted.

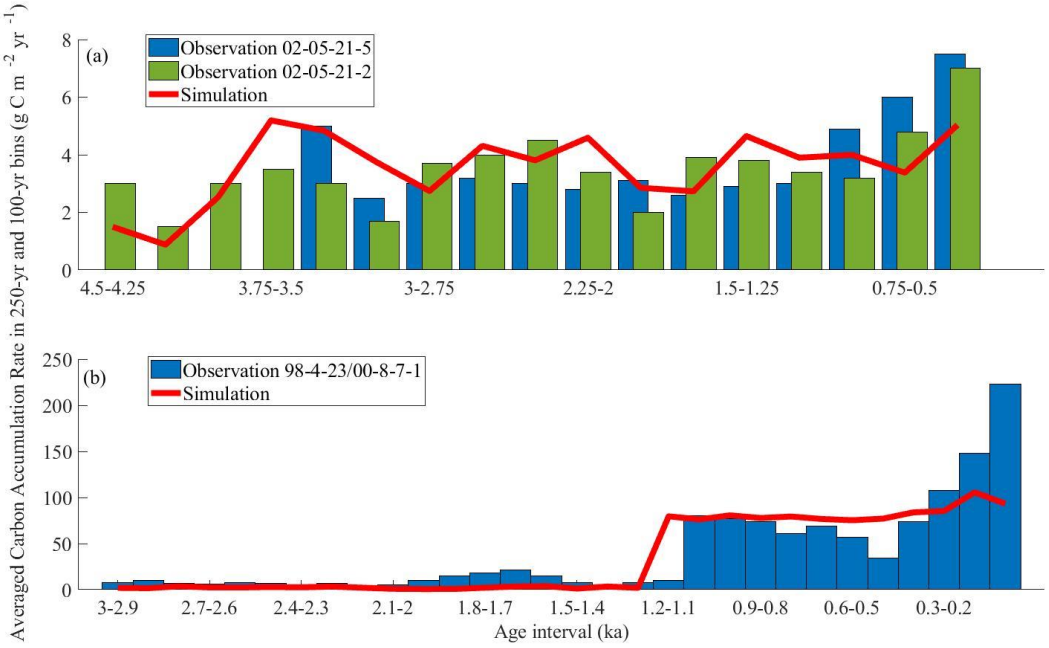

Figure 5.7. Simulated and observed carbon accumulation rates from 4.5 ka to 2014 AD (0 ka) in 250-year bins in subtropical region for (a) sawgrass; and from 3 ka to 2014 AD (0 ka) in 100-years bins for (b) sawgrass and tree island. The transition from sawgrass to tree island was assumed according to the observation (Jones et al., 2014).

5.3.2 Carbon Accumulation in North America

The peat SOC density distribution showed a large spatial variation in the region of latitude 60º-72º (Figure 5.8). Peatlands were largely distributed in the west part of the region including Alaska and western Canada. Peatlands in Alaska had a relatively low SOC density ranging from 0 to 150 kg C m^{-2} with higher density distributed in central Alaska. The western Canada has much higher SOC density up to 400 kg C m^{-2}. In the region of latitude 49º-60º, most peatlands had the current SOC density between 100 and 300 kg C m^{-2}. Low SOC density areas fell within the northern part, south central part, and eastern part of the region with SOC density from 100 to 150 kg C m^{-2}. The central part of the region exhibited a higher density with an average of 250 kg C m^{-2}. In the region of latitude 45º-49º, a lower SOC density was simulated ranging from 0 to 100 kg C m^{-2}. The northern and southern parts of the region had close to 0 kg C m^{-2} SOC density while the central part had a higher density at approximately 130 kg C m^{-2}. A small region in the western part had highest density (>350 kg C m^{-2}). In the region of latitude 40º-45º, SOC densities were moderate (~250 kg C m^{-2}) and had small spatial variations. The peatlands were mainly located in upper Michigan and Maine. In the subtropical region, peatlands were mainly distributed in the Great Everglades and the coastal area of Mexican Gulf. Lower SOC densities were modeled ranging from 0 to 120 kg C m^{-2}. The relatively lower density in the subtropical regions was presumably due to the much shorter basal age (4 ka) compared with the northern peatlands (12 ka). Peatlands in the whole Northern America showed a large variation and discontinuity, with the highest SOC density located within the northern part of central Canada (Figure 5.8). The majority of the peatlands are in Canada, Alaska, and northern conterminous USA. Peatlands in the central part, eastern part, and western part of Canada had moderate SOC density. The northern part of the USA and Alaska had lower

density. The large discontinuity among different simulation regions resulted from the implementing of different sets of model parameters during the regional simulation (Table 5.1).

The model simulated a largest peak of peat SOC accumulation rate during the period of 10 to 8 ka (Figure 5.9a). On average, the simulated SOC accumulation is 17.16 $g\ C\ m^{-2}\ yr^{-1}$ from 12 ka to 2014 AD. However, the SOC accumulation rates at 10 to 8 ka abruptly increased to 40 $g\ C\ m^{-2}\ yr^{-1}$, 2 times higher than the overall average rate during the whole simulation period. These were consistent with the findings of recent studies (Jones and Yu, 2010, Yu et al., 2009) that during the HTM, the expansion and formation of northern peatlands reached its highest. The simulated climate by CCSM3 (TraCE-21ka) model showed that the coolest temperature appeared at 15-10 ka (Figures 5.1a and 5.1b) in the whole North America (NA). In the northern part of NA, this represented colder and drier climate before the onset of the HTM (Barber and Finney, 2000; Edwards et al., 2001). The simulated long-term NPP at yearly step started to increase after the HTM and reached its maximum at 10 to 8 ka, parallel to the peak in the SOC accumulation trend (Figures 5.9a and 5.9b). When NPP started increasing at the beginning of the HTM, temperature started rising from 5 to 10 ℃ (Figure 5.1a). Meanwhile, annual precipitation during the HTM started increasing from 650 mm and continued until 5 ka to reach its highest level at 1000 mm (Figures 5.1c and 5.1d). Warmer temperature and wetter conditions during the HTM accelerated the plant photosynthesis and subsequently increased NPP, as shown by several studies (Tucker et al., 2001; Kimball et al., 2004; Linderholm, 2006). Higher annual precipitation also raised the water table in peatlands and thus allowed more space for anaerobic respiration. While warming continued after the HTM, our model indicated a decrease in SOC accumulation rates accompanied by the continued increase of heterotrophic respiration (aerobic and anaerobic) (Figure 5.9c). NPP also showed a decrease after 8 ka (Figure

5.9b). The decrease in SOC accumulation could be due to the increased soil organic matter decomposition, as warmer temperatures stimulated the soil decomposition (Nobrega et al., 2007). The simulated annual heterotrophic respiration (RH) followed a pattern similar to the temperature (Figure 5.1a). Warming also stimulated the evapotranspiration and subsequently lowered water table, opposite to the higher precipitation effect. The SOC accumulation rate slightly increased after 3 ka, presumably due to the continued wetter condition after 5 ka (Figure 5.1a) where NPP might offset the increasing RH caused by warming.

Our previous studies indicated that temperature had the most significant effect on peat SOC accumulation rate, followed by the seasonality of net incoming solar radiation (NIRR, Wang et al., 2016a, 2016b). The seasonality of temperature, the interaction of temperature and precipitation, and precipitation alone also showed significant effects. Precipitation has less effect compared to temperature. As warming continue in the 21st century, if follows the same pattern, the rapid peat SOC accumulation during the HTM under warming and wetter climate might suggest a continuous C sink in this century, as predicted by recent studies (Yu et al., 2009, 2012; Jones and Yu, 2010; Loisel et al., 2012; Spahni et al., 2013; Davidson and Janssens, 2006). Our results suggested that continue warming has positive effects on heterotrophic respiration in northern peatlands as indicated by the simulated long-term RH (Figure 5.9c). The future warming effect on soil decomposition might overwhelm its positive effect on plant photosynthesis and would possibly switch the role of the northern peatlands between a long-term carbon sink to a carbon source.

The peat SOC density (kg $C\ m^{-2}$) in each grid pixel at the resolution of 0.5 º by 0.5 º was multiplied by the percentage of wetland cover from the inundation map (Figure 5.2). It was then multiplied by the corresponding grid area (56 km by 56 km) to get the total peat SOC stock for

North America. The peatland soils are estimated to store a total of 85-174 Pg C (1 Pg C = 10^{15} g C) with a mean of 121.57 Pg C. The uncertainty range results from the random selections of the parameter sets from their posterior distribution after the model parameterization. Approximately 0.53 Pg C (0.37-0.76 Pg C) is stored in subtropical peatlands in NA with the rest of the amount stored in northern peatlands of NA.

In our previous studies on Alaskan peatlands SOC stocks (Wang et al., 2016a, 2016b), the vegetation distribution changes reconstructed from fossil pollen data (He et al., 2014) were applied through different time periods over the Holocene to mimic the peatland expansion and shrinkage. In this study, we considered that the vegetation changes through time (e.g., the peatland area changes) were static during the last 12,000 years. This might oversimplify the complicated variation and evolution of landscape by using modern peatland distribution map as vegetation shifts could happen within hundreds of years (Ager and Brubake, 1985). Further, modern inundation map was used to calculate the carbon stock within each grid pixel. As rivers and lakes included in inundation map could be classified as peatlands, we might overestimate the carbon amount for each grid. Averaging the annual variation of inundation in each grid from 1993 to 2007 to represent the static inundation map over the simulation period also caused uncertainties as inundation data vary from year to year (Figure 5.10). Using a relatively coarse resolution (56km by 56 km) for regional model simulation and subsequent carbon stock estimation might induce large uncertainty. Uncertainty also existed in the estimation of peatland basal ages. Basal age determined the time point at which peatlands started to accumulate carbon and thus it determined the length of model simulation period. As basal age was averaged from numbers of peatland sites that might not be adequate for representing the whole NA region, using the averaged basal age during the regional simulation might also induce uncertainty. The current

peat SOC density was calculated from the multiplication of simulation time period and the monthly carbon accumulation rate, the result was linearly proportional to the estimated basal age. Variations and errors in the averaged basal age would also cause large fluctuation of the current carbon amount. In summary, the model might not be appropriate when applied to simulate the peat carbon accumulation and peat density at small spatial and short time scales. Further development of both model structure and the exploration of data availability should be conducted to get a better estimation of northern or global peatland carbon dynamics.

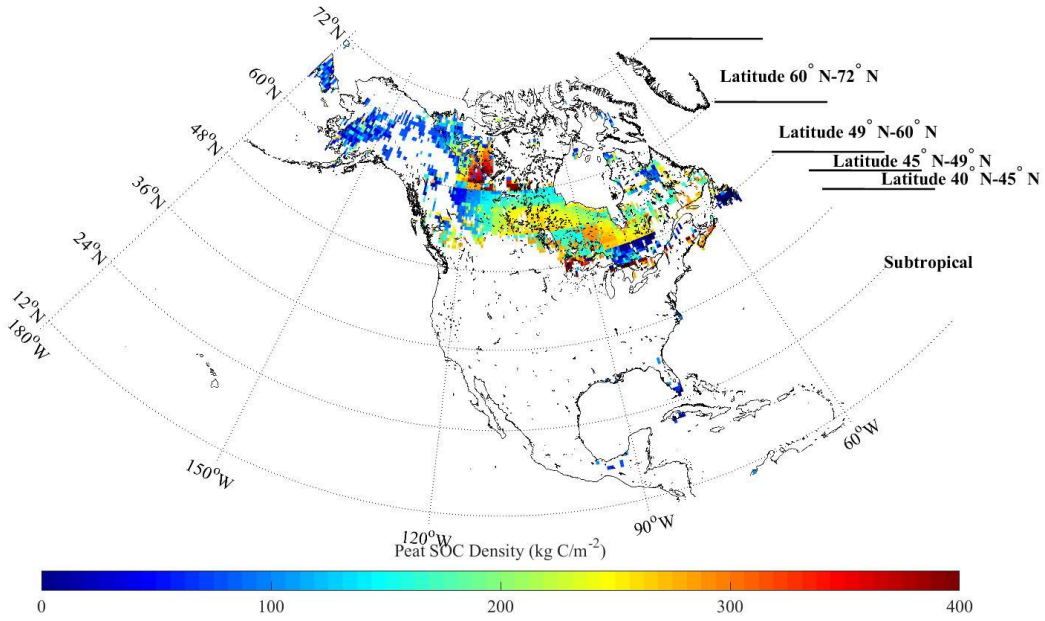

Figure 5.8. Spatial distribution of the combination of current peat SOC density ($kg\ C\ m^{-2}$) in the regions of latitude 60º-72º, latitude 49º-60º, latitude 45º-49º, latitude 40º-45º, and subtropic from 12 ka to 2014 AD.

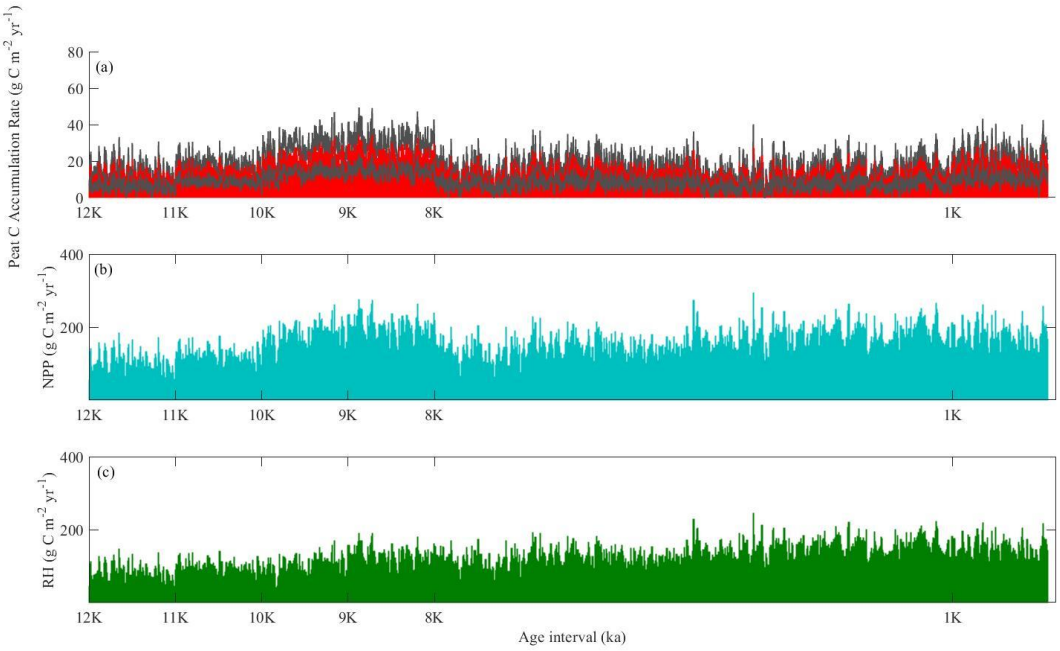

Figure 5.9. Simulated long-term annual (a) peat SOC accumulation rates (red bars) with uncertainty ranges (upper and lower gray bars), (b) NPP, and (c) heterotrophic respiration (aerobic + anaerobic) of peatlands in North America.

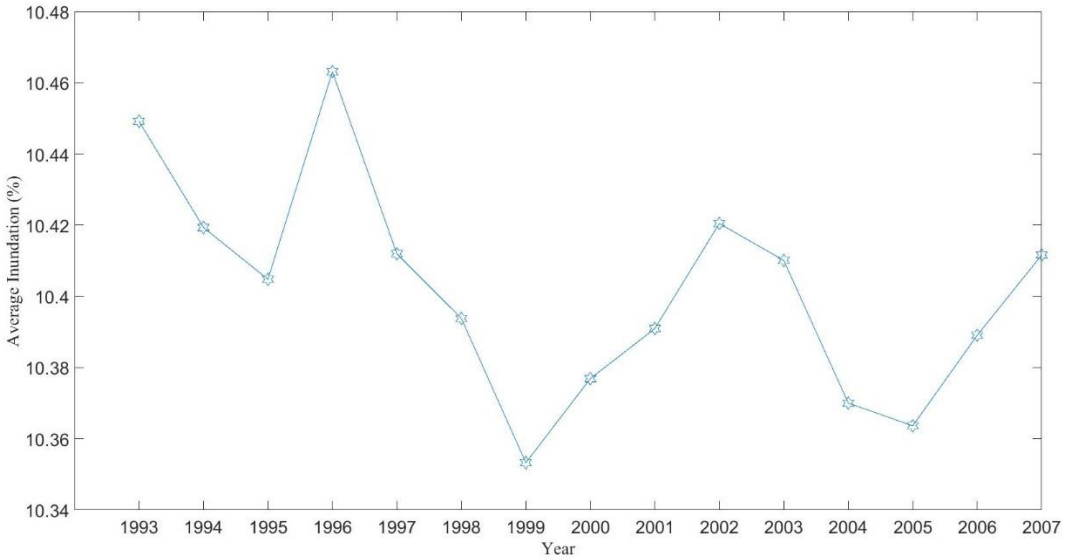

Figure 5.10. Annual average of inundation data in North America from 1993 to 2007.

5.4. Conclusions

In this study, we applied a process-based biogeochemistry peatland model to quantify the C accumulation rates and C stocks within North America peatlands over the last 12,000 years. Based on a Bayesian framework, the model parameters were optimized by comparing the modeled peat SOC accumulation rates with the observational long-term peat data at multiple sites in Alaska, Canada, the northern conterminous USA, and the subtropical regions. Consistent with our previous studies on Alaska peatlands and other studies on northern peatlands, our regional simulation captured a primary peak with the highest C accumulation rates during the late Holocene Thermal Maximum occurring at 10-8 ka. Warmer temperature along with the wetter condition might be the controlling factor to stimulate the peat formation by increasing the plant net primary production. Warmer climate decreased the peat accumulation through enhancing the heterotrophic respiration and evapotranspiration over the rest of the Holocene. Model simulations indicate that there have been 85-174 Pg C accumulated in North American peatlands over the last 12,000 years with 0.37-0.76 Pg C stored in subtropical peatlands.

CHAPTER 6. SUMMARY AND FUTURE WORK

6.1 Research Findings

In Chapter 2, I developed a model that couples the modules of hydrology, soil thermal, methane, ecosystem carbon and nitrogen to quantify long-term peat carbon accumulation in Alaska peatlands. I calibrated the model and next compared modeled soil moisture, soil temperature profiles, water table, methane fluxes, and carbon pools with the observational data. I then applied the model to four peatland sites in Alaska. The simulation suggested that high summer temperature from elevated insolation seasonality and high precipitation might be main factor for rapid carbon accumulation during the Holocene.

In Chapter 3, the SOC accumulation in Alaskan was quantified during the last 15,000 years based on the developed biogeochemistry model for both peatland and non-peatland ecosystems. The relationship between climatic factors and the historical peat accumulation trajectories were studied. Several factors such as temperature, precipitation, water table, radiation and vapor pressure, along with geographical movement of peatland (shrinkage and expansion) were quantitatively examined to find their impact on peatland formation. The study also simulated and quantified the current SOC and vegetation C stocks in both spatial and temporal patterns. Peatlands were found to contribute the most soil carbon while uplands contribute the most vegetation carbon for the region. The simulated results compared well with the field measurements at multiple sites. This study is among the first to examine the peatlands and non-peatlands C dynamics and their distributions and peat depths using core data at regional scales.

In Chapter 4, the newly developed biogeochemistry model was re-calibrated to quantify the carbon accumulation for peatland ecosystems in the Pastaza-Marañon foreland basin in the Peruvian Amazon from 12,000 years before present to 2100 AD. The study indicated that

warming accelerated peat carbon loss while increasing precipitation slightly enhanced peat carbon accumulation at millennial time scales. With these impacts, the model projected the future peat carbon dynamics by inputting the future climate data (RCP data). The simulation suggested that the basin might lose up to 0.4 Pg C by 2100 AD with the largest loss from palm swamp. If this loss rate is true for all Amazonia peatlands, the study projected that these carbon-dense peatlands might switch from a current carbon sink into a future source in this century. The study is among the first to quantify the regional C dynamics and their fates under future climate conditions using a modeling approach for Amazon basin.

In Chapter 5, the same model was re-applied to quantify the C accumulation rates and C stocks within North America peatlands over the last 12,000 years. The model was re-parameterized using observed long-term peat soil carbon accumulation rates at multiple sites in Alaska, Canada, the northern conterminous USA, and the subtropical regions. Similar to the results in Chapter 2 and Chapter 3, a primary peak with the highest C accumulation rates during the late Holocene Thermal Maximum occurred at 10-8 ka. Warmer temperature along with the wetter condition were found to be primary factors controlling peat soil carbon dynamics. The results indicated that 85-174 Pg C have been accumulated in North American peatlands over the last 12,000 years including 0.37-0.76 Pg C in subtropical peatlands.

6.2 Research Limitations

In Chapter 2, a model was developed by coupling and revising soil thermal dynamics module, carbon and nitrogen dynamics module, water table module, hydrological module and methane module. However, with numbers of parameters within the model, the model was trained and validated using limited number of available data sets. For instance, to calibrate the hydrological module, I used the soil moisture data that span only several years at monthly time

step. Also, to calibrate the methane module, monthly methane fluxes data were utilized that cover few years. The lack of data versus the large number of parameters to be calibrated may largely decrease the model accuracy during the parameterization. This will cause the model to have low performance when more and more unseen data are fed to the model, and thus involves large uncertainty. Further, the model relies heavily on sets of parameters. Although coupled with several complex sub-modules, the model structure may be still simplified considering the complicated ecosystem processes that the model is trying to simulate. More ordinary differential equations that simulate the physical and chemical processes may need to be added in the future.

In Chapter 3 and Chapter 5, besides the limitations within the model itself, there are other limitations. The vegetation changes reconstructed from fossil pollen data during different time periods followed the general climate history during the last 15,000 years. For instance, the migration of dark boreal forests over snow-covered tundra during the HTM was probably induced by the warmer and wetter climate resulted from the insolation changes (He et al., 2014). The cooler and drier climate after the mid-Holocene limited the growth of boreal broadleaf conifers (Prentice et al., 1992), and therefore resulted in the replacement of broadleaf forest with needleleaf forest and tundra ecosystems. Since the parameters of our model for individual vegetation type were static, parameterizing the model using modern site-level observations might have introduced uncertainty to parameters, which may result in regional simulation uncertainties. Assuming each parameter as constant (e.g. the lowest water-table boundary, see Wang et al. (2016) for details) over time may also weaken the model's response to different climate scenarios. Furthermore, applying static vegetation maps at millennial scales and using modern elevation and pH data may simplify the complicated changes of landscape and terrestrial ecosystems, as vegetation can shift within hundreds of years (Ager and Brubake, 1985; see He et

al. (2014) discussion section). Relatively coarse spatial resolution (0.5° ×0.5°) in P-TEM simulations may also introduce uncertainties. In addition, because I used the modern inundation map to delineate the peatland and upland within each grid cell, I might have overestimated the total peatland area since not all inundated areas are peatlands. Linking field-estimated basal ages of peat cores to the vegetation types during each period involves large uncertainties due to the limitation of the peat classification and insufficient peat samples. Thus, the estimated spatially explicit basal age data shall also introduce a large uncertainty to our regional quantification of carbon accumulation.

In Chapter 4 and Chapter 5, I quantified the regional carbon stocks by assuming there is no peatland shrinkage or expansion. I also assumed the river stays static over time. The model relies on the climate conditions rather than topographic and geological factors. However, hydrology, NPP, and SOC accumulation can also be controlled by autogenic processes of peatlands such as transition from minerotrophic to ombrotrophic conditions (Lähteenoja and Page, 2011). This transition is largely induced by the form and thickness of the peat deposit and less affected by prevailing climatic conditions – as long as the rainfall is sufficient to sustain a rain-fed bog. Interestingly, in the Aucayacu peatland, the transition from minerotrophic to ombrotrophic conditions occurred around 4 ka (3.5 ka) – exactly when precipitation started to increase. It might have been a coincidence, but it is also possible that the increased precipitation enabled the appearance of ombrotrophic bogs. If this is the case, a change in the precipitation did not affect the NPP directly but indirectly by inducing a change in the peatland type. Since our model cannot simulate the paleo-ecological change including the shifts between different peatland ecosystem types through time, our results may only partly explain the observed patterns, with much information still relying on paleo-ecological studies (Swindles et al., 2014;

Kelly et al., 2017; Roucoux et al., 2013; Lähteenoja et al., 2012). The relationship between NPP and precipitation for peatland ecosystems in the region should be further studied in the future.

Another key control of the current distribution of peat depths and SOC densities within the PMFB is the active lateral migration of rivers (Lähteenoja et al., 2012). The current distribution of peat SOC densities can be explained by both climatic and geological factors. The Amazon river networks can be affected under future climate conditions, which will affect peatland dynamics (e.g., formation and area change). Further, our model did not differentiate the minerotrophic vs. ombrotrophic conditions for the peatland ecosystems, which will introduce biases. Incorporating these dynamics into future analysis shall improve our predictions of SOC for this region.

6.3 Ongoing Works

A number of studies including long-term core analysis and modeling studies have been conducted to better understand the carbon budget in peatlands and the cycling between peat soil carbon and atmosphere. However, less attention has been paid to the corresponding role of nitrogen cycling in peatland dynamics (Hill et al., 2016; Drewer et al., 2010; Worrall et al., 2012). Due to the different hydrological conditions, nitrogen cycling in northern peatlands is unique from other ecosystems (Toberman et al., 2015). Four sources of N to peatlands have been studied, including atmospheric deposition, mineralization, N-fixation, and upwelling from regional groundwater (Bridgham et al., 1996). For bog peatlands, all N are input to the soil only through atmospheric deposition, while for fens, additional N is an input via groundwater upwelling. Northern peatlands not only store large quantity of soil organic carbon, but also form a large sink of nitrogen (Verry and Timmons, 1982). Recently, a study was conducted by Hill et

al. (2016) at two peatland sites (S3 bog) within the US Department of Agriculture's Forest Service Marcel Experimental Forest (MEF) located 40 km north of Grand Rapids, Minnesota, USA. The study includes an ombrotrophic bog and a minerotrophic fen. The soil nitrogen balance along with other climate variables and peat properties were recorded from 2010 to 2014. The nitrogen fluxes were averaged into annual rates.

Our ongoing study is focusing on developing a new model based on the original peatland model in our previous studies by incorporating nitrogen dynamics to simulate the monthly peat soil nitrogen fluxes and pools. The model is for bog only with no extra nitrogen input from groundwater upwelling. Until now, the model structure has been all finished with the code been incorporated to the original model and the model has been tested bug-free. We have added more than 5 ordinary differential equations (ODE) into the previous system pools and 30 extra processes for nitrogen fluxes were also added. The model framework follows a nitrogen cycling model framework of LPJ for non-peatland soils (Xu-Ri and Prentice, 2008, Figure 6.1). The nitrogen pools in the model include nitrate (NO_3^-), ammonium (NH_4^+), total N (TN), soil organic nitrogen, litter nitrogen pool, and plant nitrogen pool. The nitrogen fluxes were modeled monthly including nitrogen deposition though precipitation, litter fall nitrogen from plant, nitrogen mineralization (from litter fall nitrogen to NH_4^+ and from organic soil N to NH_4^+), nitrogen nitrification (from NH_4^+ to NO_3^-), NO_3^- denitrification (to NO_2^-), NH_4^+ volatilization (to NH_3), and others. The new model will be the first model for quantifying nitrogen cycling in peatland soils. The model will be parameterized based on the observational nitrogen balance and climate forcing at S3 sites in Marcel Experimental Forest from 2010 to 2014 (monthly). The climate forcing data (Figure 6.2) have been organized and the site-level simulation is ready to be conducted.

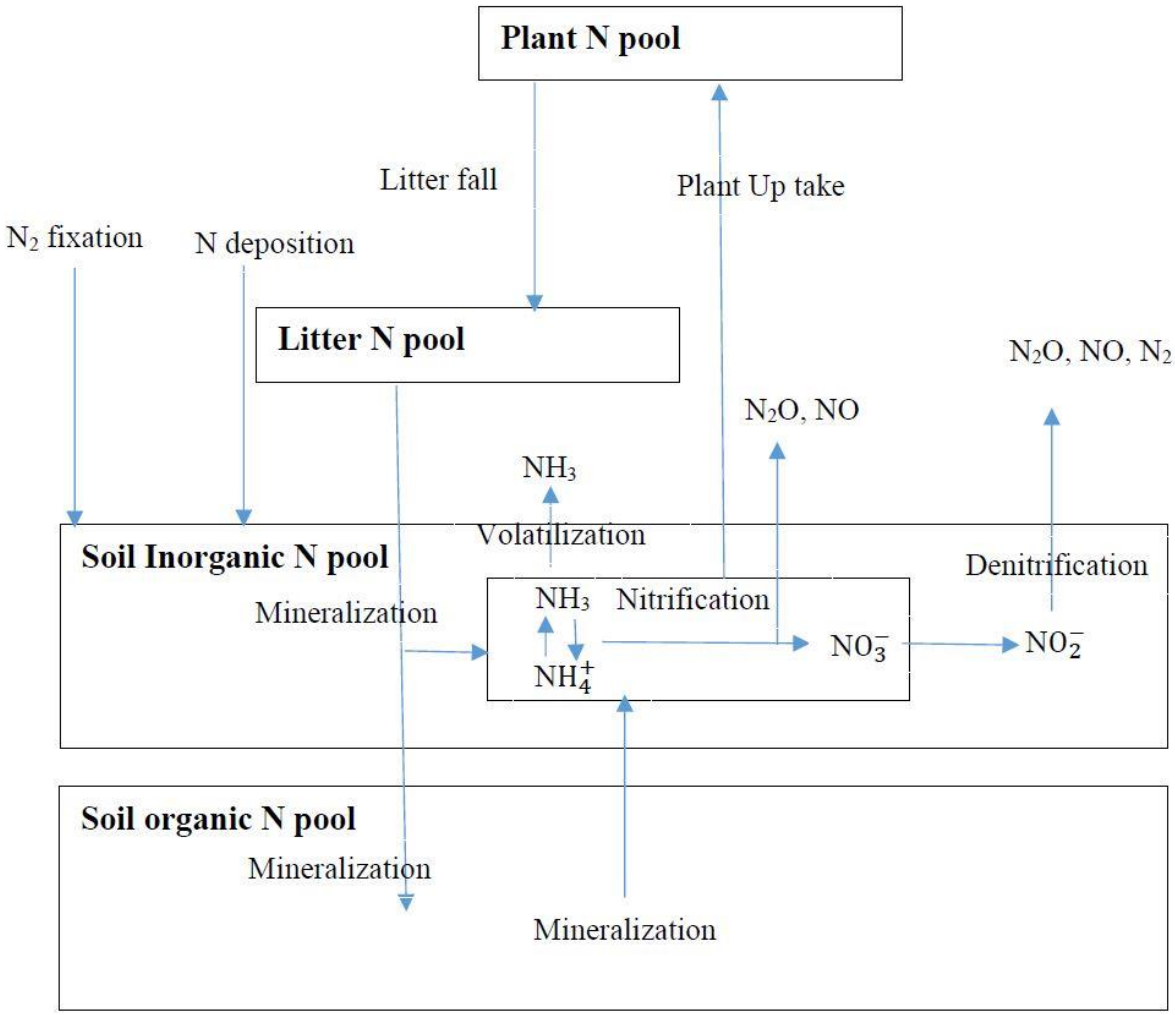

Figure 6.1. Nitrogen cycling model framework in LPG model (Xu-Ri and Prentice, 2008) for non-peatland soils.

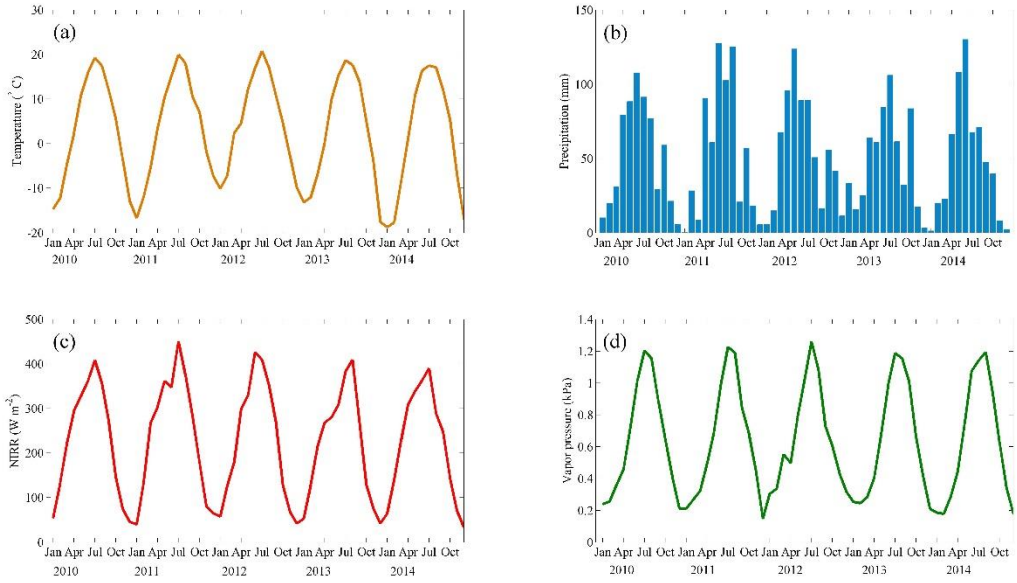

Figure 6.2. Monthly (a) air temperature; (b) precipitation; (c) NIRR; and (d) vapor pressure for model input at MEF site from 2010 to 2014.

REFERENCES

Ager, T. A., & Brubaker, L. Quaternary palynology and vegetational history of Alaska. Pollen Records of Late Quaternary North American Sediments, 353-384, 1985.

Aires, F., Miolane, L., Prigent, C., Pham-Duc, B., Fluet-Chouinard, E., Lerner, B., Papa, F. A Global Dynamic Long-Term Inundation Extent Dataset at High Spatial Resolution Derived through Downscaling of Satellite Observations. J. Hydrometeorol. doi:10.1175/JHM-D-16-0155.1, 2017.

Apps, M. J., Kurz, W. A., Luxmoore, R. J., Nilsson, L. O., Sedjo, R. A., Schmidt, R., ... & Vinson, T. S.: Boreal forests and tundra. Water, Air, and Soil Pollution, 70(1-4), 39-53, 1993.

Armentano, T. V., & Menges, E. S.: Patterns of change in the carbon balance of organic soil-wetlands of the temperate zone. The Journal of Ecology, 755-774, 1986.

Assessment, A. C. I. Forests, land management and agriculture. Arctic Climate Impact Assessment, 781-862, 2005.

Baker, T. R. et al. Variation in wood density determines spatial patterns in Amazonian forest biomass. Global Change Biology, 10: 545–562. doi:10.1111/j.1365-2486.2004.00751.x (2004).

Balshi, M. S., McGuire, A. D., Zhuang, Q., Melillo, J., Kicklighter, D. W., Kasischke, E., ... & Burnside, T. J.: The role of historical fire disturbance in the carbon dynamics of the pan-boreal region: A process-based analysis. Journal of Geophysical Research: Biogeosciences, 112(G2), 2007.

Barber, V. A., & Finney, B. P. Late Quaternary paleoclimatic reconstructions for interior Alaska based on paleolake-level data and hydrologic models. Journal of Paleolimnology, 24(1), 29-41, 2000.

Belyea, L. R. Nonlinear dynamics of peatlands and potential feedbacks on the climate system. Carbon cycling in northern peatlands, 5-18, 2009.

Berger, A., & Loutre, M. F.: Insolation values for the climate of the last 10 million years. Quaternary Science Reviews, 10(4), 297-317, 1991.

Bigelow, N. H., Brubaker, L. B., Edwards, M. E., Harrison, S. P., Prentice, I. C., Anderson, P. M., ... & Kaplan, J. O.: Climate change and Arctic ecosystems: 1. Vegetation changes north of 55 N between the last glacial maximum, mid-Holocene, and present. Journal of Geophysical Research: Atmospheres, 108(D19), 2003.

Booth RK, Jackson ST, Gray CED, Paleoecology and high-resolution paleohydrology of a kettle peatland in upper Michigan. Quat Res 61:1–13, 2004.

Bridgham, S. D., Megonigal, J. P., Keller, J. K., Bliss, N. B., & Trettin, C.: The carbon balance of North American wetlands. Wetlands, 26(4), 889-916, 2006.

Bridgham, S. D., Pastor, J., Dewey, B., Weltzin, J. F., & Updegraff, K. Rapid carbon response of peatlands to climate change. Ecology,89(11), 3041-3048, 2008.

Bridgham, S.D., Pastor, J., Janssens, J.A., Chapin, C., Malterer, T.J. Multiple limiting gradients in peatlands: a call for a new paradigm. Wetlands 16, 45–65, 1996.

Camill, P., A. Barry, E. Williams, C. Andreassi, J. Limmer, and D. Solick. Climate-vegetation-fire interactions and their impact on long-term carbon dynamics in a boreal peatland landscape in northern Manitoba, Canada, J. Geophys. Res., 114, G04017, doi:10.1029/2009JG001071, 2009.

Carlson, A. E. et al. Modeling the surface mass-balance response of the Laurentide Ice Sheet to Bølling warming and its contribution to Meltwater Pulse 1A. Earth and Planetary Science Letters, 315, 24-29 (2012).

Carter, A. J., & Scholes, R. J.: SoilData v2. 0: generating a global database of soil properties. Environmentek CSIR, Pretoria, South Africa, 2000.

Castaneda-Moya E, Twilley RR, Rivera-Monroy VH. Allocation of biomass and net primary productivity of mangrove forests along environmental gradients in the Florida coastal Everglades, USA. Forest Ecology and Management 307: 226–241, 2013.

Change, I. C.: Mitigation of Climate Change. Contribution of Working Group III to the Fifth Assessment Report of the Intergovernmental Panel on Climate Change. Cambridge University Press, Cambridge, UK and New York, NY, 2014.

Change, I. C.: The Physical Science Basis: Working Group I Contribution to the Fifth Assessment Report of the Intergovernmental Panel on Climate Change. New York: Cambridge University Press, 1, 535-1, 2013.

Chapin, F. S., P. A. Matson, and H. A. Mooney. Principles of Terrestrial Ecosystem Ecology, Springer, New York, 2002.

Charman D, Beilman D, Blaauw M et al. Climate-related changes in peatland carbon accumulation during the last millennium. Biogeosciences 10: 929–944. DOI: 10.5194/bg-10-929-2013, 2013.

Charman, D.J., Amesbury, M.J., Hinchliffe, W., Hughes, P.D.; Mallon, G., Blake, W.H.; Daley, T.J., Gallego-Sala, A.V., Mauquoy, D. Drivers of Holocene peatland carbon accumulation across a climate gradient in northeastern North America. Quat. Sci. Rev. 121, 110–119, 2015.

Chivers, M. R., Turetsky, M. R., Waddington, J. M., Harden, J. W., & McGuire, A. D.: Effects of experimental water table and temperature manipulations on ecosystem CO2 fluxes in an Alaskan rich fen.Ecosystems, 12(8), 1329-1342, 2009.

Christensen, J. H., & Christensen, O. B. A summary of the PRUDENCE model projections of changes in European climate by the end of this century. Climatic change, 81(1), 7-30, 2007.

Churchill, A. The response of plant community structure and productivity to changes in hydrology in Alaskan boreal peatlands. Master Thesis, University of Alaska, Fairbanks, AK, USA. 119 pp, 2011.

Cleveland, C. C. et al. A comparison of plot-based satellite and Earth system model estimates of tropical forest net primary production. Global Biogeochem. Cycles, 29, 626–644. doi: 10.1002/2014GB005022 (2015).

Clymo, R.S. Sphagnum, the peatland carbon economy, and climate change. In Bryology for the 21st century. Edited by J.W. Bates, N.W. Ashton, and J.G. Duckett. Maney Publishing Company, Leeds, and the Bryological Society. pp. 361–368, 1998.

Conrad, R. Contribution of hydrogen to methane production and control of hydrogen concentrations in methanogenic soils and sediments.FEMS Microbiology Ecology, 28(3), 193-202, 1999.

Coughlan, J. C., & Running, S. W. Regional ecosystem simulation: A general model for simulating snow accumulation and melt in mountainous terrain. Landscape Ecology, 12(3), 119-136, 1997.

Cox, P. M. et al. Amazonian forest dieback under climate-carbon cycle projections for the 21st century. Theoretical and applied climatology, 78(1), 137-156 (2004).

Cox, P. M. et al. Modelling vegetation and the carbon cycle as interactive elements of the climate system. International Geophysics, 83, 259-279 (2002).

Crill, P. M., Bartlett, K. B., Harriss, R. C., Gorham, E., Verry, E. S., Sebacher, D. I., ... & Sanner, W. Methane flux from Minnesota peatlands. Global Biogeochemical Cycles, 2(4), 371-384, 1988.

Dargie, G. C. et al. Age, extent and carbon storage of the central Congo Basin peatland complex. Nature, 542, 86-90 (2017).

Davidson, E. A., & Janssens, I. A. Temperature sensitivity of soil carbon decomposition and feedbacks to climate change. Nature, 440(7081), 165-173, 2006.

Davidson, E. A., Trumbore, S. E., & Amundson, R.: Biogeochemistry: soil warming and organic carbon content. Nature, 408(6814), 789-790, 2000.

Del Aguila-Pasquel, J. et al. The seasonal cycle of productivity, metabolism and carbon dynamics in a wet aseasonal forest in north-west Amazonia (Iquitos, Peru). Plant Ecology and Diversity, 7, 71–83 (2014).

Delbart, N. et al. Mortality as a key driver of the spatial distribution of aboveground biomass in Amazonian forest: results from a vegetation model. BG, 7(10), 3027-3039 (2010).

Deng, J., Li, C., & Frolking, S. Modeling impacts of changes in temperature and water table on C gas fluxes in an Alaskan peatland. Journal of Geophysical Research: Biogeosciences, 120(7), 1279-1295, 2015.

Dorrepaal, E., Toet, S., van Logtestijn, R. S., Swart, E., van de Weg, M. J., Callaghan, T. V., & Aerts, R. Carbon respiration from subsurface peat accelerated by climate warming in the subarctic. Nature, 460(7255), 616-619, 2009.

Draper, F. C. et al. The distribution and amount of carbon in the largest peatland complex in Amazonia. Environmental Research Letters, 9(12), 124017 (2014).

Drewer, J., Lohila, A., Aurela, M., Laurila, T., Minkinen, K., Penttila, T., Dinsmore, K.J., McKenzie, R.M.M., Helfter, C., Flechard, C., Sutton, M.A., Skiba, U.M. Comparison of greenhouse gas fluxes and nitrogen budgets froman ombrotrophic bog in Scotland and a minerotrophic sedge fen in Finland. Eur. J. Soil Sci. 61, 640–650, 2010.

Dumont, J. F. et al. Morphostructural provinces and neotectonics in the Amazonian lowlands of Peru. Journal of South American Earth Sciences, 4(4), 373-381 (1991).

Dumont, J. F. et al. Wetland and upland forest ecosystems in Peruvian Amazonia: plant species diversity in the light of some geological and botanical evidence. Forest Ecology and Management, 33, 125-139 (1990).

Edwards, M. E., Mock, C. J., Finney, B. P., Barber, V. A., & Bartlein, P. J. Potential analogues for paleoclimatic variations in eastern interior Alaska during the past 14,000 yr: atmospheric-circulation controls of regional temperature and moisture responses. Quaternary Science Reviews, 20(1), 189-202, 2001.

Euskirchen, E. S., McGuire, A. D., & Chapin, F. S.: Energy feedbacks of northern high-latitude ecosystems to the climate system due to reduced snow cover during 20th century warming. Global Change Biology,13(11), 2425-2438, 2007.

Ewe, S. M. L., E. E. Gaiser, D. L. Childers, D. Iwaniec, V. H. Rivera-Monroy, and R. R. Twilley. Spatial and temporal patterns of aboveground net primary productivity (ANPP) along two freshwater-estuarine transects in the Florida coastal Everglades, Hydrobiologia, 569, 459–474, 2006.

Field, C. B., Barros, V. R., Dokken, D. J., Mach, K. J., Mastrandrea, M. D., Bilir, T. E., ... & Girma, B. IPCC, 2014: Climate Change 2014: Impacts, Adaptation, and Vulnerability. Part A: Global and Sectoral Aspects. Contribution of Working Group II to the Fifth Assessment Report of the Intergovernmental Panel on Climate Change, 2014.

Freeman, C., Lock, M. A., & Reynolds, B. Fluxes of CO2, CH4 and N2O from a Welsh peatland following simulation of water table draw-down: potential feedback to climatic change. Biogeochemistry, 19(1), 51-60, 1992.

Frolking, S., Roulet, N. T., Tuittila, E., Bubier, J. L., Quillet, A., Talbot, J., & Richard, P. J. H. A new model of Holocene peatland net primary production, decomposition, water balance, and peat accumulation. Earth System Dynamics, 1(1), 1-21, 2010.

Frolking, S., Talbot, J., Jones, M. C., Treat, C. C., Kauffman, J. B., Tuittila, E. S., & Roulet, N. Peatlands in the Earth's 21st century climate system. Environmental Reviews, 19(NA), 371-396, 2011.

Gerdol, R., Bragazza, L., & Brancaleoni, L. Heatwave 2003: high summer temperature, rather than experimental fertilization, affects vegetation and CO2 exchange in an alpine bog. New Phytologist, 179(1), 142-154, 2008.

Gilmanov, T. G., & Oechel, W. C.: New estimates of organic matter reserves and net primary productivity of the North American tundra ecosystems. Journal of Biogeography, 723-741, 1995.

Glatzel, S., Basiliko, N., & Moore, T. Carbon dioxide and methane production potentials of peats from natural, harvested and restored sites, eastern Québec, Canada. Wetlands, 24(2), 261-267, 2004.

Goodman, R. C. et al. Amazon palm biomass and allometry. Forest Ecology and Management, 310, 994-1004 (2013).

Gore, A. J. P. (Ed.) Mires: Swamp, Bog, Fen, and Moor, Elsevier, Amsterdam, 1983.

Gorham, E. Northern peatlands: role in the carbon cycle and probable responses to climatic warming. Ecological applications, 1(2), 182-195, 1991.

Gorham, E. The biogeochemistry of northern peatlands and its possible responses to global warming. In Biotic feedbacks in the global climate system: will the warming feed the warming? Edited by G.M. Woodwell and F.T. Mackenzie. Oxford University Press, New York. pp. 169–186, 1995

Gorham, E. V. I. L. L. E.: Biotic impoverishment in northern peatlands. The earth in transition: patterns and processes of biotic impoverishment. Cambridge University Press, Cambridge, UK, 65-98, 1990.

Gorham, E., Janssens, J. A., & Glaser, P. H. Rates of peat accumulation during the postglacial period in 32 sites from Alaska to Newfoundland, with special emphasis on northern Minnesota. Canadian Journal of Botany, 81(5), 429-438, 2003.

Gorham, E., Lehman, C., Dyke, A., Clymo, D., & Janssens, J. Long-term carbon sequestration in North American peatlands. Quaternary Science Reviews, 58, 77-82, 2012.

Granberg, G., Grip, H., Löfvenius, M. O., Sundh, I., Svensson, B. H., & Nilsson, M. A simple model for simulation of water content, soil frost, and soil temperatures in boreal mixed mires. Water resources research,35(12), 3771-3782, 1999.

Guimberteau, M. et al. Future changes in precipitation and impacts on extreme streamflow over Amazonian sub-basins. Environmental Research Letters, 8(1), 014035 (2013).

Guzmán Castillo, W. Valor económico del manejo sostenible de los ecosistemas de aguaje (Mauritia flexuosa). In International Congress on Development, Environment and Natural Resources: Multi-level and Multi-scale Sustainability (Vol. 3, pp. 1513-1521) (2007).

Hanson PJ, Phillips JR, Riggs JS, Nettles WR, Todd DE SPRUCE Large-Collar In Situ CO_2 and CH_4 Flux Data for the SPRUCE Experimental Plots. Carbon Dioxide Information Analysis Center, Oak Ridge National Laboratory, U.S. Department of Energy, Oak Ridge, Tennessee, U.S.A. http://dx.doi.org/10.3334/CDIAC/spruce.006, 2014.

Hanson PJ, Riggs JS, Dorrance C, Nettles WR, Hook LA. SPRUCE Environmental Monitoring Data: 2010-2014. Carbon Dioxide Information Analysis Center, Oak Ridge National Laboratory, U.S. Department of Energy, Oak Ridge, Tennessee, U.S.A. doi:http://dx.doi.org/10.3334/CDIAC/spruce.001, 2015.

Harden JW, Sundquist ET, Stallard RF et al. Dynamics of soil carbon during deglaciation of the Laurentide ice sheet. Science 258: 1921–1924, 1992.

Hay, L.E., Wilby, R.L., Leavesley, G.H. A comparison of delta change and downscaled GCM scenarios for three mountainous basins in the United States. Journal of the American Water Resources Association 36, 387–397, 2000.

He, Y., Jones, M. C., Zhuang, Q., Bochicchio, C., Felzer, B. S., Mason, E., & Yu, Z. Evaluating CO 2 and CH 4 dynamics of Alaskan ecosystems during the Holocene Thermal Maximum. Quaternary Science Reviews, 86, 63-77, 2014.

Helvey, J. D., A summary of rainfall interception by certain conifers of North America, in Proceedings of the Third International Symposium for Hydrology Professors Biological Effects in the Hydrological Cycle, edited by E. J. Monke, 103– 113 pp., Purdue Univ., West Lafayette, Ind, 1971.

Hill BH, Jicha TM, Lehto LLP, Elonen CM, Sebestyen SD, Kolka RK. Comparisons of soil nitrogen mass balances for an ombrotrophic bog and a minerotrophic fen in northern Minnesota. Science of the Total Environment 550:880–892, 2016.

Hinzman, L. D., Viereck, L. A., Adams, P. C., Romanovsky, V. E., & Yoshikawa, K. Climate and permafrost dynamics of the Alaskan boreal forest. Alaska's Changing Boreal Forest, 39-61, 2006.

Hobbie, S. E., Schimel, J. P., Trumbore, S. E., & Randerson, J. R. Controls over carbon storage and turnover in high-latitude soils. Global Change Biology, 6(S1), 196-210, 2000.

Hobbie, S. E.: Interactions between litter lignin and nitrogenitter lignin and soil nitrogen availability during leaf litter decomposition in a Hawaiian montane forest. Ecosystems, 3(5), 484-494, 2000.

Houghton, R. A. et al. The spatial distribution of forest biomass in the Brazilian Amazon: a comparison of estimates. Global Change Biology, 7(7), 731-746 (2001).

Hugelius, G., Strauss, J., Zubrzycki, S., Harden, J. W., Schuur, E., Ping, C. L., ... & O'Donnell, J. A.: Estimated stocks of circumpolar permafrost carbon with quantified uncertainty ranges and identified data gaps.Biogeosciences, 11(23), 6573-6593, 2014.

Huybers, P. Early Pleistocene glacial cycles and the integrated summer insolation forcing. Science, 313(5786), 508-511, 2006.

Iman, R. L. et al. An investigation of uncertainty and sensitivity analysis techniques for computer models, Risk Anal., 8, 71 – 90, 1988.

Iversen CM, Hanson PJ, Brice DJ, Phillips JR, McFarlane KJ, Hobbie EA, Kolka RK. SPRUCE Peat Physical and Chemical Characteristics from Experimental Plot Cores, 2012. Carbon Dioxide Information Analysis Center, Oak Ridge National Laboratory, U.S. Department of Energy, Oak Ridge, Tennessee, U.S.A.http://dx.doi.org/10.3334/CDIAC/spruce.005, 2014.

Jenkinson, D. S. et al. Model Estimates of CO (2) Emissions from Soil in Response to Global Warming. Nature, 351(6324), 304 (1991).

Jobbágy, E. G., & Jackson, R. B.: The vertical distribution of soil organic carbon and its relation to climate and vegetation. Ecological applications, 10(2), 423-436, 2000.

Jones, M. C., & Yu, Z. Rapid deglacial and early Holocene expansion of peatlands in Alaska. Proceedings of the National Academy of Sciences,107(16), 7347-7352, 2010.

Jones, M.C., Bernhardt, C.E. & Willard, D.A. Late Holocene vegetation, climate, and land-use impacts on carbon dynamics in the Florida Everglades. Quaternary Science Reviews, 90, 90–105, 2014.

Jones, P. D., & Moberg, A.: Hemispheric and large-scale surface air temperature variations: An extensive revision and an update to 2001. Journal of Climate, 16(2), 206-223, 2003.

Juszli GM. Patterns in belowground primary productivity and belowground biomass in marshes of the Everglades' oligohaline ecotone. M.Sc. Thesis, Florida International University, Miami, FL, 2006.

Kalliola et al. Upper Amazon channel migration: implications for vegetation perturbance and succession using bitemporal Landsat images. Naturwissenschaften, 79, 75 –79 (1992).

Kane, E. S., Turetsky, M. R., Harden, J. W., McGuire, A. D., & Waddington, J. M. Seasonal ice and hydrologic controls on dissolved organic carbon and nitrogen concentrations in a boreal-rich fen. Journal of Geophysical Research: Biogeosciences, 115(G4), 2010.

Kaufman, D. S., Ager, T. A., Anderson, N. J., Anderson, P. M., Andrews, J. T., Bartlein, P. J., ... & Dyke, A. S. Holocene thermal maximum in the western Arctic (0–180 W). Quaternary Science Reviews, 23(5), 529-560, 2004.

Kaufman, D.S., Axford, Y.L., Henerson, A., McKay, N.P., Oswald, W.W., Saenger, C., Anderson, R.S., Bailey, H.L., Clegg, B., Gajewski, K., Hu, F.S., Jones, M.C., Massa, C., Routson, C.C., Werner, A., Wooller, M.J., Yu, Z. Holocene climate changes in eastern Beringia (NW North America) e a systemic review of multi-proxy evidence. Quaternary Science Reviews, this volume. http://dx.doi.org/10.1016/ j.quascirev.2015.10.021, 2016.

Keller, J. K., & Bridgham, S. D. Pathways of anaerobic carbon cycling across an ombrotrophic–minerotrophic peatland gradient. Limnology and Oceanography 52 : 96 –107, 2007.

Keller, J. K., & Takagi, K. K. Solid-phase organic matter reduction regulates anaerobic decomposition in bog soil. Ecosphere, 4(5), 1-12, 2013.

Kelly, T. J. et al. The vegetation history of an Amazonian domed peatland. Palaeogeography, Palaeoclimatology, Palaeoecology, 468, 129-141 (2017).

Kimball, J. S., McDonald, K. C., Running, S. W., & Frolking, S. E. Satellite radar remote sensing of seasonal growing seasons for boreal and subalpine evergreen forests. Remote Sensing of Environment, 90(2), 243-258, 2004.

Kirschbaum, M. U. A modelling study of the effects of changes in atmospheric CO2 concentration, temperature and atmospheric nitrogen input on soil organic carbon storage. Tellus B, 45(4), 321-334, 1993.

Kirschbaum, M. U. F. The temperature dependence of organic-matter decomposition—still a topic of debate. Soil Biology and Biochemistry, 38(9), 2510-2518, 2006.

Kirschbaum, M. U. The temperature dependence of soil organic matter decomposition, and the effect of global warming on soil organic C storage. Soil Biology and biochemistry, 27(6), 753-760, 1995.

Kirschbaum, M. U. Will changes in soil organic carbon act as a positive or negative feedback on global warming?. Biogeochemistry, 48(1), 21-51, 2000.

Kivinen, E., and P. Pakarinen. Geographical distribution of peat resources and major peatland complex types in the world. Annales Academiae Scientarum Fennicae, Series A, Number 132, 1981.

Kleinen, T., Brovkin, V., & Schuldt, R. J. A dynamic model of wetland extent and peat accumulation: results for the Holocene.Biogeosciences, 9(1), 235-248, 2012.

Knorr, W., Prentice, I. C., House, J. I., & Holland, E. A. Long-term sensitivity of soil carbon turnover to warming. Nature, 433(7023), 298-301, 2005.

Kuhry, P., & Vitt, D. H. Fossil carbon/nitrogen ratios as a measure of peat decomposition. Ecology, 77(1), 271-275, 1996.

Lähteenoja, O. et al. Amazonian floodplains harbour minerotrophic and ombrotrophic peatlands. Catena, 79(2), 140-145, 2009b.

Lähteenoja, O. et al. Amazonian peatlands: an ignored C sink and potential source. Global Change Biology, 15(9), 2311-2320, 2009a.

Lähteenoja, O. et al. The large Amazonian peatland carbon sink in the subsiding Pastaza-Marañón foreland basin, Peru. Global Change Biology, 18(1), 164-178, 2012.

Lähteenoja, O., & Page, S. High diversity of tropical peatland ecosystem types in the Pastaza-Marañón basin, Peruvian Amazonia. Journal of Geophysical Research: Biogeosciences, 116(G2), 2011.

Lappalainen E. General review on world peatlands and peat resources. In: Lappalainen E (ed.) Global Peat Resources. Jyvaskyla: International Peat Society, pp. 53–56, 1996.

Lavoie, M. and Richard, P.J.H. Paléoécologie de la tourbière du lac Malbaie, dans le massif des Laurentides (Québec): évaluation du rôle du climat sur l'accumulation de la tourbe. Géographie physique et Quaternaire 54, 169–85, 2000.

Li, W. et al. Future precipitation changes and their implications for tropical peatlands, Geophys. Res. Lett., 34, L01403, doi:10.1029/2006GL028364 (2007).

Linderholm, H. W. Growing season changes in the last century.Agricultural and Forest Meteorology, 137(1), 1-14, 2006.

Liu, H., Randerson, J. T., Lindfors, J., & Chapin, F. S. Changes In The Surface Energy Budget After Fire In Boreal Ecosystems Of Interior Alaska: An Annual Perspective, Journal Of Geophysical Research, 110(D13), 2005.

Loisel, J., Gallego-Sala, A. V., & Yu, Z. Global-scale pattern of peatland Sphagnum growth driven by photosynthetically active radiation and growing season length. Biogeosciences, 9(7), 2737-2746, 2012.

Loisel, J., Yu, Z., Beilman, D. W., Camill, P., Alm, J., Amesbury, M. J., ... & Belyea, L. R. (2014). A database and synthesis of northern peatland soil properties and Holocene carbon and nitrogen accumulation. The Holocene, 0959683614538073, 1996.

Loisel, J., Yu, Z., Beilman, D. W., Camill, P., Alm, J., Amesbury, M. J., ... & Belyea, L. R. A database and synthesis of northern peatland soil properties and Holocene carbon and nitrogen accumulation. the Holocene, 0959683614538073, 2014.

MacDonald GM, Beilman DW, Kremenetski KV et al. Rapid early development of circum-arctic peatlands and atmospheric CH4 and CO2 variations. Science 314: 285–288, 2006.

Malhi, Y. et al. The regional variation of aboveground live biomass in old-growth Amazonian forests. Global Change Biology 12, 1107–1138 (2006).

Maltby E and Immirzi P. Carbon dynamics in peatlands and other wetland soils, regional and global perspectives. Chemosphere 27: 999–1023, 1993.

Manabe, S., & Wetherald, R. T.: On the distribution of climate change resulting from an increase in CO2 content of the atmosphere. Journal of the Atmospheric Sciences, 37(1), 99-118, 1980.

Manabe, S., & Wetherald, R. T.: Reduction in summer soil wetness induced by an increase in atmospheric carbon dioxide. Science, 232(4750), 626-628, 1986.

Marcott, S. A., Shakun, J. D., Clark, P. U., & Mix, A. C.: A reconstruction of regional and global temperature for the past 11,300 years.science, 339(6124), 1198-1201, 2013.

Marengo, J. A. et al. Development of regional future climate change scenarios in South America using the Eta CPTEC/HadCM3 climate change projections: Climatology and regional analyses for the Amazon, Sa˜o Francisco and the Parana River Basins. Clim Dyn 38:1829–1848. doi:10.1007/s00382- 011-1155-5 (2012).

Martin, A. R., & Thomas, S. C. A reassessment of carbon content in tropical trees. PloS one, 6(8), e23533 (2011).

Matthews, E., & Fung, I.: Methane emission from natural wetlands: Global distribution, area, and environmental characteristics of sources.Global biogeochemical cycles, 1(1), 61-86, 1987.

McGuire, A. D. et al. Interactions between carbon and nitrogen dynamcs in estimating net primary productivity for potential vegetation in North America. Global Biogeochemical Cycles, 6(2), 101-124 (1992).

McGuire, A. D., & Hobbie, J. E.: Global climate change and the equilibrium responses of carbon storage in arctic and subarctic regions. InModeling the Arctic system: A workshop report on the state of modeling in the Arctic System Science program, pp. 53-54, 1997.

McGuire, A. D., Anderson, L. G., Christensen, T. R., Dallimore, S., Guo, L., Hayes, D. J., ... & Roulet, N. Sensitivity of the carbon cycle in the Arctic to climate change. Ecological Monographs, 79(4), 523-555, 2009.

McGuire, A. D., Melillo, J. M., Kicklighter, D. W., & Joyce, L. A. Equilibrium responses of soil carbon to climate change: empirical and process-based estimates. Journal of Biogeography, 785-796, 1995.

McGuire, A. D., Melillo, J. M., Randerson, J. T., Parton, W. J., Heimann, M., Meier, R. A., ... & Sauf, W. Modeling the effects of snowpack on heterotrophic respiration across northern temperate and high latitude regions: Comparison with measurements of atmospheric carbon dioxide in high latitudes. Biogeochemistry, 48(1), 91-114, 2000.

Melillo, J. M., Kicklighter, D. W., McGuire, A. D., Peterjohn, W. T., & Newkirk, K.: Global change and its effects on soil organic carbon stocks. In Dahlem Conference Proceedings, John Wiley and Sons, New York, John Wiley & Sons, Ltd., Chichster, pp. 175-189, 1995.

Miettinen, J. et al. Two decades of destruction in Southeast Asia's peat swamp forests. Frontiers in Ecology and the Environment, 10(3), 124-128 (2011).

Mitchell, T. D., Carter, T. R., Jones, P. D., Hulme, M., & New, M.: A comprehensive set of high-resolution grids of monthly climate for Europe and the globe: the observed record (1901–2000) and 16 scenarios (2001–2100).Tyndall centre for climate change research working paper, 55(0), 25, 2004.

Moore, T. R., & Knowles, R. The influence of water table levels on methane and carbon dioxide emissions from peatland soils. Canadian Journal of Soil Science, 69(1), 33-38, 1989.

Moore, T. R., Bubier, J. L., Frolking, S. E., Lafleur, P. M., & Roulet, N. T. Plant biomass and production and CO2 exchange in an ombrotrophic bog. Journal of Ecology, 90(1), 25-36, 2002.

Nebel, G. et al. Litter fall, biomass and net primary production in flood plain forests in the Peruvian Amazon. Forest Ecology and Management, 150(1), 93-102 (2001).

Neller RJ et al. On the formation of blocked valley lakes by channel avulsion in Upper Amazon foreland basins. Zeitschrift fu ¨r Geomorphologie, 36, 401–411 (1992)

Nobrega, S., & Grogan, P. Deeper snow enhances winter respiration from both plant-associated and bulk soil carbon pools in birch hummock tundra. Ecosystems, 10(3), 419-431, 2007.

Oechel, W. C., Hastings, S. J., Vourlrtis, G., Jenkins, M., Riechers, G., & Grulke, N.: Recent change of Arctic tundra ecosystems from a net carbon dioxide sink to a source. Nature, 361(6412), 520-523, 1993.

Oechel, W. C.: Nutrient and water flux in a small arctic watershed: an overview. Holarctic Ecology, 229-237, 1989.

Oksanen, P. O., Kuhry, P., & Alekseeva, R. N.: Holocene development of the Rogovaya river peat plateau, European Russian Arctic.The Holocene, 11(1), 25-40, 2001.

Page, S. E. et al. A record of Late Pleistocene and Holocene carbon accumulation and climate change from an equatorial peat bog (Kalimantan, Indonesia): implications for past, present and future carbon dynamics. Journal of Quaternary Science, 19(7), 625-635, 2004.

Page, S. E. et al. Global and regional importance of the tropical peatland carbon pool. Global Change Biology, 17(2), 798-818, 2011.

Page, S. E. et al. The amount of carbon released from peat and forest fires in Indonesia during 1997. Nature, 420(6911), 61-65 (2002).

Peteet, D., Andreev, A., Bardeen, W., & Mistretta, F.: Long-term Arctic peatland dynamics, vegetation and climate history of the Pur-Taz region, western Siberia. Boreas, 27(2), 115-126, 1998.

Post, W. M., Emanuel, W. R., Zinke, P. J., & Stangenberger, A. G. Soil carbon pools and world life zones. Nature 298: 156–159, 1982.

Powell, T. L. et al. Confronting model predictions of carbon fluxes with measurements of Amazon forests subjected to experimental drought. *New Phytologist*, 200: 350–365. doi: 10.1111/nph.12390 (2013).

Prentice, I. C., Cramer, W., Harrison, S. P., Leemans, R., Monserud, R. A., & Solomon, A. M.: Special paper: a global biome model based on plant physiology and dominance, soil properties and climate. Journal of biogeography, 117-134, 1992.

Raich, J. W., Rastetter, E. B., Melillo, J. M., Kicklighter, D. W., Steudler, P. A., Peterson, B. J., ... & Vorosmarty, C. J. Potential net primary productivity in South America: application of a global model. Ecological Applications, 1(4), 399-429, 1991.

Rammig, A. et al. Estimating the risk of Amazonian forest dieback. New Phytologist, 187: 694-706. doi:10.1111/j.1469-8137.2010.03318.x (2010).

Räsänen, M. E. et al. Evolution of the western Amazon lowland relief: impact of Andean foreland dynamics. Terra Nova, 2(4), 320-332 (1990).

Räsänen, M. E. et al. Recent and ancient fluvial deposition systems in the Amazonian foreland basin, Peru. Geological Magazine, 129(03), 293-306 (1992).

Renssen, H., Seppä, H., Heiri, O., Roche, D. M., Goosse, H., & Fichefet, T. The spatial and temporal complexity of the Holocene thermal maximum. Nature Geoscience, 2(6), 411-414, 2009.

Restrepo-Coupe, N. et al. Do dynamic global vegetation models capture the seasonality of carbon fluxes in the Amazon basin? A data-model intercomparison. Glob Change Biol, 23: 191–208. doi:10.1111/gcb.13442 (2017).

Rieley, J. O. et al. Tropical peatlands: carbon stores, carbon gas emissions and contribution to climate change processes. Peatlands and Climate Change. International Peat Society, Vapaudenkatu, 12(40100), 148-182 (2008).

Rieley, J. O., & Page, S. E. Wise use of tropical peatlands: focus on Southeast Asia: synthesis of results and conclusions of the UK Darwin Initiative and the EU INCO EUTROP, STRAPEAT and RESTORPEAT Partnerships together with proposals for implementing wise use of tropical peatlands. ALTERRA–Wageningen University and Research Centre and the EU INCO–STRAPEAT and RESTORPEAT Partnerships, 266 (2005).

Roucoux, K. H. et al. Vegetation development in an Amazonian peatland. Palaeogeography, Palaeoclimatology, Palaeoecology, 374, 242-255, 2013.

Roucoux, K.H. et al. Threats to intact tropical peatlands and opportunities for their conservation. Conservation Biology. Accepted Author Manuscript. doi:10.1111/cobi.12925 (2017).

Roulet, N. T., Lafleur, P. M., Richard, P. J., Moore, T. R., Humphreys, E. R., & Bubier, J. I. L. L. Contemporary carbon balance and late Holocene carbon accumulation in a northern peatland. Global Change Biology, 13(2), 397-411, 2007.

Rowland, L. et al. Modelling climate change responses in tropical forests: similar productivity estimates across five models, but different mechanisms and responses, *Geosci. Model Dev*., 8, 1097-1110, doi:10.5194/gmd-8-1097-2015 (2015).

Running, S. W., Nemani, R. R., Heinsch, F. A., Zhao, M., Reeves, M., & Hashimoto, H. A continuous satellite-derived measure of global terrestrial primary production. Bioscience, 54(6), 547-560, 2004.

Ruokolainen, K. et al. On Amazonian peatlands. International Mire Conservation Group Newsletter, 4, 8-10 (2001).

Saarinen, T., Tolonen, K. & Vasander, H. Use of 14 C labelling to measure below-ground biomass of mire plants', Suo. **43**, 245–247, 1992.

Saarinen, T. Biomass and production of two vascular plants in a boreal mesotrophic fen. Canadian Journal of Botany, 74(6), 934-938, 1996.

Sánchez, E. et al. Regional climate modelling in CLARIS-LPB: a concerted approach towards twentyfirst century projections of regional temperature and precipitation over South America. Climate Dynamics, 45(7-8), 2193-2212 (2015).

Schulman et al. Parameters for global ecosystem models. Nature, 399(6736), 535-536 (1999).

Schuur, E. A., Bockheim, J., Canadell, J. G., Euskirchen, E., Field, C. B., Goryachkin, S. V., ... & Mazhitova, G.: Vulnerability of permafrost carbon to climate change: implications for the global carbon cycle.BioScience, 58(8), 701-714, 2008.

Senkowsky, S. A burning interest in Boreal forests: Researchers in Alaska link fires with Climate Change. BioScience, 51(11), 916-921, 2001.

Shi, X., Thornton, P. E., Ricciuto, D. M., Hanson, P. J., Mao, J., Sebestyen, S. D., ... & Bisht, G. Representing northern peatland microtopography and hydrology within the Community Land Model. Biogeosciences, 12(21), 6463-6477, 2015.

Sitch, S., Smith, B., Prentice, I. C., Arneth, A., Bondeau, A., Cramer, W., ... & Thonicke, K.: Evaluation of ecosystem dynamics, plant geography and terrestrial carbon cycling in the LPJ dynamic global vegetation model.Global Change Biology, 9(2), 161-185, 2003.

Skare, Ø. et al. Improved sampling importance resampling and reduced bias importance sampling, Scand. J. Stat., 30, 719 – 737, 2003.

Smith ND et al. Anatomy of an avulsion. Sedimentology, 36,1 –23 (1989).

Spahni, R., Joos, F., Stocker, B. D., Steinacher, M., & Yu, Z. C. Transient simulations of the carbon and nitrogen dynamics in northern peatlands: From the Last Glacial Maximum to the 21st century. Climate of the Past, 9(3), 1287-1308, 2013.

Stieglitz, M., Déry, S. J., Romanovsky, V. E., & Osterkamp, T. E. The role of snow cover in the warming of arctic permafrost. Geophysical Research Letters, 30(13), 2003.

Stocker, B. D., Spahni, R., & Joos, F.: DYPTOP: a cost-efficient TOPMODEL implementation to simulate sub-grid spatio-temporal dynamics of global wetlands and peatlands. Geoscientific Model Development, 7(6), 3089-3110, 2014.

Stocker, B. D., Strassmann, K., & Joos, F.: Sensitivity of Holocene atmospheric CO 2 and the modern carbon budget to early human land use: analyses with a process-based model. Biogeosciences, 8(1), 69-88, 2011.

Swindles, G. et al. Ecology of testate amoebae in an Amazonian peatland and development of a transfer function for palaeohydrological reconstruction. Mic. Ecol. 68, 284–298, 2014.

Tang, J., & Zhuang, Q. A global sensitivity analysis and Bayesian inference framework for improving the parameter estimation and prediction of a process-based Terrestrial Ecosystem Model. Journal of Geophysical Research: Atmospheres, 114(D15), 2009.

Tang, J., & Zhuang, Q. Equifinality in parameterization of process-based biogeochemistry models: A significant uncertainty source to the estimation of regional carbon dynamics. Journal of Geophysical Research: Biogeosciences, 113(G4), 2008.

Tang, J., Zhuang, Q., Shannon, R. D., & White, J. R. Quantifying wetland methane emissions with process-based models of different complexities. Biogeosciences, 7(11), 3817-3837, 2010.

Tarnocai, C., Canadell, J. G., Schuur, E. A. G., Kuhry, P., Mazhitova, G., & Zimov, S. Soil organic carbon pools in the northern circumpolar permafrost region. Global biogeochemical cycles, 23(2), 2009.

Thiemann, M. et al. Bayesian recursive parameter estimation for hydrologic models, Water Resour. Res., 37(10), 2521 – 2536 (2001).

Tian, H. et al. Climatic and biotic controls on annual carbon storage in Amazonian ecosystems. Global Ecology and Biogeography, 9(4), 315-335 (2000).

Tian, H. et al. Effect of interannual climate variability on carbon storage in Amazonian ecosystems. Nature, 396(6712), 664-667 (1998).

Timm, O., & Timmermann, A.: Simulation of the Last 21 000 Years Using Accelerated Transient Boundary Conditions*. Journal of Climate,20(17), 4377-4401, 2007.

Toberman, H., Tipping, E., Boyle, J.F., Helliwell, R.C., Lilly, A., Henrys, P.A. Dependence of ombrotrophic peat nitrogen on phosphorus and climate. Biogeochemistry 125, 11–20, 2015.

Trumbore, S. E., O. A. Chadwick, and R. Amundson. Rapid exchange between soil carbon and atmospheric carbon dioxide driven by temperature change, Science, 272, 393–396, doi:10.1126/science.272.5260.393, 1996.

Tucker, C. J., Slayback, D. A., Pinzon, J. E., Los, S. O., Myneni, R. B., & Taylor, M. G. Higher northern latitude normalized difference vegetation index and growing season trends from 1982 to 1999. International journal of biometeorology, 45(4), 184-190, 2001.

Turetsky, M. R., Kotowska, A., Bubier, J., Dise, N. B., Crill, P., Hornibrook, E. R., ... & Olefeldt, D. A synthesis of methane emissions from 71 northern, temperate, and subtropical wetlands. Global change biology, 20(7), 2183-2197, 2014.

Turetsky, M. R., Treat, C. C., Waldrop, M. P., Waddington, J. M., Harden, J. W., & McGuire, A. D. Short-term response of methane fluxes and methanogen activity to water table and soil warming manipulations in an Alaskan peatland. Journal of Geophysical Research: Biogeosciences,113(G3), 2008.

Turunen, J., Tomppo, E., Tolonen, K., & Reinikainen, A. Estimating carbon accumulation rates of undrained mires in Finland–application to boreal and subarctic regions. The Holocene, 12(1), 69-80, 2002.

Verry, E.S., Timmons, D.R. Waterbourne nutrient flow through an upland-peatland watershed in Minnesota. Ecology 63, 1456–1467, 1982.

Vitt, D. H., Halsey, L. A., Bauer, I. E., & Campbell, C.: Spatial and temporal trends in carbon storage of peatlands of continental western Canada through the Holocene. Canadian Journal of Earth Sciences, 37(5), 683-693, 2000.

Wang, S. et al. Quantifying peat carbon accumulation in Alaska using a process-based biogeochemistry model. Journal of Geophysical Research. Biogeosciences, 121(8), 2172-2185, 2016a.

Wang, S. et al. Quantifying soil carbon accumulation in Alaskan terrestrial ecosystems during the last 15000 years. Biogeosciences, 13(22), 6305, 2016b.

Wang, S., Zhuang, Q., Lätheenoja, O., Draper, F.C., Cadillo-Quiroz, H. Potential shift from a carbon sink yo a source in Amazionian peatlands under a changing climate. Proc. Natl. Acad. Sci. USA, 115, 12407–12412, 2018.

Wang, Y. P., & Polglase, P. J. Carbon balance in the tundra, boreal forest and humid tropical forest during climate change: scaling up from leaf physiology and soil carbon dynamics. Plant, Cell & Environment, 18(10), 1226-1244, 1995.

Worrall, F., Clay, G.D., Burt, T.P., Rose, B. The multi-annual nitrogen budget of a peat-covered catchment—changing from sink to source? Sci. Total Environ. 433, 178–188, 2012.

Xu-Ri, Prentice IC. Terrestrial nitrogen cycle simulation with a dynamic global vegetation model. Global Change Biology 14: 1745–1764, 2008.

Yavitt, J. B., Lang, G. E., & Wieder, R. K. Control of carbon mineralization to CH4 and CO2 in anaerobic, Sphagnum-derived peat from Big Run Bog, West Virginia. Biogeochemistry, 4(2), 141-157, 1987.

Yu, Z. C. Northern peatland carbon stocks and dynamics: a review. Biogeosciences, 9(10), 4071-4085, 2012.

Yu, Z., Beilman, D. W., & Jones, M. C. Sensitivity of northern peatland carbon dynamics to Holocene climate change. Carbon cycling in northern peatlands, 55-69, 2009.

Yu, Z., Loisel, J., Brosseau, D. P., Beilman, D. W., & Hunt, S. J. Global peatland dynamics since the Last Glacial Maximum. Geophysical Research Letters, 37(13), 2010.

Yu, Z., Loisel, J., Brosseau, D.P., Beilman, D.W., Hunt, S.J. Global peatland dynamics since the Last Glacial Maximum. Geophys. Res. Let. 37 (13), L13402, 2010.

Zhuang, Q., McGuire, A. D., Melillo, J. M., Clein, J. S., Dargaville, R. J., Kicklighter, D. W., ... & Hobbie, J. E. Carbon cycling in extratropical terrestrial ecosystems of the Northern Hemisphere during the 20th century: a modeling analysis of the influences of soil thermal dynamics. Tellus B, 55(3), 751-776, 2003.

Zhuang, Q., McGuire, A. D., O'neill, K. P., Harden, J. W., Romanovsky, V. E., & Yarie, J. Modeling soil thermal and carbon dynamics of a fire chronosequence in interior Alaska. Journal of Geophysical Research: Atmospheres, 107(D1), 2002.

Zhuang, Q., Melillo, J. M., Kicklighter, D. W., Prinn, R. G., McGuire, A. D., Steudler, P. A., ... & Hu, S. Methane fluxes between terrestrial ecosystems and the atmosphere at northern high latitudes during the past century: A retrospective analysis with a process-based biogeochemistry model. Global Biogeochemical Cycles, 18(3), 2004.

Zhuang, Q., Melillo, J. M., McGuire, A. D., Kicklighter, D. W., Prinn, R. G., Steudler, P. A., ... & Hu, S.: Net emissions of CH4 and CO2 in Alaska: Implications for the region's greenhouse gas budget. Ecological Applications, 17(1), 203-212, 2007.

Zhuang, Q., Melillo, J. M., Sarofim, M. C., Kicklighter, D. W., McGuire, A. D., Felzer, B. S., ... & Hu, S. CO2 and CH4 exchanges between land ecosystems and the atmosphere in northern high latitudes over the 21st century. Geophysical Research Letters, 33(17), 2006.

Zhuang, Q., Romanovsky, V. E., & McGuire, A. D. Incorporation of a permafrost model into a large-scale ecosystem model: Evaluation of temporal and spatial scaling issues in simulating soil thermal dynamics. Journal of Geophysical Research: Atmospheres, 106(D24), 33649-33670, 2001.

Zhuang, Q., Zhu, X., He, Y., Prigent, C., Melillo, J. M., McGuire, A. D., ... & Kicklighter, D. W. Influence of changes in wetland inundation extent on net fluxes of carbon dioxide and

methane in northern high latitudes from 1993 to 2004. Environmental Research Letters, 10(9), 095009, 2015.

Zhuang, Q., Zhu, X., He, Y., Prigent, C., Melillo, J. M., McGuire, A. D., ... & Kicklighter, D. W. Influence of changes in wetland inundation extent on net fluxes of carbon dioxide and methane in northern high latitudes from 1993 to 2004. Environmental Research Letters, 10(9), 095009, 2015.

Zimov, S. A., Schuur, E. A., & Chapin III, F. S. Permafrost and the global carbon budget. Science(Washington), 312(5780), 1612-1613, 2006.

Zoltai, S. C. Permafrost distribution in peatlands of west-central Canada during the Holocene warm period 6000 years BP. Géographie physique et Quaternaire, 49(1), 45-54, 1995.

Zulkafli, Z. et al. Projected increases in the annual flood pulse of the Western Amazon. Environmental Research Letters, 11(1), 014013 (2016).

VITA

EDUCATION

Aug.14-Present	Department of Earth, Atmospheric, and Planetary Sciences, Purdue University,
Aug.10-Jul.14	University of Science and Technology of China, School of Earth and Planetary Sciences, B.S. in Atmospheric Physics

PUBLICATIONS

1. **Wang, S**., Q. Zhuang, Z. Yu, S. Bridgham, and J. K. Keller (2016), Quantifying peat carbon accumulation in Alaska using a process-based biogeochemistry model, *J. Geophys. Res. Biogeosci.*, 121, doi: 10.1002/2016JG003452.
2. **Wang, S.,** Q. Zhuang, and Z. Yu (2016), Quantifying soil carbon accumulation in Alaskan terrestrial ecosystems during the last 15 000 years, *Biogeosciences*, 13, 6305-6319, doi:10.5194/bg-13-6305-2016.
3. **Wang, S.,** Zhuang, Q., Lähteenoja, O., Draper, F., and Cadillo-Quiroz, H (2018), Potential shift from a carbon sink to a source in Amazonian peatlands under a changing climate, *Proceedings of the National Academy of Sciences* Nov 2018, 201801317; DOI: 10.1073/pnas.1801317115.
4. **Wang, S.,** Zhuang, Q., and Aires, F (2019), Quantifying peat soil carbon accumulation in North America during the last 12,000 years (Submitted to *JGR-Biogeosciences*).
5. Xu, X., …**Wang, S** (2016), Factors influencing industrial carbon emissions and strategies for carbon mitigation in the Yangtze River Delta of China, *Journal of Cleaner Production*, ISSN 0959-6526, http://dx.doi.org/10.1016/j.jclepro.2016.10.107